TOWARDS A TERRADYNAMICS OF LEGGED LOCOMOTION ON HOMOGENEOUS AND HETEROGENEOUS GRANULAR MEDIA THROUGH ROBOPHYSICAL APPROACHES

A Thesis
Presented to
The Academic Faculty

by

Feifei Qian

In Partial Fulfillment
of the Requirements for the Degree
Doctor of Philosophy in the
Electrical and Computer Engineering

Georgia Institute of Technology
December 2015

TOWARDS A TERRADYNAMICS OF LEGGED LOCOMOTION ON HOMOGENEOUS AND HETEROGENEOUS GRANULAR MEDIA THROUGH ROBOPHYSICAL APPROACHES

Approved by:

Dr. Ayanna M. Howard,
Committee Chair
School of Electrical and Computer Engineering
Georgia Institute of Technology

Professor Daniel I. Goldman, Advisor
School of Physics
Georgia Institute of Technology

Dr. Henrik I. Christensen
College of Computing
Georgia Institute of Technology

Dr. Kurt Wiesenfeld
School of Physics
Georgia Institute of Technology

Dr. Patricio Vela
School of Electrical and Computer Engineering
Georgia Institute of Technology

Dr. Robert J. Full
Department of Integrative Biology
University of California, Berkeley

Dr. Simon Sponberg
School of Physics
Georgia Institute of Technology

Date Approved: 9 Nov 2015

ACKNOWLEDGEMENTS

In full gratitude I would like to thank everyone who encouraged, inspired, supported, and assisted me in my pursuit of a my PhD degree, who have made this dissertation possible and because of whom my graduate life an unforgettable experience for me.

Firstly, I would like to express my sincere gratitude to my advisor Prof. Daniel Goldman for his continuous support of my Ph.D study and research. His enthusiasm and immense knowledge inspired me to become a better researcher. He showed me how to conduct cool research, how to effectively communicate my work, and how to mentor students. He always believed in my abilities and gave me a lot of opportunities to try my ideas, but whenever I was confused he was always there to provide guidance. I benefit from his guidance not just for my Ph.D research but also for my entire career. I could not have imagined having a better advisor for my Ph.D study.

Besides my advisor, I would also like to thank my co-adviser, Prof. Henrik I. Christensen, and the rest of my thesis committee: Prof. Ayanna M. Howard, Prof. Kurt Wiesenfeld, Prof. Robert J. Full, Prof. Simon Sponberg, and Prof. Patricio Vela, for their for their encouragement, insightful comments, and questions which inspired me to widen my research from various perspectives.

I am deeply grateful to Dr. Paul Umbanhowar for the helpful discussions that helped me sort out the technical details of my work. My sincere thanks also goes to my collaborators: I thank Dr. Haldun Komsuoglu, Deniz Ilhan, and Prof. Daniel

Koditschek of University of Pennsylvania, for their support in the SandBot experiments; Dr. Aaron M. Hoover, Paul Birkmeyer, Andrew Pullin, and Prof. Ronald Fearing of UC Berkeley, for their support in the DynaRoACH experiments; and Prof. Pierangelo Masarati of Politecnico di Milano for his support in the MbDyn simulation.

I would like to thank my dear friends and colleagues in the CRAB lab, whom I had a great time and pleasure working with and learned so much from. Special thanks to Chen Li, my lab mentor who gave me numerous guidance on research and career. Many thanks to Sarah Sharpe and Nicole Mazouchova, who always selflessly share with me their experiences and patiently help me when I was a junior graduate student in the lab. Many thanks to Nick Gravish and Andrei Savu who extended a great amount of assistance in helping me with my experimental setup and giving me guidance on electrical and mechanical techniques. And my sincere thanks to my fellow labmates, Jeffrey Aguilar, Tingnan Zhang, Daria Monaenkova, Hamid Marvi, Mark Kingsbury, Vadim Linevich and Perrin Schiebel, for the stimulating discussions, and for all the fun we have had these years. I am also deeply thankful to my undergraduate and high school research assistants, Jeffery Shen, Kevin Daffon, Jessica Chau, Duncan Hathaway, Luke Buffardi, Thomas Board, Amrita Sen, and Patrick Shin, without whose great effort this work could not have been accomplished.

I owe my gratitude to my previous teachers, Yu Wei and Qizhong Hu, who have always believed in me and given me invaluable advice that lead me here. I thank Dr. David Hu whose research greatly inspired me and whose invaluable advice helped me learned how to enjoy my work.

I would like to thank my dear friends, Sijie Zhang, Mingge Wu, Patricia Yang, Zhuo Chen, Miao He, Liting Hu, Jingwen Qu, Sadie Ali, and Chuanshu Shi, for always

being there for me whenever I needed encouragement and support, and for giving me so much happiness during the last few years. I thank Feng Wang and Wenlong Yu for helping me during my first year when I was struggling with my physics classes and cooking skills. My sincere thanks also goes to Al and Elaine Lacour for their generous host and support when I first arrived at US. I also want to thank Jane Chrisholm for helping me proofreading the introduction section of this thesis.

Most importantly, none of this would have been possible without the love and support of my family. My deepest gratitude to my parents, Jianhua Mao and Jianhua Qian, who always believe in me, encourage me, and support me to pursue my dreams. I want to thank my fiance, Dapeng Zhang, for being a constant source of support and strength for me throughout the years.

Last but not least, I would like to acknowledge the funding agencies: Army Research Laboratory (ARL) Micro Autonomous Systems and Technology (MAST), Defense Advanced Research Projects Agency (DARPA), Army Research Office (ARO), the Burroughs Wellcome Fund, and National Science Foundation (NSF) Physics of Living Systems (PoLS), for financially supporting the research discussed in this dissertation.

TABLE OF CONTENTS

LIST OF FIGURES

SUMMARY

In traditional navigation planning, robots are generally required to find a "collision free path" and avoid interacting with obstacles. This is reasonable for most wheeled or treaded robots which must circumvent obstacles, but for legged robots, traversing obstacles by stepping over or upon them is a valid and possibly a more effective option. Allowing robots to gracefully interact with the ground heterogeneities, or even manipulating the locomotion environments, will open a new avenue for strategic navigation planning and significantly expand viable exploration space.

The objectives of this dissertation were to discover the principles of legged locomotion on homogeneous and heterogeneous loose ground and to create the models of animal and robot interaction within such environments. Since interactions with natural substrates were too complicated to model, this work took a robophysics approach: We created a terrain generation system called SCATTER in which the properties of granular substrates were systematically varied to emulate a wide range of natural terrains. The control of such substrates allowed for the systematic exploration of the parameters of substrate properties, particularly substrate stiffness and heterogeneity. With this terrain creation system, this work systematically explored the locomotion of simplified laboratory robots when traversing over terrains with various properties.

For locomotion on homogeneous granular substrates, this work systematically examined the dynamics and performance of locomotors over a wide range of mass scales, appendage morphologies, and gaits. Using a 2.5 kg SandBot and a 20 g DynaRoACH as physical models that represent locomotors of different mass scales, we discovered

that at low leg frequency, both heavy and lightweight robots used a quasi-static "rotary walking" mechanism, in which the substrate yielded as legs penetrated and then solidified once vertical force balance was achieved. For locomotors that propelled themselves using this ground solidification mechanism, their locomotion performance depended primarily on the insertion depth of their legs in the substrates. Despite variation in morphology and gait, the performance of lizards, geckos, and crabs was also determined by their leg penetration ratio. For both robotic and biological locomotors, appendage designs that reduced foot pressure helped them passively minimize leg penetration ratio as the ground weakened, and consequently permitted maintenance of effective locomotion on low stiffness ground. At high leg frequencies, lightweight locomotors such as DynaRoACH used a distinct propulsion mechanism to achieve effective locomotion: By rapidly slapping their feet on the granular surface and fluidizing the granular particles, lightweight locomotors could generate a large lifting force from the substrate inertia, and propel themselves during rapid running by exploiting a speed-dependent fluid-like response of the granular substrates.

For locomotion on heterogeneous granular substrates, this work used SCATTER to embed boulders and rocks in the smaller granular grains, and systematically examined the trajectory and dynamics of a small robot interacting with such complex substrates. We noticed that robot trajectories exhibited chaotic dynamics and sensitivity to initial conditions, and the interaction between the robot and each ground heterogeneity could be modelled as a scattering event. The scattering magnitude depended sensitively on the initial contact position between the robot and the ground heterogeneity, but was relatively insensitive to the heterogeneity geometry, orientation, and texture. For a larger heterogeneous field with multiple "scatterers", the trajectory of a robot could be estimated using a superposition of the scattering angles from each scatterer.

A key feature of this dissertation is the ability to generate general interaction models of locomotor appendages with such complex substrates. These models aid in the design and control of future robots with morphologies and control strategies that allow for effective navigation on a large diversity of terrains and expand the applicability of terradynamics to heterogeneous terrestrial substrates.

CHAPTER I

INTRODUCTION

1.1 Motivation and Overview

The ability to successfully and rapidly maneuver on complex terrains is crucial for both biological and robotic systems. Animals locomote to find food and mates, escape predators, or relocate to more suitable habitats. In most of these scenarios, having strong locomotion ability directly results in an increase in the probability of survival. For autonomous robots, the ability to navigate in complex environments or negotiate with rough terrains is critical for transportation, search and rescue, planetary scientific exploration, and so on.

Natural environments come in a staggering variety of forms, with which locomotor strategies adapt accordingly. Animals can walk, run, jump, crawl on the ground, fly in the air, and swim in the water (Figure 1); and many robotic platforms have been developed that can effectively run on fractured rigid ground [105, 109], crawl within concave surfaces [133], and even climb on walls [57] (Figure 2). However, locomotor performance decreases significantly on soft, loose ground such as sand, gravel, snow and leaf litter (Figure 3), because unlike hard ground, such substrates can support only a limited amount of stress (i.e., yield stress). During interactions between legs or wheels and such substrates, the substrates can yield and flow when the yield stress is exceeded, producing complex and dynamic interactions that can result in poor locomotor performance for both biological and robotic locomotors.

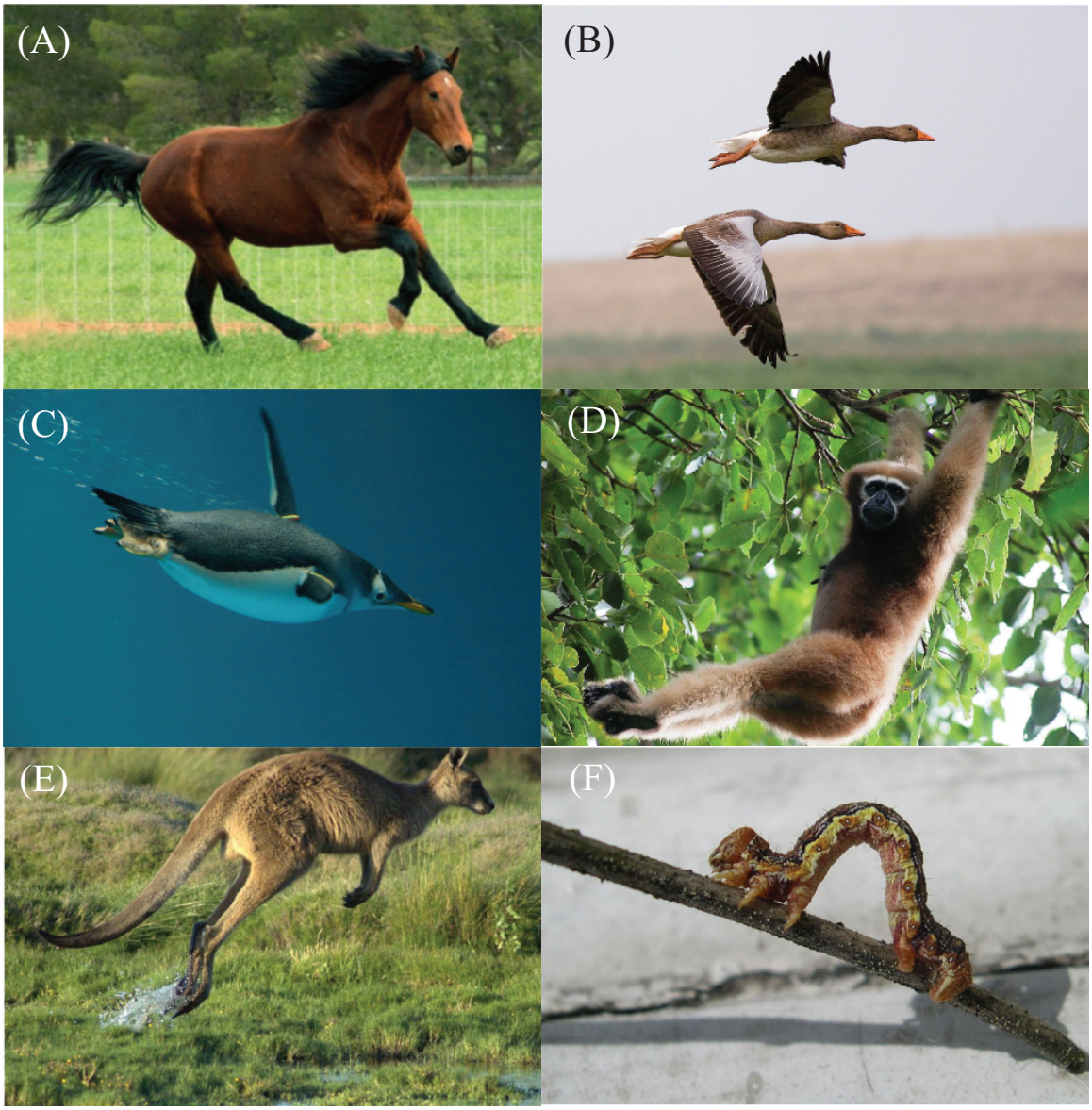

Figure 1: Animals' locomotion in various environments. (A) A horse running on land. (B) Two Greylag geese (*Anser anser*) flying in the sky. (C) A Gentoo Penguin swimming underwater. (D) A Forester (Eastern Grey Kangaroo) jumping on grassland. (E) A gibbon brachiating in the tree. Photos courtesy of Wikipedia.org

Studying how biological and robotic locomotors respond to such substrates can reveal key parameters that govern the locomotor performance, provide insights into the function of morphological features of animal feet and the effect of different gaits, and therefore facilitate robot appendage design and control strategy to improve robots' locomotion performance on these challenging terrains. Many studies have explored locomotor morphology and kinematics, granular (sand) physics, and robot controls on rough terrains. However, few studies have systematically investigated how different substrate responses affect locomotor performance, or how a locomotor could adjust its morphology/gait to successfully locomote on loose, flowable ground. Understanding the connection between locomotor performance and substrate response requires developing apparatus that can systematically control substrate properties (engineering), as well as understanding both morphological functions of locomotor appendages (biomechanics) and material responses of complex substrates (physics).

This dissertation combines engineering, physics and biomechanics to investigate the interaction between locomotors and complex substrates, and to develop general principles that govern the mechanism of locomotion on such terrains. We call this approach "locomotion robophysics" [3], an approach that searches for the underlying physics principles of moving systems (biological and robotic locomotors) and provides the fundamental understanding of their interactions with environments. In particular, we develop novel ground-control techniques that allow the extension of terradynamic (analogous to hydro and aerodynamics, which provide predictive power for aquatic and aerial vehicles) principles to arbitrary ground stiffness and heterogeneity distribution. Using these ground-control techniques, we systematically test legged robot and animal locomotion to explore the dependence of locomotor performance on leg morphology, kinematics, and ground properties. This study not only advances our understanding of ambulatory locomotion on complex granular substrates, but also

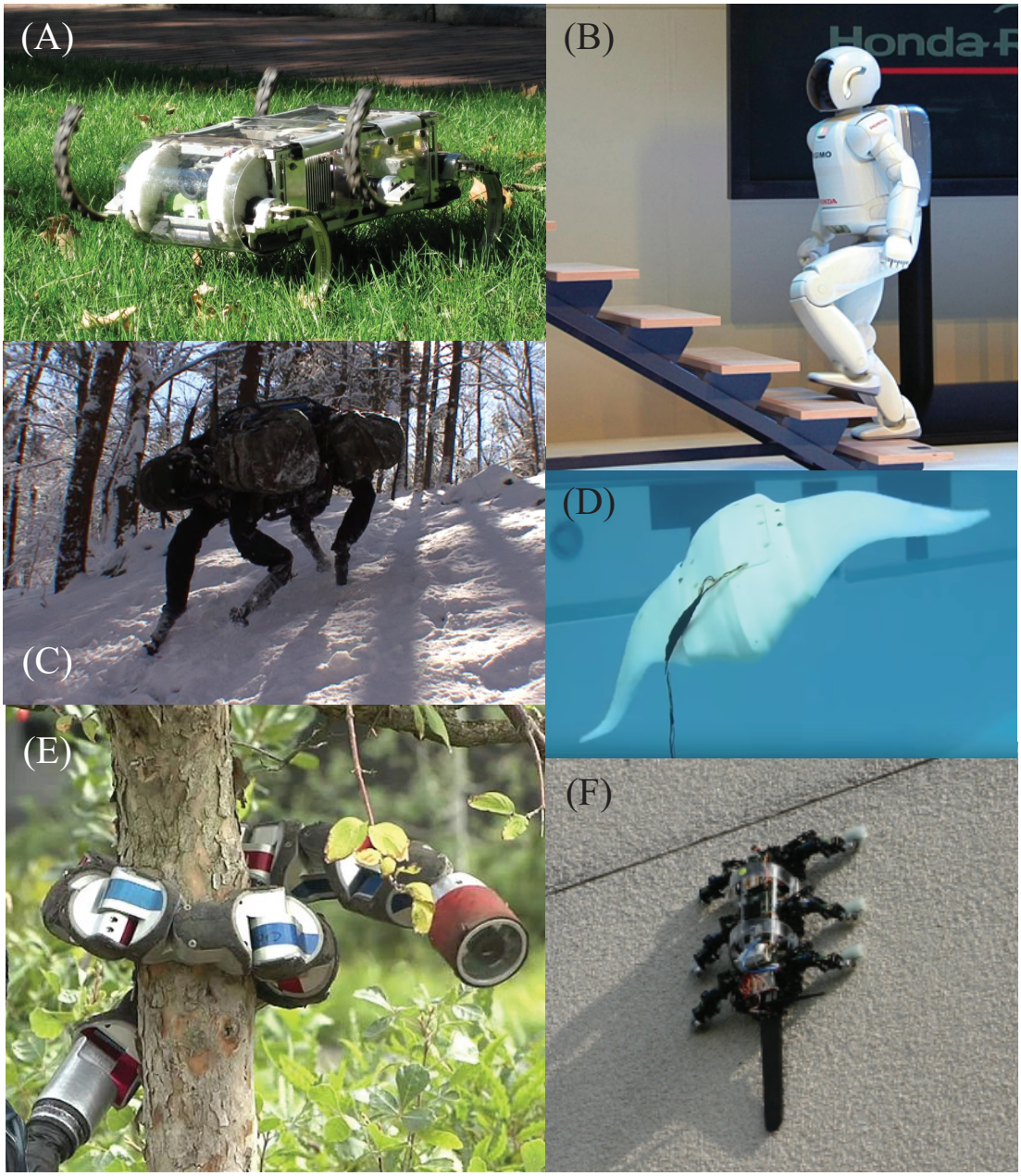

Figure 2: Robots' locomotion in various environments. (A) A cockroach-inspired hexapedal robot, RHex, running on grass. Photo courtesy of KodLab, University of Pennsylvania. (B) A humanoid robot, ASIMO, walking up stairs. Photo courtesy of HONDA. (C) A dog-inspired robot, Big Dog, walking on snow slope. Photo courtesy of Boston Dynamics. (D) A robotic ray swimming in a pool. Photo courtesy of BIER Lab, University of Virginia. (E) A snake-inspired robot, CMU SnakeBot, climbing up a tree. Photo courtesy of CMU Biorobotics Lab. (F) A gecko-inspired robot, RiSE, climbing a vertical wall. Photo courtesy of Boston Dynamics.

demonstrates the feasibility of using bio-inspired robots as simplified models to test biological hypotheses and to develop general terradynamic models. These models allow quantitative analyses of complex limb-ground interactions and aid in future design of legged robots by improving their mobility over a range of terradynamically challenging surfaces. In the following sections of this chapter, we review previous work and describe experimental techniques that provide the scientific and technical basis of this dissertation.

1.2 Robophysics – An Intersection of Engineering and Physics

Modern robots are expected to traverse a wide variety of land or even explore remote planets [125, 106]. Driven by engineering and computer science, many platforms have been developed to negotiate a large number of challenging ground conditions. As examples, Big Dog [103] (Figure 2C) can walk on slippery ice and uneven surfaces with high stability, and the CMU Snake robot [133] (Figure 2E) can perform a variety of bio-inspired gaits [74] to climb up poles, move inside pipes, and even swim in water. Many of these robots employ biological inspirations (e.g., morphological design, bio-inspired gaits, neural control pattern) to improve their mobility. These improvements normally relies heavily on sensor accuracy and careful control of foot trajectories/footholds [90], or limited to specific platforms. Development of general principles that allow high mobility requires a fundamental understanding of mechanisms behind optimal performance or failure.

Within the last few years, a new approach called "locomotion robophysics", complementing the traditional control and learning methods, has emerged to aid robot mobility. Robophysics is an approach that obtains a fundamental understanding of the general principles that explains complex systems and dynamics by studying these

Figure 3: Natural flowable ground such as (A) sand, (B) snow, (C) mud, and (D) leaf litter.

phenomena in simplified man-made devices. Similar to the discovery of thermodynamics through the improvements of steam engines [15] and the understanding of aerodynamics through the attempts of designing airplanes, many of these theories have been inspired from the progress of specific technological improvements but lead to fundamental knowledge that can be applied to more general phenomena in nature. Similarly, in locomotion robophysics, robots are used as simplified, controllable models of more complex animals or platforms that allow systematic study and development of basic principles that govern the mechanism of their locomotion and their interaction dynamics with the environments. These model robots allow for high controllability and comprehensive exploration of parameters, and help the identification of the key parameters in the locomotion of more complex systems (e.g., to uncover biological locomotor strategies and to reveal the mechanisms behind their optimal performance). As an example, inspired by the high performance of a sand-swimming lizard, *Scincus scincus* (Figure 4A), Maladen et al. used a seven-link robot, a minimal model that produced undulatory motion (Figure 4B, C), to systematically vary undulation parameters. They discovered that for a single period sinusoidal wave, forward swimming speed in sand could be maximized with a certain undulatory wave pattern (wave amplitude to wavelength, $A/\lambda \approx 0.2$) (Figure 4D), which explains how the sandfish lizards achieve high performance, and how robots can achieve such high performance with simple design and controls [79].

Unlike so-called biomimetic robots [54, 97] which usually attempt to replicate the appearance of an organism, robophysics type devices (e.g., the sandfish robot) are usually abstracted from specific features of appendage-induced locomotion (e.g., legs [71], flippers[84], tails [73, 53, 59, 60], and fins [23]), and they carry only minimal geometric/control resemblance necessary to produce dynamics similar to those of more complex locomotors (i.e., robots and animals) that they were derived from. However,

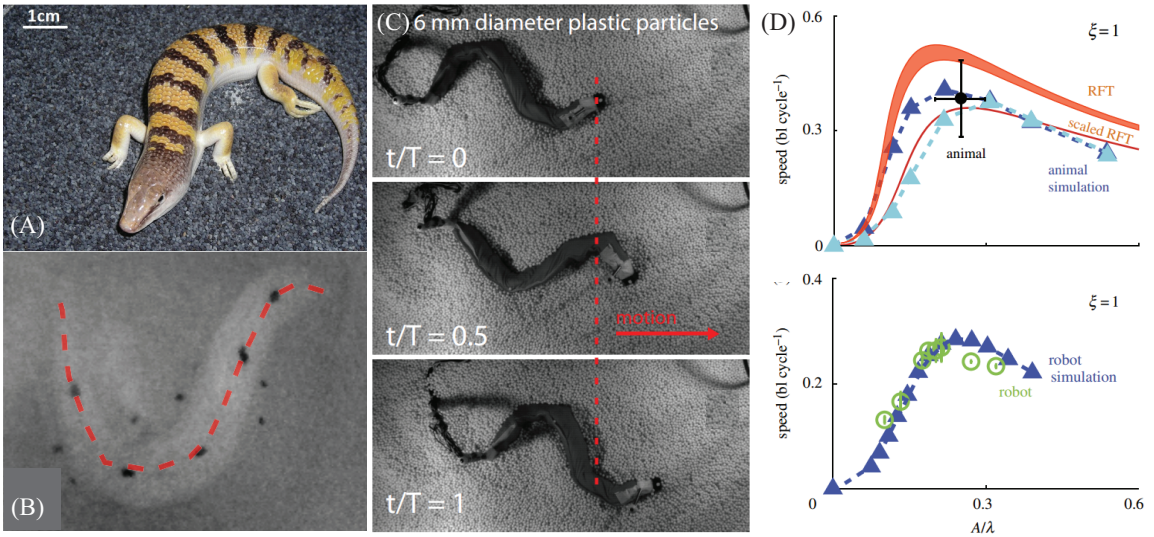

Figure 4: Sand-swimming animal and robot. (A) The sandfish Scincus scincus, a sand-swimming lizard that inhabits the Saharan desert, (B) Sandfish swimming subsurface where the X-ray image shows the body (light area) and opaque markers fixed to limbs and midline. Red dashed line indicates tracked midline. (C) Top view images of the sand-swimming robot tested on the surface of the 6 mm diameter plastic particles. (D) Robophysics experiments and simulation reveals that animal uses the kinematics that maximize swimming speed. Reproduced from [78] and [79].

the principles developed using these simplified models lead to a better understanding of the interaction dynamics and failure mechanisms, and aid in the control and design of more complex systems that have greater mobility in complex environments. For example, the CMU SnakeBot is extremely effective in a diversity of environments including hard ground, pipes, poles and water, but it had difficulties ascending sand inclines until robophysics experiments revealed that effective ascent of sandy slopes could be generated through a modulation of the snake-sand contact length, which reduced the stress on the sand below the granular material yield stress and kept the substrate remaining solid-like. By implementing this simple strategy, the snake robot was able to climb up sand inclines of more than 20 degrees [81], close to the angle of maximum slope stability.

The use of robophysics is especially important and useful for locomotion within

complex environments (e.g., sand, snow, grass), where direct modeling is extremely difficult and experimental methods are necessary for an understanding of the locomotor-environment interactions. For such situations, improvements in robot performance are almost impossible without understanding the interaction dynamics and failure mechanisms resulting from different substrate responses, and one needs simplified systems to generate and analyze such dynamics. This dissertation employs the robophysics approach to obtain such understanding in the following ways: the use of legged robots as physical models to study the effect of locomotor characteristics, and the development of terrain creation and control systems to systematically study the effect of terrain properties.

1.3 Legged robots – Model Locomotors

Blickhan and Full [13] found that legged locomotion in biological organisms (regardless of leg number) such as walking and running can generally be described as a spring-mass monopode (Figure 5), in which locomotors store and return energy gravitationally (walking) or elastically (running). During walking, the height of the center of mass (CoM) increases during the first half of the stance, and the kinetic energy transforms into gravitational potential energy. During the later half of the stance, the gravitational potential energy transforms back to kinetic energy and CoM height decreases. These kinematics can be modelled as an inverted pendulum. Similarly, running can be modelled as a spring loaded inverted pendulum (the SLIP model), in which elastic potential energy is stored and released during each step. This pendulous energy exchange saves energy during walking, while, during running, loading and unloading of elastic elements stores and returns energy, thus aiding speed and stability.

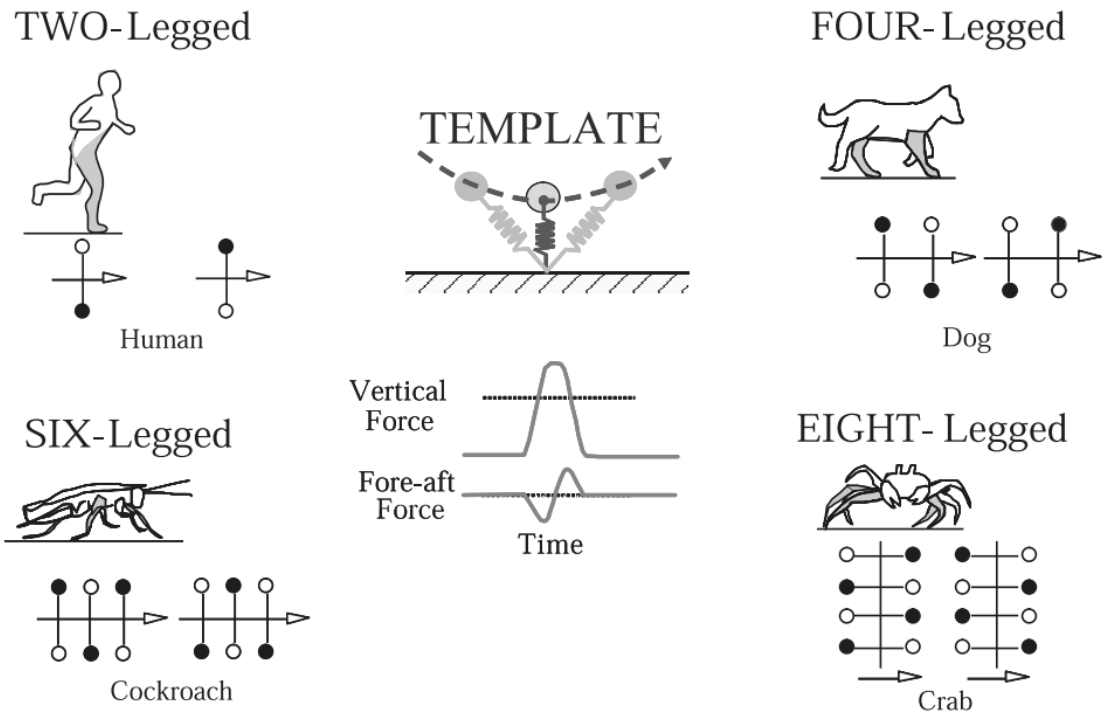

Figure 5: The Spring Loaded Inverted Pendulum (SLIP) model for multi-legged locomotion. COM dynamics for running animals with two to eight legs. Groups of legs act in concert so that the runner is an effective biped, and mass center falls to its lowest point at midstride. Stance legs are shown shaded, with qualitative vertical and fore-aft force patterns through a single stance phase at bottom center. The SLIP, which describes these dynamics, is shown in the center of the figure. Reproduced from [40].

Legged locomotion performance depends sensitively on locomotor characteristics such as appendage morphology and kinematics [45][44]. Many biological locomotors have developed morphologies and gaits that uniquely adapted to the environments of their habitats, and these features and functions often inspire innovative solutions in Engineering design and control of bio-inspired robotic devices. However, the morphological features in animals are often complicated and may not be optimized exclusively for locomotion purposes. Blindly mimicking the entire appearance of animals is not only impossible but also do not guarantee the generation of good performance. Improvement in effective bio-inspired design and control is almost impossible without the knowledge of the basic principles that governs the mechanism of locomotion.

Legged terrestrial devices have been used to uncover principles of contact physics between terrestrial locomotor foot and ground [21, 71], test hypothesis of biological locomotor strategies [6, 84], and conduct comparative study between robots and animals [110]. Such robots allow for high controllability and comprehensive exploration of parameters, such as foot size, joint angle, gait frequency [71, 36], body undulation amplitude [6], as well as novel mechanisms for robotic locomotion features such as anisotropic leg friction [65], steering and forward movement with a single actuator [134], scaled-impulse galloping [95], and various mechanisms that enhance climbing [87]. In this dissertation, we use legged robots as physical models to study how different locomotor characteristics (e.g., body mass, appendage size, stride frequency) affect locomotion performance on homogeneous and heterogeneous granular ground.

1.3.1 SandBot

SandBot is a 2.5 kg, bio-inspired hexapedal robot [105] (Figure 6A) derived from the RHex class robots [105] (Figure 2A). Inspired by the alternating gaits of insects, SandBot's six legs function as two alternating tripods. Legs in each tripod rotate synchronously with a half-cycle lag between the two tripods. This bio-inspired gait allows RHex robots to perform a bouncing monopode like locomotion [13] on hard ground, achieving dynamically stable running across a variety of landform (e.g., grassland, stairways) with simple design and controls.

SandBot's limb kinematics are precisely controlled. Each leg rotation is composed of a fast phase and a slow phase (Figure 6B). The angular extent and center position of the slow phase, the duty cycle of the slow phase (i.e. fraction of the period spent in the slow phase), and the cycle-average stride frequencies, can be set and varied for each test. In a previous study [71], Li et al. investigated a c-legged SandBot on packed granular media, and discovered that its locomotion performance depended sensitively on granular packing state, robot leg frequencies, and intra-cycle gait parameters. Li. et al found that the locomotor performance of the SandBot could be optimized for different packing states by adjusting these parameters. For loosely packed sand, SandBot gait parameters should be fined tuned to a Soft Ground Kinematics (SGK) to produce effective locomotion [70].

In this dissertation, we used a cylindrical-leg SandBot as our physical model, to further investigate the effect of foot size and gait frequency for locomotion on low-stiffness Granular media. The simpler leg geometry facilitated foot size characterization and theoretical modeling of the leg-ground interaction, while the larger foot area (as compared to the previous c-leg) enabled the robot to move effectively over an

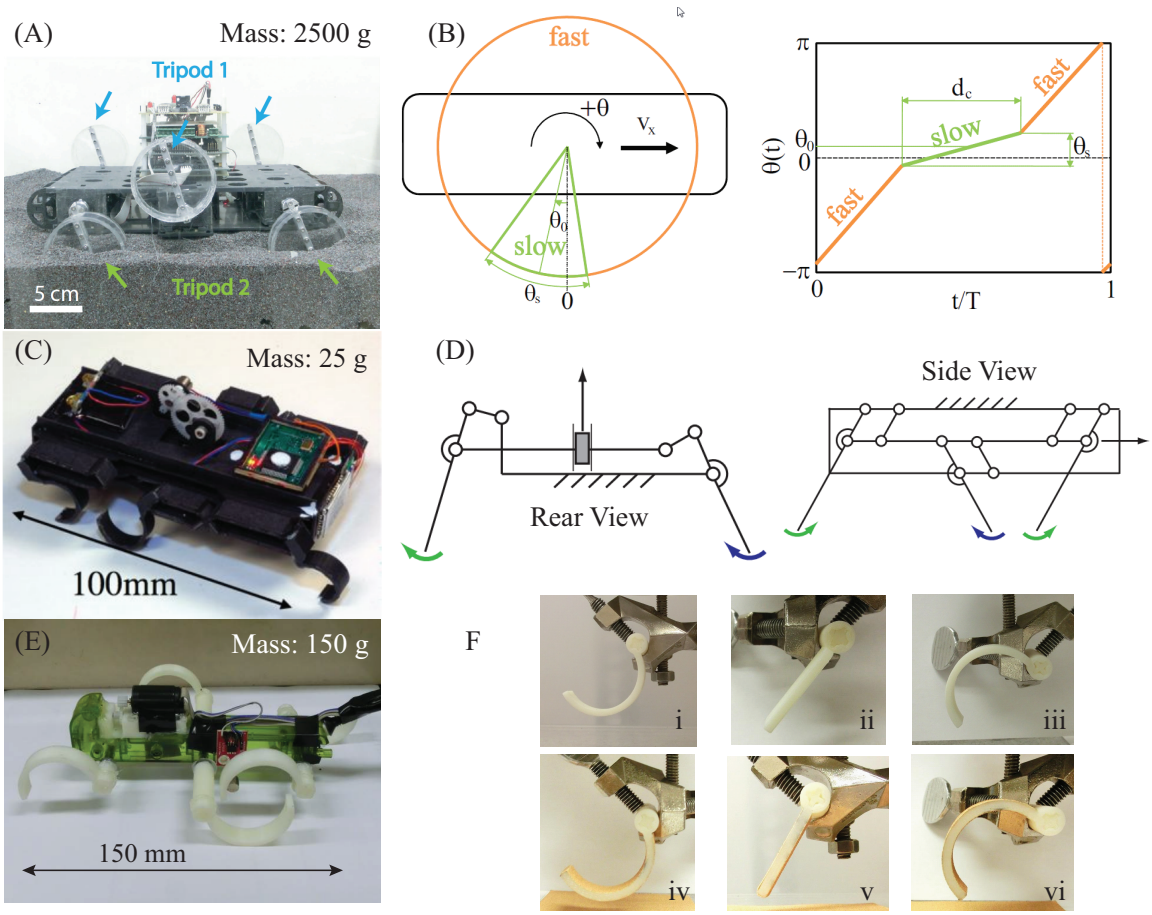

Figure 6: Legged robots as model locomotors. (A) SandBot. (B) SandBot intr-cycle limb kinematics. (C) DynaRoACH. (D) Body structure enabled leg kinematics of the DynaRoACH robot from rear view and side view. (E) Xplorer. (F) Switchable leg shapes and leg roughness for Xplorer robot: i)Low-frictional C leg with positive curvature. ii)Low-frictional flat leg. iii)Low-frictional C leg with negative curvature. iv)High-frictional C leg with positive curvature. v)High-frictional flat leg. vi)High-frictional C leg with negative curvature.

extended range of ground conditions, making it possible to compare the robot performance on such extreme terrains with sand-expert organisms (fast-running lizards and crabs), allowing for models developed using the robot to be generalized to biological locomotors with more complicated morphologies and gaits.

1.3.2 DynaRoACH

The DynaRoACH robot[1] (Figure 6C) is a small, lightweight (10 cm, 25 g), bio-inspired hexapedal robot [41]. Similar to the RHex robot, it has six c-shaped legs (radius 1 cm) and uses an alternating tripod gait. In DynaRoACH, all six legs are driven by a single motor through body linkages. The motor is controlled by a centralized controller mounted close to the center of mass (CoM) of the robot. During a cycle, each leg rotates backward about the hip (retraction), lifts-up sideways, and swings forward (protraction) (Figure 6D). Control parameters such as stride frequency, running time, and PID control gains are set on a PC and communicated to the controller through a Bluetooth wireless interface.

While possessing a similar gait to the SandBot, DynaRoACH is 100 times lighter than SandBot. Manufactured using Smart Composite Manufacturing (SCM) technique [12], the DynaRoACH robot's bodyweight is only 25 grams, about one magnitude lighter as compared to other small legged robot of the same size such as iSprawl [56] and Mini-Whegs [88], and comparable to lizards and crabs (among other myriad desert vertebrates and invertebrates [89], [17]) that can achieve rapid running on flowable ground. Therefore, DynaRoACH provides a promising physical model to study how effective legged locomotion can be achieved on granular substrates in small, high-performing animals (Chapter *III*).

[1] in collaboration with R. Fearing's group at University of California, Berkeley.

1.3.3 Xplorer

The Xplorer robot (Figure 6E) is a 15 cm, 150 g hexapedal robot, which we modified from a SmartLabs Xplorer toy by stripping down the case, replacing the motor and installing 3D-printed legs. The Xplorer used in this dissertation has six C-shaped legs and uses an alternating tripod gait. The gait frequency of the robot is controlled by a DC motor (Micromo 1724-SR with IE2-1024 encoder) using pulse width modulation (PWM). A Hall effect sensor is attached to the robot body to control the initial leg phase and to track leg tip positions during the run. Controlled under open-loop, the Xplorer robot provides the simplest model to study the mechanics dominated interaction with heterogeneous GM.

Xplorer's leg shape, size, and roughness can be easily varied (Figure 6F) to test the effect of different appendage properties on robot interaction dynamics with homogeneous and heterogeneous GM. In addition, since the Xplorer robot is lightweight and rigid, it can be picked up by a robotic gripper installed in our automated locomotion testing system [99], allowing for a large amount of data collection for various terrain configurations. In this dissertation, we use Xplorer as a physical model to test robot locomotion and interaction with heterogeneous GM (Chapters $IV \sim VI$). In Chapter VI, this robot was also equipped with a GM-jamming tail to test anticipatory trajectory control in negotiation with ground heterogeneities.

1.4 Granular Media – Model Substrates

The environments of the natural world contain materials of incredible complexity. If future robots are to effectively maneuver across terrains such as disaster sites, forests,

and extraterrestrial planets, we must understand the mechanisms of effective movement in such terrains, and this will only be possible through the parametrization and systematic creation of such complex substrates. In this dissertation we are particularly interested in flowable ground such as sand, gravel, snow, and leaf litter. These terrains exist widely in natural environments (e.g., deserts, beaches, Martian terrains) that animals and robots have to traverse. When moving on such terrains, the limb of the animal or the tread/wheel of a robot could fluidize the small particles, causing large slippage to the locomotor and resulting in significant performance loss. One challenge in performing systematic locomotion studies on such substrates is due to the astonishing diversity of the forms of such terrains in nature. Natural flowable terrains vary in constitution, cohesiveness, particle size, angularity, compaction, and so on, making it nearly impossible to perform exhaustive locomotion testings. Granular media (GM) such as glass beads and poppy seeds (Figure 7), while exhibiting a wide variety of similar behaviors in response to external forcing [72], have more regular shapes than natural sand and can be modelled as an ensemble of individual particles that interacts through repulsive, dissipative forces. These features allows for precise experimental controllability of substrate properties, and provides relative simple model to compute the interactions numerically. Therefore, granular media makes a simple, representative, and controllable model for natural flowable terrains. The results obtained using granular media can be generally applied to natural sand with greater polydispersity and angularity of grains [72].

1.4.1 Granular forces

Granular media are defined as a collection of discrete, rigid particles, typically with particle size larger than 100 μm [5]. At the grain level, forces between a pair of granular particles are normally described by normal forces and tangential forces [46]. The

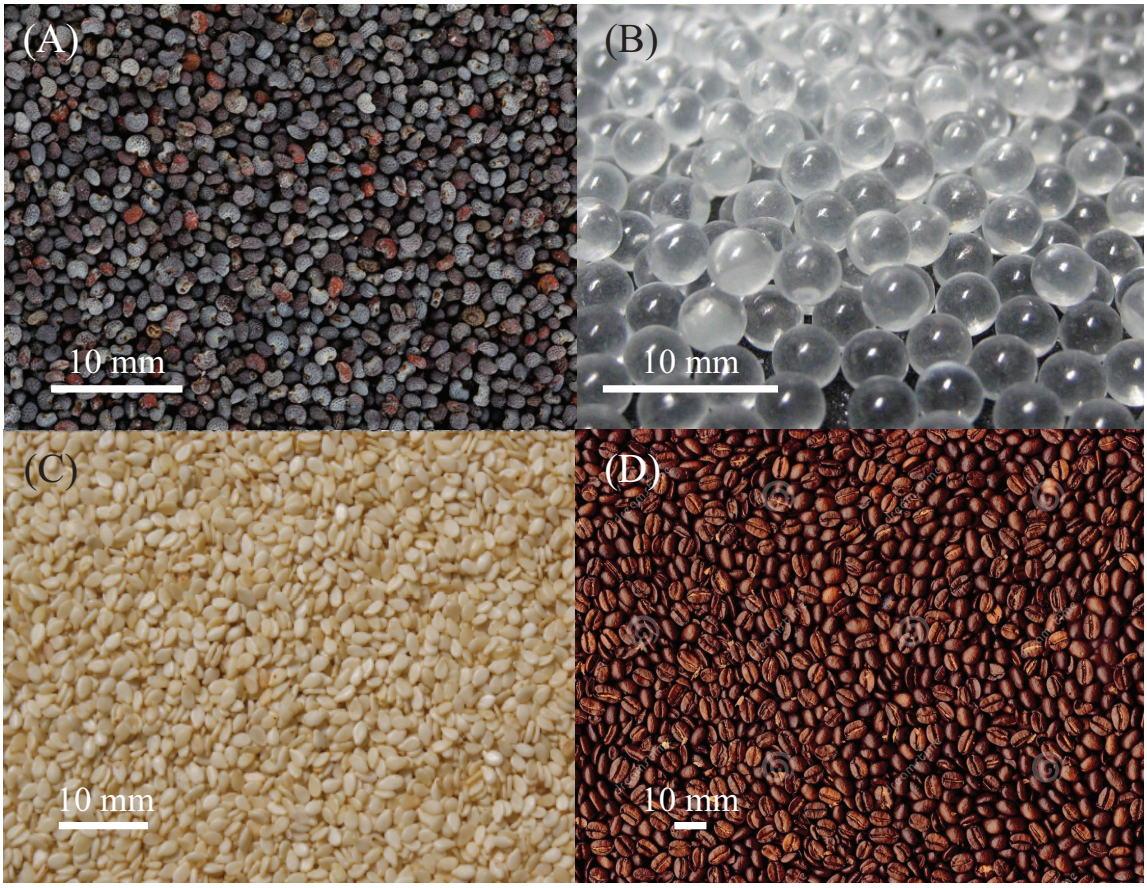

Figure 7: Granular media such as (A) poppy seeds, (B) glass beads, (C) sesame seeds, and (D) coffee beans.

normal force results from the elastic deformation of the bodies in contact, whereas the tangential force is due to the friction between the contacting surfaces. Individual grains interact with each other through this dissipative, repulsive contact forces [49], and forces in granular media were carried by a small fraction of grains along spatially inhomogeneous force chains [76], resulting in a complex dynamics in the bulk assembly.

Without external disturbances, the bulk granular material by default remains in a solid-like state. To break the solid-like state of a granular medium, the penetration force per unit area needs to exceed a critical stress (i.e., the yield stress) of the medium. Once the yield stress is exceeded, the grains begin moving and rearranging in front of the intruder, while exerting a resistive force on the intruder. For slow intrusion or drag, the force acting on the intruder is independent of the intrusion speed [4, 38]. Albert et al. studied the horizontal drag force acting on a cylinder slowly moving horizontally through granular media, and found that this velocity independence is limited to the regime of velocities smaller than the velocity of the grains rearranging in front of the cylinder ($\sqrt{2gd_g}$, where d_g is the grain diameter). Within this range, the horizontal drag force increases linearly with the cylinder diameter, quadratically with the depth of insertion, and is insensitive to intrusion velocity [4]. Similarly, for vertical penetration at low speed, the penetration force is also independent of speed, and linearly dependent on the depth of intrusion, projected area of the intruder, and the penetration resistance of the media, as long as the intruder is far enough from the bottom of the container to trigger the boundary effect [117]. Both vertical and horizontal granular forces do not have a systematic dependence upon the grain diameter [4][116], given that the grain diameter much smaller than the dimension of the penetrating object.

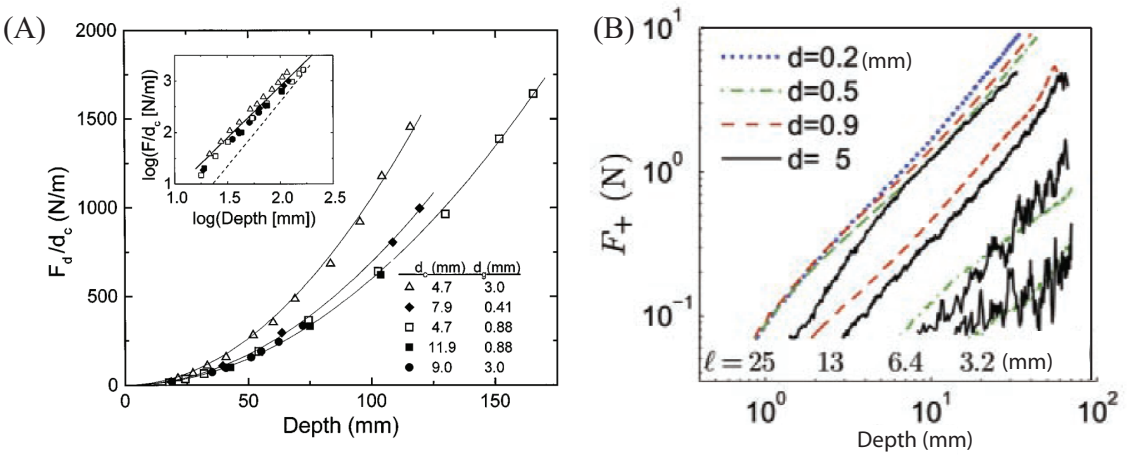

Figure 8: Granular force during low speed drag and intrusion. (A) The depth (H) dependence of the drag force F_d. The data were all taken at $v = 1.5mm/sec$ with various grain diameters (d_g) and cylinder diameters (d_c), and the drag force was normalized to the cylinder size. The solid lines are parameter fit of the form $F_d/d_c = \eta g \rho H^2$. Reproduced from [4]. (B) The depth (z) dependence of the vertical plunging forces $F+$ of a spherical intruder. The data were taken in beds of monodisperse glass beads with particle diameter d and with various spherical intruders diameters l. Reproduced from [38].

At higher intrusion speed, the inertia of the grains is no longer negligible and the intrusion force becomes velocity dependent. Previous studies [128, 55, 30] discovered that forces acting on a high speed penetration or drag object can be decomposed into the sum of a depth-dependent frictional component plus a velocity dependent inertial component, where the inertial component depends quadratically on the intrusion speed. In 2003, Wassgren et al. [128] and Chehata et al [16] investigated the drag force exerted on stationary objects in steady granular flows for both dilute and dense flows. In 2010, Katehara et al. [119] directly examined the high speed drag force exerted on a disk obstacle moving in the granular media at different constant speeds, and found that the drag force was proportional to the square of the drag velocity. Same phenomena was also observed in impact studies. Katsuragi et al. [55] and Goldman et al [30] measured the impact force exerted on large projectiles as they penetrate into dry granular media. Both studies suggested that hydrodynamic forces scaling

like v^2 dominate in the high velocity/shallow penetration regime. In [30] it was also found that at deeper penetration and decreasing velocity, frictional/hydrostatic forces dominates and the force and acceleration no longer vary as v^2 but instead linear in velocity with a non-zero offset at $v = 0$.

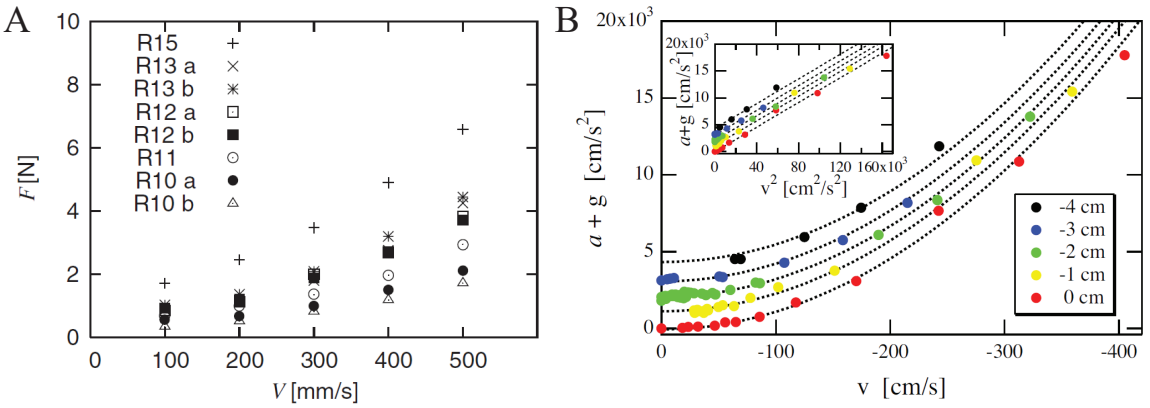

Figure 9: Granular force during high speed drag and intrusion. (A) Plots of the average drag force as a function of moving velocity for different radii of the obstacle (R = 10, 11, 12, 13 and 15 mm) where each data point is obtained from ten-drag experiments. Reproduced from [119]. (B) Net acceleration $a+g$ vs velocity, at various fixed depths. The inset shows the same plot but vs v^2, in order to demonstrate the quadratic dependence on speed. Reproduced from [55].

1.4.2 Solid-fluid transition

Forced granular media can exhibit solid-like or fluid-like (Figure 10) behavior when respond to external perturbations, depending on whether the external forcing exceeds the critical yield stress [91]. If the external forcing per unit area is below the critical yield stress, GM remained solid and drag/penetration stops. Otherwise if the external forcing per unit area exceeded the yield stress, GM started to flow like a fluid with grains keep rearranging in front of the intruder. This unique property presents great challenges for terrestrial locomotors, similar to many natural flowable ground, and makes interaction with granular media fundamentally different from interaction with either fluids or solids. When intruders (such as a robot wheel or animal leg) contact

with granular media, the substrate deforms and the force can dissipate into the substrate, which is different from interaction with elastic solids. However, the granular fluids also differs from viscous fluids because the forces exerted on the intruder are typically independent of drag/intrusion velocity at low impact speed. For different granular substrates, the yield stress depends on parameters including packing state, cohesiveness, particle size, and heterogeneity.

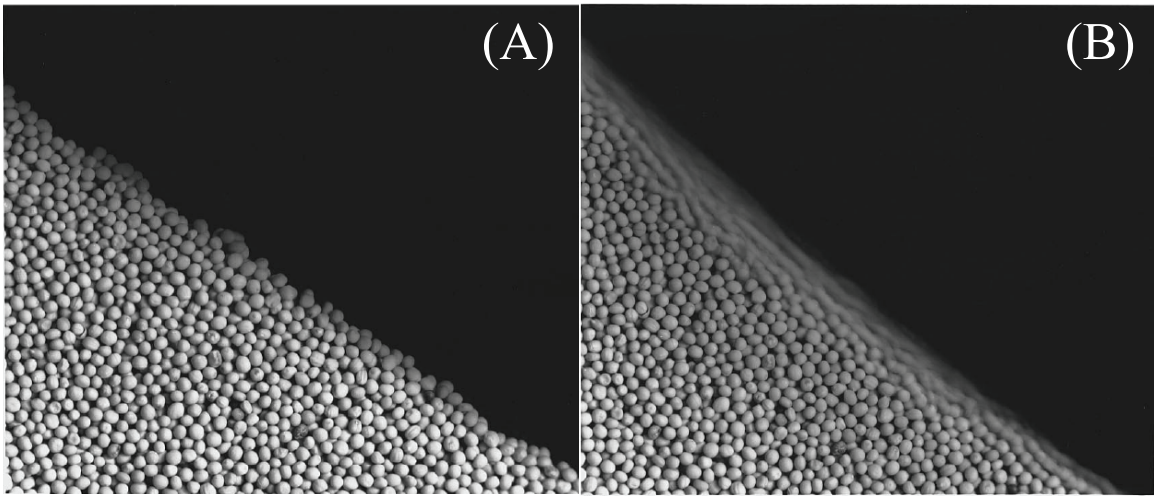

Figure 10: Solid and fluid behaviors of granular media. (A) A pile of mustard seeds that is tilted to an angle lower than the angle of repose. (B) The same pile after the slope has been increased slightly to create an avalanche. The flow occurs only along the surface and that the seeds deeper within the pile remain stationary. Reproduced from [49].

1.4.3 Volume fraction

The packing state of GM can be characterized using the volume fraction ϕ, the ratio of solid grain volume to the occupied volume. Volume fraction varies as a result of particle arrangement. For tightly packed granular media, the volume fraction is larger, whereas for loosely packed granular media, the volume fraction is smaller. For homogeneous (i.e., mono-size) granular media, the volume fraction usually varies between the range of $\phi \approx 0.57$ to $\phi \approx 0.64$ [26], although this range is influenced by

particle coefficient of friction [51].

Different packing states affects when the solid-fluid transition in GM (e.g., yield stress, slope stability) occurs under external perturbations (e.g., intrusion, drag, tilt). Generally, granular media in a more tightly packed state exhibit higher stability (i.e., more solid-like). Previous studies have shown that both the penetration resistance (an indication of the granular medium stiffness) [71] and the initial angle of avalanche (an indication of granular slope stability) [33] increase with the packing fraction ϕÀs a result, terrestrial locomotor performance depends sensitively on the volume fraction of the medium [71].

Experiments have also shown that loosely and tightly packed granular media respond differently to shear. A loosely packed granular medium compacts under shear, whereas a tightly packed granular media dealates [108, 33]. Through bed height measurements and force measurements, Schroter et al. [111] and Gravish et al. [34] previously found that the phase transition occurs at a volume fraction of $\phi = 0.6$ (the critical packing state [108]). The dependence of penetration force on volume fraction [111], the rate of change in bed height [111], the compaction-dilation response [34], and the mean granular displacement during avalanching [33], all exhibited significantly different behavior for loosely ($\phi < 0.6$) and tightly packed ($\phi > 0.6$) granular media (Figure 11).

For size-heterogeneous granular media, the packing configuration depends on the particle size ratio, concentration, and so on. Two extreme cases of packing configuration for a mixture of bidisperse spherical granular grains are shown in Figure 12A. The first situation has a large concentration of large particles, and all the small particles fit inside the gap of large particles. In the second situation the concentration of

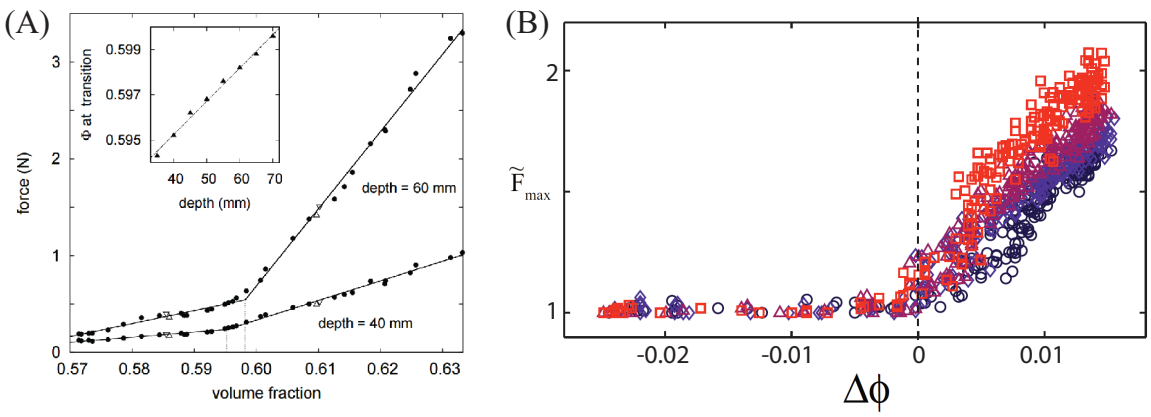

Figure 11: Phase transition at the critical packing state. (A) The dependence of the penetration force on volume fraction at depth of 40 mm and 60 mm. The inset displays the dependence of the transition point on the penetration depth. Reproduced from [111]. (B) Peak force developed over 1 cm displacement normalized by force at x = 1 cm vs. initial volume fraction ϕ (2 cm/s circles, 4 cm/s diamonds, 6 cm/s triangles, 8 cm/s squares). Reproduced from [33].

large particle is low, and the few large grains lies in a bath of small grains [19]. And the volume fraction of this bidisperse packing can be characterized as a function of the mass concentration of the large particles for different diameter ratios (Figure 12B).

1.4.4 Preparation and Control

For homogeneous granular substrate, ground stiffness (i.e., the penetration resistance) significantly affects locomotion performance. Traditionally, researchers use single-wheel testbeds filled with granular material such as Mojave Martian Simulant [112], quartz sand, and Ottawa sand [86] for robotic vehicle motion testing on homogeneous granular ground (Figure 13). These studies measure ground properties and analyze wheel-ground interaction, but few of them systematically control and vary ground stiffness. In nature, ground stiffness varies widely among terrestrial environments. To systematically vary ground penetration resistance to emulate various ground stiffness in nature, a previous study [71] used air pulses to control packing states of granular media in a fluidized bed.

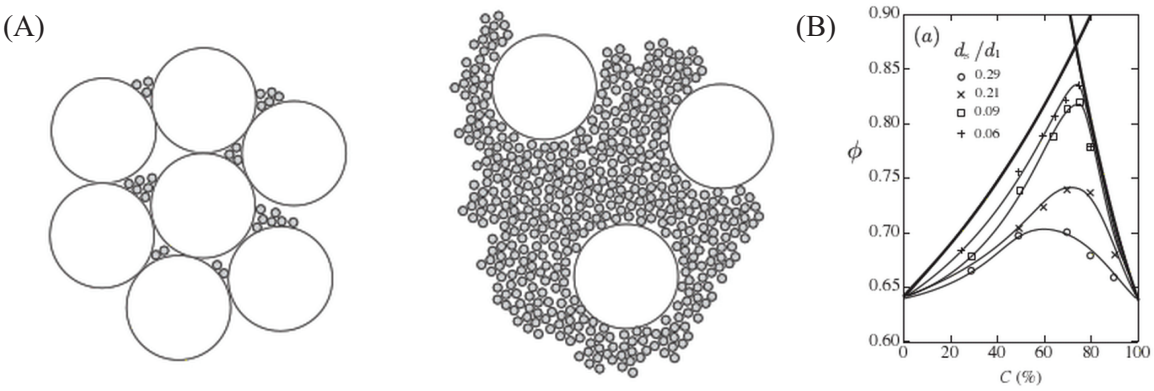

Figure 12: Packing configuration and volume fraction for size-heterogeneous granular media. (A) Two extreme cases of bidisperse packing. Reproduced from [5]. (B) The volume fraction of bidispersed packings as a function of the mass concentration of large particles. Different curves indicates different particle diameter ratios. Reproduced from [19].

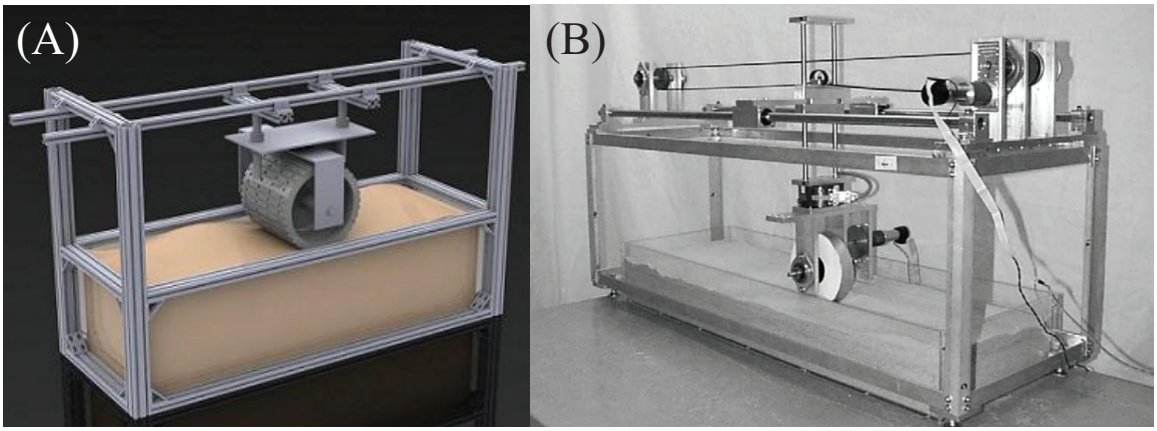

Figure 13: (A) CAD design of a single-wheel testbed. (B) Terrain characterization testbed photo reproduced from [113].

A typical fluidized bed consists of a granular bed, several air inlets, and a flow distributer layer [47] (Figure 14). A gas from the bottom of the granular bed flows upward through the distributer, evenly fluidizes the granular media in the bed, eliminates any previous perturbation history and leaves the granular media in a loosely

packed state when the air is gently removed. Previous investigation of particle dynamics during fluidization shows that, when the air flow initially increased from 0, the normal forces between the granular particles were reduced, but the air pressure drop through the grains was smaller than the weight of the bed and thus the grains remained immobile. As the air flow increased, the pressure drop increased. When the pressure drop reached the weight of the granular bed, the bed height began to increase and the granular material inside started to exhibit fluid-like properties [121]. The flow rate at this transition onset was defined as the onset of fluidization. During de-fluidization, granular particles such as poppy seeds [27] exhibited a hysteresis behavior – the height of the granular media was greater than during fluidization (increasing air speed) at the same air speed.

By increasing the flow rate to the fluidization transition and then decreasing it to zero, a loosely packed state (volume fraction $\sim 0.590 \pm 0.004$) can be achieved for homogeneous GM, independent of particle size and container shape [93]. To achieve higher ground stiffness than loosely packed state, shaking and vibration are often used. Using pulses of fluidization, granular materials like poppy seeds and glass beads can be packed into a dense state with volume fraction of ~ 0.63 [34, 111, 71]. Few studies have investigated locomotion on GM of lower stiffness than loosely packed state. In nature, terrains such as snow or leaf litter can exhibit much lower penetration resistances than loosely packed sand. For example, natural snowpack has a minimum penetration resistance per unit area of only 0.17 N/cm^3 [107]. New ground control techniques are needed to obtain such low stiffness to prepare robots for these terradynamically challenging surfaces.

For heterogeneous granular media, the ground property can no longer simply controlled by air pulses or shaking because mixing and segregation occurs under shear

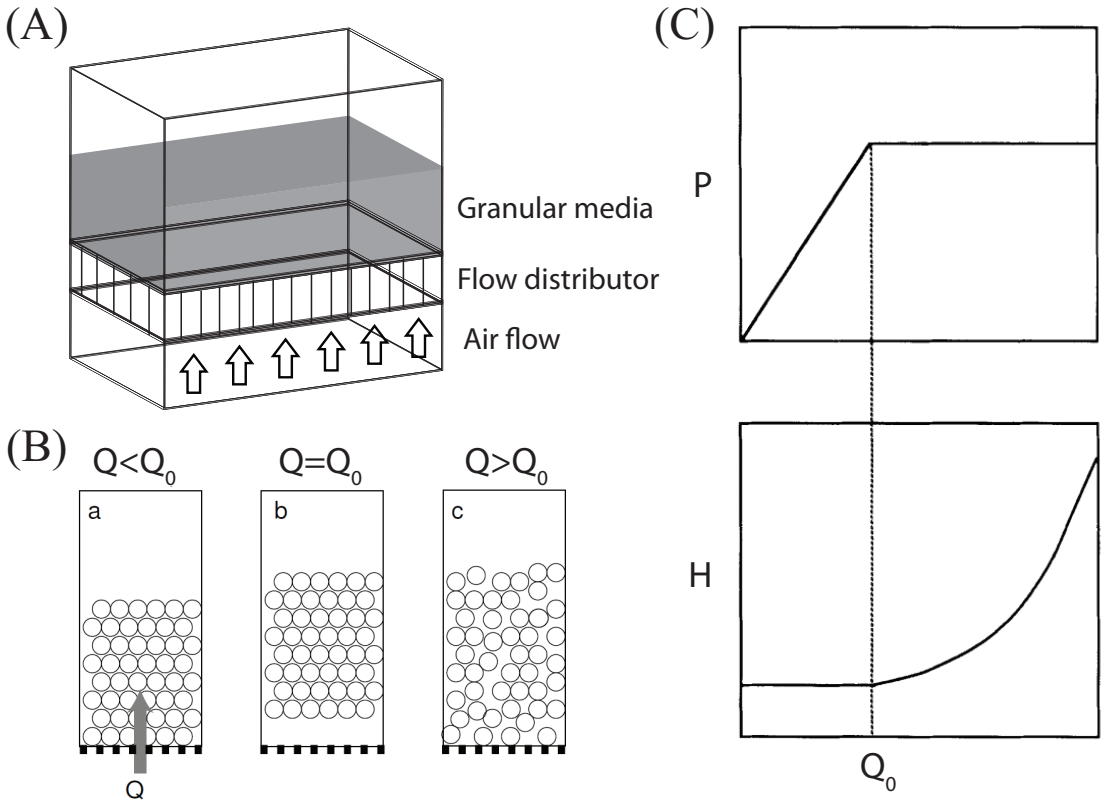

Figure 14: Fluidized bed. (A) Diagram of fluidized bed. (B) A schematic illustrating the behavior of grains as the flow rate, Q, is increased through fluidization (C) Dependence of pressure drop and bed height on flow rate for ideal fluidization. Reproduced from [121].

– large particles typically rise to the top and small particles descend to the bottom. While there exist investigations on segregation rate [31], dilation and compression behavior during the transition [83], techniques to systematically prepare heterogeneous granular state at comparable level of homogeneous GM do not yet exist.

1.5 Legged Locomotion on Granular Media – Challenges and Previous Efforts

Locomotion can occur in various environments, and locomotor performance depends sensitively on environment characteristics [135]. Investigating locomotion problem requires understanding of both the locomotor characteristics (e.g., morphology, gait) and the environmental effects, and more importantly, the interaction between the two. For terrestrial locomotors, substrate properties and responses presents great influence on locomotor performance and strategy [122]. On hard ground, legs can store and return energy gravitationally (walking) or elastically (running). Pendulous energy exchange can save energy during walking, while, during running, loading and unloading of elastic elements can store and return energy, thus aiding speed and stability. The situation is quite different during walking and running on deformable ground. When the ground becomes deformable and dissipative, energy [62] can be transferred to the ground and this can affect locomotor style and performance, making locomotion on granular substrates challenging. Previous studies on human locomotors suggested that humans use 60% more energy running on deformable and dissipative substrates (e.g., sand) compared to rigid ground due to an increase in the work done on the ground and a decrease in muscle-tendon efficiency [66]. Pandolf et al. investigated the metabolic energy expenditure for human walking on snow, and found that energy expenditure increased linearly with increasing depth of footprint depression [94]. Furthermore, due to the solid/fluid transition property of the substrate material [49],

yielding and re-solidification can occur unpredictably and multiple times during foot/-leg penetration [30], dynamically changing the terrain profile and substrate response, and equations of motions for such complex interactions are not yet known.

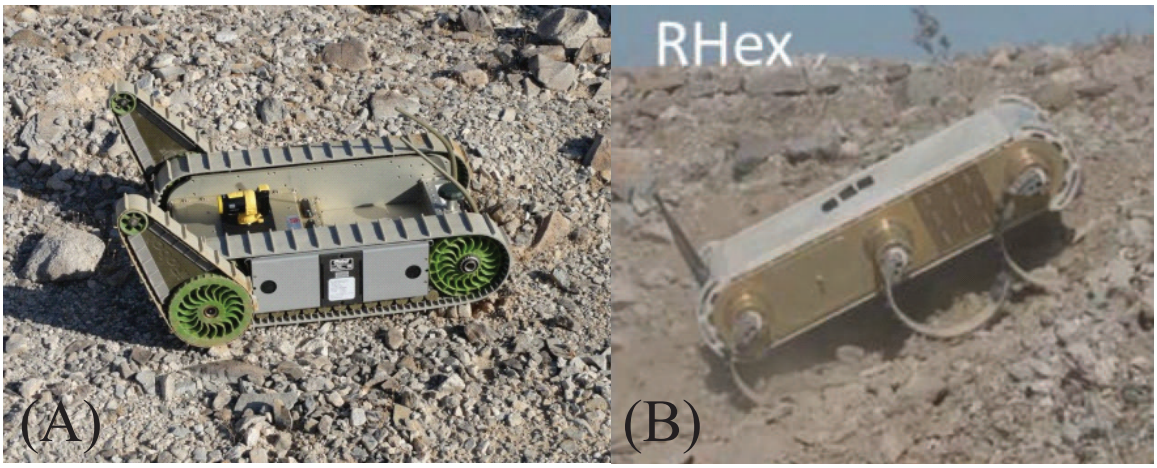

Figure 15: Challenges in locomotion on heterogeneous granular terrains (A)PackBot moving on Mojave Desert. (B) RHex traveling across heterogeneous gravel substrate (photo courtesy Alfred Rizzi, Boston Dynamics).

The situation can become more challenging when heterogeneities are present. Substrates that are rocky and loose that found in environments can be size/shape heterogeneous and often contain GM with particle sizes spanning multiple orders of magnitude. When small robotic locomotors such as PackBot or RHex travel across these flowable types of terrain (Figure 15), they exhibit characteristic failure modes (slips, unstable foot-holds, impassable barriers, or a limb/tread fluidization of a thin layer of smaller particles), which significantly affect robot stability, trafficability and power consumption. Approaches to systematic creation of heterogeneous multi-component terrain for systematic locomotion study do not yet exist.

Two of the major challenges in studying locomotion on flowable substrates are the lack of analytical models at the level of the Navier-Stokes equations for locomotion in air and water [124], and the lack of experimental control and measurement

techniques like the wind tunnel for aerodynamic studies or the force platforms [10] for hard ground. Over the past few decades, researchers have made extensive efforts to address both deficits.

1.5.1 Terramechanics

Since the 1950s, terramechanics approaches have been used to understand the interactions between robot/vehicle wheels and the deformable ground. In [7] and [130], Bekker and Wong systematically analyzed the normal load distribution of a vehicle wheel/track and the soil/snow mechanics and deformation under such load. Using the pressure-sinkage relations (Figure 16), shear stress and vehicle performance can be accurately predicted for large wheeled and tracked vehicles. However, for smaller scale vehicles (wheel diameter smaller than 50 cm), the prediction accuracy decreased significantly due to the sharp curvature of the loading area, which was not considered in the Bekker flat-plate pressure-sinkage model assumptions [86]. Therefore, the classical terramechanics is not sufficient to accurately describe leg-ground interactions for small scale locomotors, especially for locomotor appendages of complex geometry like robot/animal legs.

1.5.2 Rotary walking

In 2009, Li et al. systematically studied the locomotion of a C-legged RHex robot, a legged device that was tuned to run on hard ground [105], and discovered that ground reaction forces and robot dynamics on granular media depended sensitively on actuation parameters such as leg frequency [71] and intra-cycle leg kinematics (relative phasing between fast and slow leg rotations) [70]. Li et al. found that a small change in ground volume fraction ($\triangle\phi < 1\%$) could result in either rapid motion or failure to move, and that the robot kinematics at low leg frequency could be described

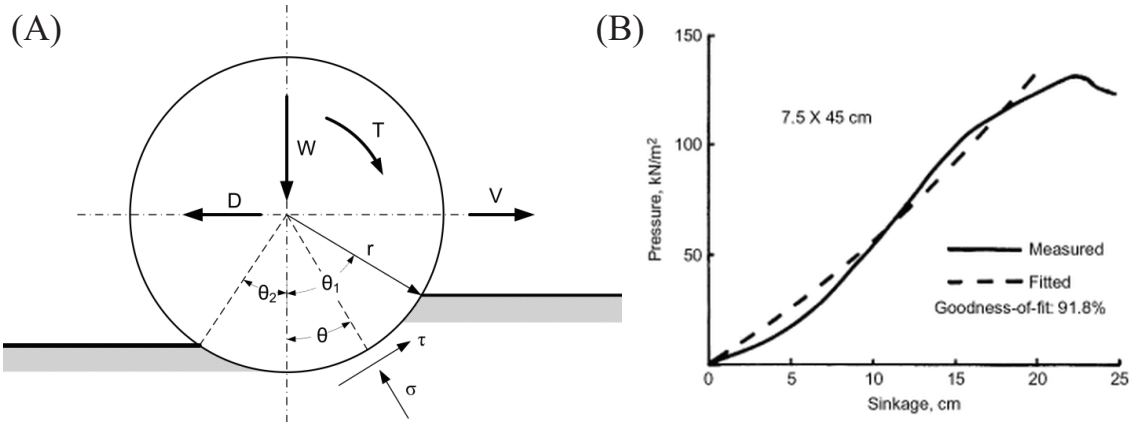

Figure 16: Terramechanics model. (A) Wheel-soil contact model diagram for a rigid wheel. Reproduced from [131] (B) Flat plate pressure-sinkage relationship. Reproduced from [130].

using a Rotary Walking model [71] (RW model). According to this model, the legs penetrated a yielding substrate until the increasing granular reaction forces balanced robot weight and body inertia, at which point the substrate solidified and the legs stopped penetrating and began rotating to propel the body forward. This solidification strategy enabled the SandBot to walk effectively at up to 1 body length/s on granular media at low to intermediate stride frequencies. At high stride frequencies, however, the robot legs kept encountering previously disturbed ground, the granular material around the legs became continuously fluidized, and the robot "swam" forward slowly ($\sim$ 0.01 body length/s) using drag on the legs to overcome belly drag. The rotary walking model reveals how sensitive the robot's locomotion performance is to the granular state, and provides accurate prediction of the robot step length and forward speed. However, the prediction power of the rotary walking model was limited to the specific platform studied in [71], and the applicability for robots and animals with more complex morphologies and gaits was unclear.

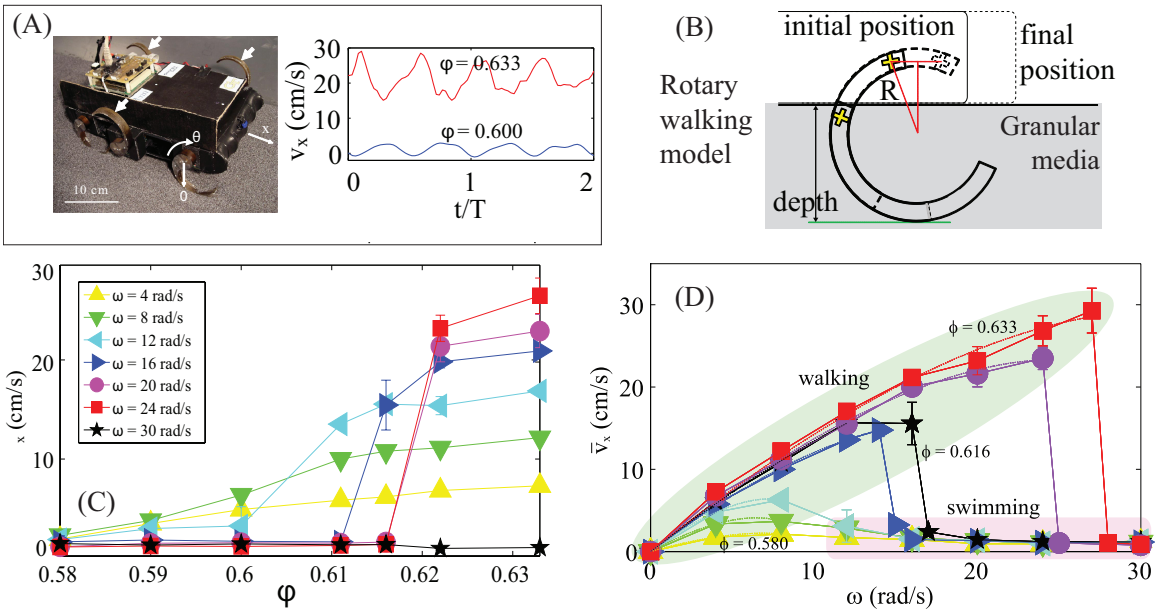

Figure 17: Rotary walking model. (A) The c-legged RHex-class robot, SandBot, and its speed on two granular substrates with various volume fraction ϕ. (B) Diagram of the Rotary Walking model. (C)Average robot speed vs. volume fraction ϕ. (D) Average robot speed vs. limb frequency ω. The solid lines and symbols are experimental measurements for $\phi = 0.580, 0.590, 0.600, 0.611, 0.616, 0.622$, and 0.633. The dashed lines are fits from the Rotary Walking model.

1.5.3 Discrete Element Methods

To further advance understandings of homogeneous granular media responses to locomotor intrusion, Maladen et al. coupled a multi-particle discrete element method (DEM) [104] simulation with a multi-body simulator software package Working Model 2D, to investigate the interaction between a sand-swimming lizard, the sandfish *Scincus scincus*, with a 3 mm model granular medium. The discrete element method (DEM) models the force and flow in granular media by computing the normal and tangential forces between each interacting pair of particles (Figure 18A). The normal contact force is typically given by a Hertzian repulsion and a velocity dependent dissipation, whereas the tangential contact force is modeled as Coulomb friction. Force parameters such as friction and dissipation coefficient can be empirically tuned by

matching the simulated forces on intruders moving in a granular medium to experimental measurements [78, 22] (Figure 18B). Once the parameters are set correctly, DEM can predict the granular forces and flow fields over a wide range of conditions. Particularly when DEM was coupled with multi-body dynamic simulator, DEM can be used to accurately capture body-media interactions during locomotion, facilitating parameter variation and the development of locomotor principles [78, 79]. One deficit of the DEM simulation is that, since it is based on force models at grain level, for large numbers of particles it requires long computation time, which is not useful for rapid iteration.

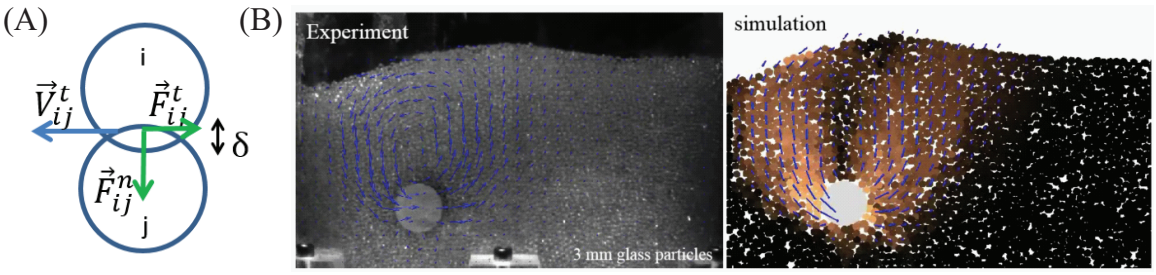

Figure 18: Discrete element method. (A) Diagram of a interacting pair of particles. DEM computes the normal force F_{ij}^{n} and the tangential force F_{ij}^{t} between the two particles i and j. δ is the deformation (virtual overlap) between the contacting particles, and v_{ij}^{t} is the tangential component of relative velocity. (B) The flow field of granular media in the surroundings of a rod slowly dragging through $3mm$ glass beads. The DEM simulation prediction of granular forces and flow fields matched the experimental measurements.

1.5.4 Resistive Force Theory

Recently, a resistive force theory (RFT) approach was developed to capture the terradynamic performance of robots and animals on homogeneous granular substrate. RFT was originally developed to model motion in low Reynolds number viscous fluids [35] and was adapted in [77] to calculate granular reaction forces on objects moving in the horizontal plane. In [72] RFT was extended to describe intrusion in the vertical

plane, which is relevant for surface locomotion where the granular force on robot/animal limbs is calculated as a linear superposition of independent surface element forces (Figure 19A) with varying depth, orientation, and moving direction. The coefficients used to calculate the element forces can be empirically measured using intrusion by a rigid plate. By using the bulk response of the granular media, RFT can predict locomotor performance on GM (Figure 19B, C) without computing detailed grain interactions, and thus significantly speed up the simulation as compared to DEM. On the other hand, due to this simplification, the usage of RFT is unclear for fast granular locomotion [102] (e.g., high speed impact) or when substrates contain larger and/or complex obstacles [101], where grain inertia and size heterogeneity needs to be considered.

1.5.5 Interaction analysis for multi-component substrates

The presence of pebbles, rocks and boulders in the sand further complicates the interaction between the locomotors and the substrates. These multi-component heterogeneous substrates environments widely exists in environments that robots need to traverse [32]. However, the understanding of the interactions between robots and such heterogeneous substrates was limited. In traditional navigation planning, robots were generally required to find a "collision free path" and avoid interacting with obstacles. This is reasonable for most wheeled/treaded robots which must circumvent obstacles, but for legged robots, traversing obstacles by stepping over or upon them[63] can be a valid and possibly more effective option. Allowing robots to gracefully interact with obstacles[9], or even manipulating the locomotion environment [67], can open a new avenue for strategic navigation planning and significantly expand viable exploration space.

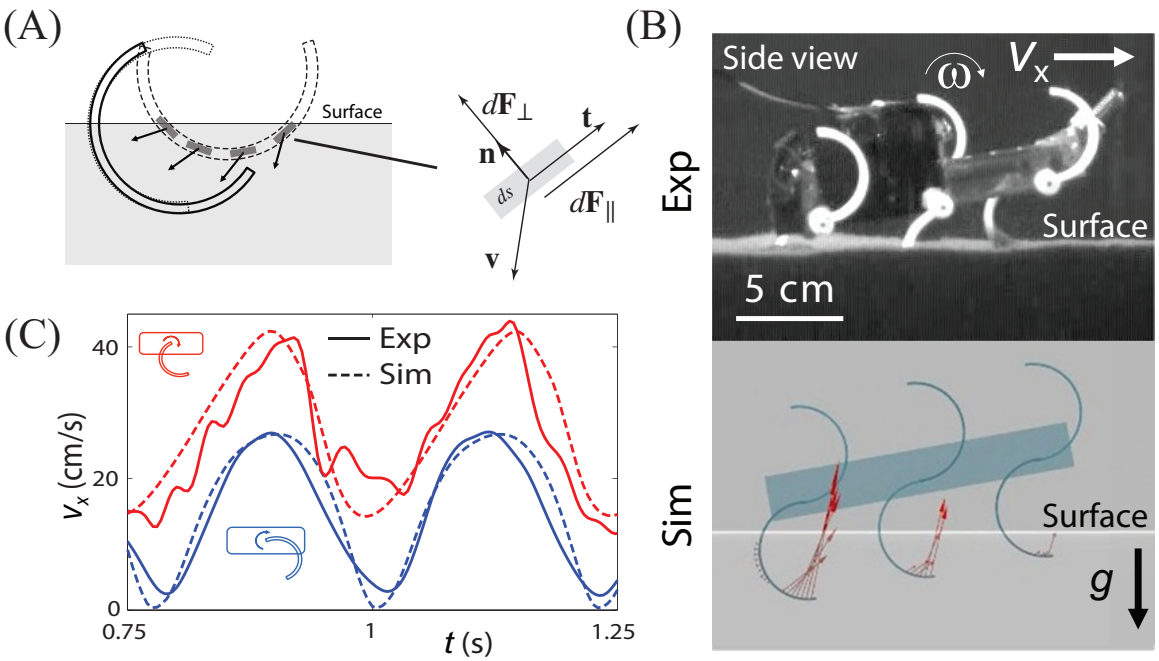

Figure 19: Resistive force theory. (A) Illustration of the Resistive Force Theory (RFT) method. For a RHex c-leg moving into granular media, each infinitesimal element ds on the intruding leg is characterized by its tangent direction $\hat{\mathbf{t}}$ (or normal direction $\hat{\mathbf{n}}$) and its velocity $\mathbf{v}$; each element experiences a force $d\mathbf{F}_{\perp,\parallel}$ that can be experimentally measured using a rigid plate. Granular force on the c-leg can then be estimated as a linear superposition of these independent element forces. (B) Experiment and RFT simulation of a RHex-like robot (Xplorer) during alternating tripod gait locomotion on granular media. Red arrows indicate granular reaction forces at each segment calculated using RFT. (C) Comparison of forward speed vs time between an experimental robot and corresponding RFT simulation using c-legs and reversed c-legs. Adapted from [72].

Many previous studies have started to investigate robot mobility on irregular terrains such as steps [58], slopes [39, 127], gaps, sideways tilts [58], and ground unevenness [123]. However, these studies largely focused on optimizing locomotor control and planning strategies while interaction physics with the environments were not fully understood. In addition, in most of these studies the terrain irregularities were assumed to be static, while in nature terrain heterogeneities such as pebbles, boulders and rocks in sand can exhibit complicated dynamics upon contact (i.e., when robot/animal leg steps on such heterogeneities, rocks and boulders in sand can sink, rotate, slide, or remain still). Development of obstacle-interactive legged robot locomotion control on ground heterogeneities that possess mobility relative to the substrates underneath requires fundamental understanding of the complex interaction dynamics between the robot and the heterogeneous flowable substrate.

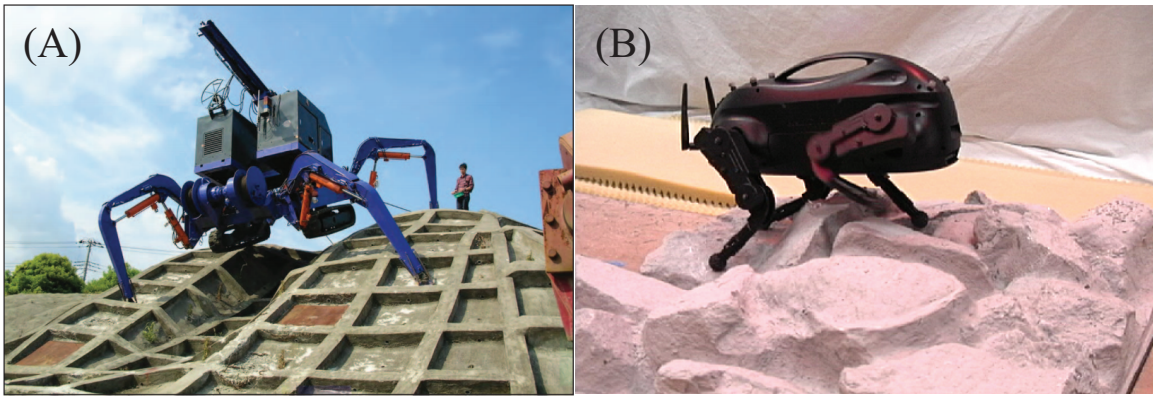

Figure 20: Robot negotiating irregular terrains. (A)TITAN XI climbing a unstructured slope. Reproduced from [39]. (B) Little Dog traversing uneven terrain. Reproduced from [123].

The challenge of achieving such understanding comes from the nearly infinite variety of naturally occurring heterogeneous terrains (with variation in size, shape, mobility, distribution, and so on). Studying such complex dynamics often results in intractable complexities. Recently, researchers started to use robophysics approach to

systematically create simplified 3D-component environments, to examine the interactions between locomotors and complex, multi-component environments and develop basic understandings to help improve robot locomotion. One example is a recent study of locomotor interaction with tall slender obstacles (i.e., small insects or micro robots traverse through grass, shrubs, tree slabs, fungi, etc.). By analyzing the interaction of a legged robot through a field of densely packed, grass-like bendable beams, Li et al. [69] discovered that a discoid body shape helped cockroach traverse through cluttered "grass" field with opening size narrower than body width, by inducing a passive "rolling" behavior. By implementing this body shape to small legged robots, Li et al. significantly increased the traversal ability of small robots through cluttered multi-component environments without any complicated control. Another example is a recent study of interaction between undulatory locomotor and shrubs, branches, etc. in their environments. To enable snake robots to effectively maneuver in such environments, Schiebel et al. constructed a peg board [3] to allow systematic variation of environment geometry. By adjusting the spacing of the peg array, they systematically examined the effect of narrow peg spacing on snake locomotion and kinematics, and found that snakes can modulate its undulation wavelength to adapts to different peg spacings. These studies have taken a first step in systematic creation and control of simplified environments for locomotor-environment interaction studies. In this dissertation, we discuss a novel robophysical apparatus [99] to parameterize and systematic create heterogeneous granular terrain and to test robotic locomotion and extract informative models on such challenging substrates.

1.6 Organization of this thesis

Within the framework of this dissertation, Chapters $II \sim III$ discuss how locomotor foot size, ground stiffness and substrate inertia affect locomotion performance on homogeneous granular ground, Chapters $IV \sim VI$ discuss how substrate heterogeneity can be controlled by an automated system and how it affects the chaotic dynamics and universal scattering of legged locomotion. Chapter VII concludes the contribution of this dissertation and outlines the research to be completed in future work.

CHAPTER II

EFFECT OF LOCOMOTOR APPENDAGE DESIGN ON TERRADYNAMIC PERFORMANCE FOR HOMOGENEOUS GRANULAR GROUND

2.1 Summary

Natural substrates like sand, soil, leaf litter and snow vary widely in penetration resistance. To search for principles of appendage design in robots and animals that permit high performance on such flowable ground, we developed a ground control technique by which the penetration resistance of a dry granular substrate could be widely and rapidly varied. The approach was embodied in a device consisting of an air fluidized bed trackway in which a gentle upward flow of air through the granular material resulted in a decreased penetration resistance. As the volumetric air flow, Q, increased to the fluidization transition, the penetration resistance decreased to zero. Using a bio-inspired hexapedal robot as a physical model, we systematically studied how locomotor performance (average forward speed, v_x) varies with ground penetration resistance and robot leg frequency. Average robot speed decreased with increasing Q, and decreased faster for higher leg frequency, ω. A universal scaling model revealed that the leg penetration ratio (foot pressure relative to penetration force per unit area per depth and leg length) determined v_x for all ground penetration resistances and robot leg frequencies. To extend our result to include continuous variation of locomotor foot pressure, we used a resistive force theory (RFT) based terradynamic approach to perform numerical simulations. The terradynamic model successfully predicted locomotor performance for low resistance granular states. Despite variation in morphology and gait, the performance of running lizards, geckos and crabs on

flowable ground was also determined by the leg penetration ratio. Appendage designs with reduced foot pressure can passively maintain minimal leg penetration ratio as the ground weakens, and consequently permit maintenance of effective high-speed running over a range of terradynamically challenging surfaces [1].

2.2 Introduction

Legged locomotor performance depends sensitively on substrate properties, locomotor morphology and gait. Deformable substrates like loose sand, new snow, mud, and leaf litter can be particularly challenging due to their low penetration resistance, which we define here as the vertical ground resistance force per depth during intrusion. During interaction, such substrates can yield and flow, producing complex and dynamic interactions that can result in poor locomotor performance. Despite the ubiquity of such interactions, general biological principles linking appendage morphology and performance are unknown.

That said, there have been a number of specific studies in recent years which give hints about the importance of limb-substrate interaction on such surfaces. For example, a previous study concluded that humans use 60% more energy running on deformable and dissipative substrates like sand compared to rigid ground due to an increase in the work done on the ground and a decrease in muscle-tendon efficiency [66]. Pandolf et al. investigated the metabolic energy expenditure for humans walking on snow, and found that energy expenditure increased linearly with increasing depth of the footprint depression [94]. For non-human locomotors, Li et al. found that the elongated hind foot of the zebra-tailed lizard, *Callisaurus draconoides*, functioned as an energy-saving spring on solid ground, but on yielding sand, the foot acted as a force-generating paddle [68]. It was also suggested in [68] that for a given animal,

[1] This Chapter is a paper by Feifei Qian, Tingnan Zhang, Wyatt L. Korff, Paul B. Umbanhowar, Robert J. Full, and Daniel I. Goldman, *Bioinspiration & Biomimetics* [98]

larger foot area can reduce energy loss to yielding granular substrates. Irschick and Jayne [43] tested two sand lizards species, *U. Scoparia* and *C. draconoides*, on a sand-covered racetrack, and examined how body posture, hindlimb kinematics related to their sprinting performance on different inclinations. Korff et al. [61] further compared the sprinting performance of *U. Scoparia* and *C. draconoides* in their natural habitat substrates, dune and wash sand, and investigated whether habitat distribution and the presence of toe fringes contributed to their performance difference. These studies provided better understanding of how morphology and kinematics can contribute to locomotor performance on flowable ground, but the substrate resistances were not controlled and systematically varied. Further, locomotor responses to low resistance flowable substrates were relatively unexplored.

Studying how biological and robotic locomotors respond to low penetration resistance substrates can provide insights into the function of morphological features of animal feet, facilitate robot appendage design and improve the terradynamic performance of robots on challenging terrains. We suspect that foot penetration depth, foot size and limb length play important roles in determining locomotor performance on flowable ground, and we investigate these parameters here by studying the locomotion of a bio-inspired robot as a simplified model locomotor. Robots are increasingly used as physical models to systematically vary morphological and kinematic parameters and to test biological hypotheses on granular media. For example, Li et al. used a bio-inspired hexapedal robot as a model legged locomotor on granular media and found that the robot exploited the solid-like response of granular media and advanced via a kinematic form of walking [71] when ground penetration was relatively small. Using an undulating sandfish-inspired robot, Maladen et al. found that the desert-dwelling sandfish lizard (*Scincus scincus*) swam within sand with optimal wave efficiency [77]. With a turtle-inspired robot named FlipperBot, Mazouchova et al. [84] discovered

that a free wrist joint kept the stress applied by the flipper below the substrate yield stress and allowed FlipperBot to advance its body kinematically with no slip. Using an undulatory snake inspired robot, Marvi et al. [81] revealed that sidewinding snakes control ground contact length to reduce ground shear stress and avoid slipping when ascending granular inclines.

There are many challenges associated with studying locomotion on flowable ground and discovering the principles by which effective movement is achieved. One challenge in performing systematic locomotion studies on flowable ground is that natural deformable terrain comes in a staggering variety of forms, making exhaustive locomotion testing on each substrate impossible. Single-wheel testbeds with granular material such as Mojave Martian Simulant [112], quartz sand, and Ottawa sand [86] have been used for robotic vehicle motion testing studies. Most of these studies measured ground properties to analyze wheel-ground interaction, but few of them systematically controlled and varied the ground properties, especially for low penetration resistance ground. In a previous study [71] of locomotion on dry granular media, we used air pulses to control granular media compaction from closely packed to loosely packed. The associated volume fractions ϕ (the ratio of solid grain volume to occupied volume) varied from 0.62 to 0.58 respectively, with corresponding penetration resistances per unit area of 1.6 N/cm^3 to 0.3 N/cm^3 (note that air flow was turned off during locomotion tests in these studies). However, ground penetration resistance varies even more widely in terrestrial environments, and terrains like leaf litter or snow can exhibit even lower penetration resistances than can be achieved in loose packing of model laboratory materials. For example, snowpacks can have a minimum penetration resistance per unit area of only 0.17 N/cm^3 [107], which is below the limit of the loose compaction state in dry granular media like sand. New ground control techniques are needed to attain such low resistance states.

Another challenge to the study of locomotion on flowable ground lies in the difficulties in modelling the ground interactions that occur when locomotors move on yielding substrates. Researchers have traditionally used terramechanics [7][130] approaches to understand the interactions between robot/vehicle wheels and deformable ground. The classical terramechanics method is based on flat-plate pressure-sinkage relations, which works well for large wheeled and tracked vehicles. However, for small scale locomotors and especially for locomotor appendages of complex geometry like robot/animal legs, classical terramechanic models are not sufficient to accurately describe leg-ground interactions [86]. Recently, a resistive force theory (RFT) based terradynamic approach was developed to capture the terradynamic performance of robots and animals. RFT was originally applied to motion in low Reynolds number viscous fluids [35] and was adapted in [77] to calculate granular reaction forces on objects moving in the horizontal plane. In [72] the RFT was extended to describe intrusion in the vertical plane, which is relevant for surface locomotion where the granular force on robot/animal limbs is calculated as a linear superposition of independent surface element forces.

In this paper, we apply a new approach that allows precise control and broad variation of ground penetration resistance using continuous upward air flow through the bed [93]. Using this new ground control technique, we systematically investigate the effects of ground strength on robot and animal locomotion performance over a range of penetration resistances in both experiment and RFT-based terradynamic simulation, and we find good agreement between the simulation and the robot experiment. We develop a universal scaling model that successfully captures kinematic legged robot locomotion performance for low resistance granular states, and show that our model can be further extended to explain locomotor performance of animals with

more complex morphologies and gaits. Our ground control technique opens a new avenue for systematic study of the limits of animal and robot locomotor performance over a wide range of granular substrates, and the use of the RFT method allows us to achieve continuous variation of locomotor scaling parameters (mass, foot size, etc.). Our approach allows extension of granular terradynamics (RFT in particular) to loose substrates of arbitrary ground stiffness, and advances our understanding of legged animal and robot locomotion on low resistance ground.

2.3 Materials and Methods

Locomotor performance is sensitive to the mechanical properties of the ground, which vary widely between different terrestrial environments. To systematically reproduce a wide range of ground properties for robot and animal testing, we utilized an air-fluidized granular trackway to vary and precisely control the ground penetration resistance via continuous upward air flow. For different substrate properties, we performed robot and animal locomotion experiments to investigate the effects of morphology and kinematics on locomotor performance. We also conducted force measurements and modelling to analyze in detail the deformable substrate response during leg intrusion.

2.3.1 Fluidized bed trackway

To emulate natural terrains with low penetration resistance, we used a 2.1 m long, 0.5 m wide fluidized bed trackway [71]. The trackway was filled with ≈ 1 mm diameter poppy seeds, a model granular substrate, to a depth of 12 cm (Fig. 21A). Four leaf blowers (Toro, Model No. 51599, 300 liters per minute (LPM)) connected below the trackway forced a continuous flow of air through a porous flow distributer to evenly fluidize the granular substrate inside the trackway. The superficial speed of the air, q, was measured by an anemometer (Omega Engineering, FMA-900) mounted 3 cm

above the granular surface and was controlled by varying the blower voltage.

Using a camera that monitored the bed from the side through transparent walls, we characterized the height of the granular media as q varied from 0 to 0.4 m s^{-1} in increments of 0.01 m s^{-1}. A hysteresis curve (Fig. 21B) was observed during the fluidization and de-fluidization process, similar to the fluidized bed behavior reported previously [93]. When the air flow initially increased (from 0 to the onset of fluidization), the normal forces between the granular particles were reduced, but the air pressure drop through the grains was smaller than the weight of the bed and thus the grains remained immobile. When the air speed exceeded the threshold of fluidization, the pressure drop reached the weight of the bed, and the granular medium exhibited fluid-like properties [121]. Due to the large horizontal extent of our fluidized bed, the flow distribution varied across the trackway: the "onset" of fluidization from the bed height measurement ranged from $q = 0.27$ to 0.37 m s^{-1}. We also measured the onset of fluidization from penetration force measurements; this approach gave a more accurate value of $q = 0.3$ m s^{-1}. The hysteresis loop closed at $q = 0.39$ m s^{-1}, which coincided with the onset of bubbling [48]. During de-fluidization, the height of the granular media was greater than during fluidization (increasing air speed) at the same air speed.

We prepared the bed to the same initial packing state before each test. To do so, we increased the air flow from 0 to 0.5 m s^{-1} to fully fluidize the bed, and then decreased the air flow to zero at approximately 0.03 ms^{-2}, which left the material with the desired volume fraction of $\phi = 0.58$. Then we increased the air flow to the desired speed and maintained this fixed flow for the duration of the test. Using this method, we varied the ground penetration resistance from the loosely packed value (zero air flow) to zero (air flow at or above fluidization onset). The upward air flow through

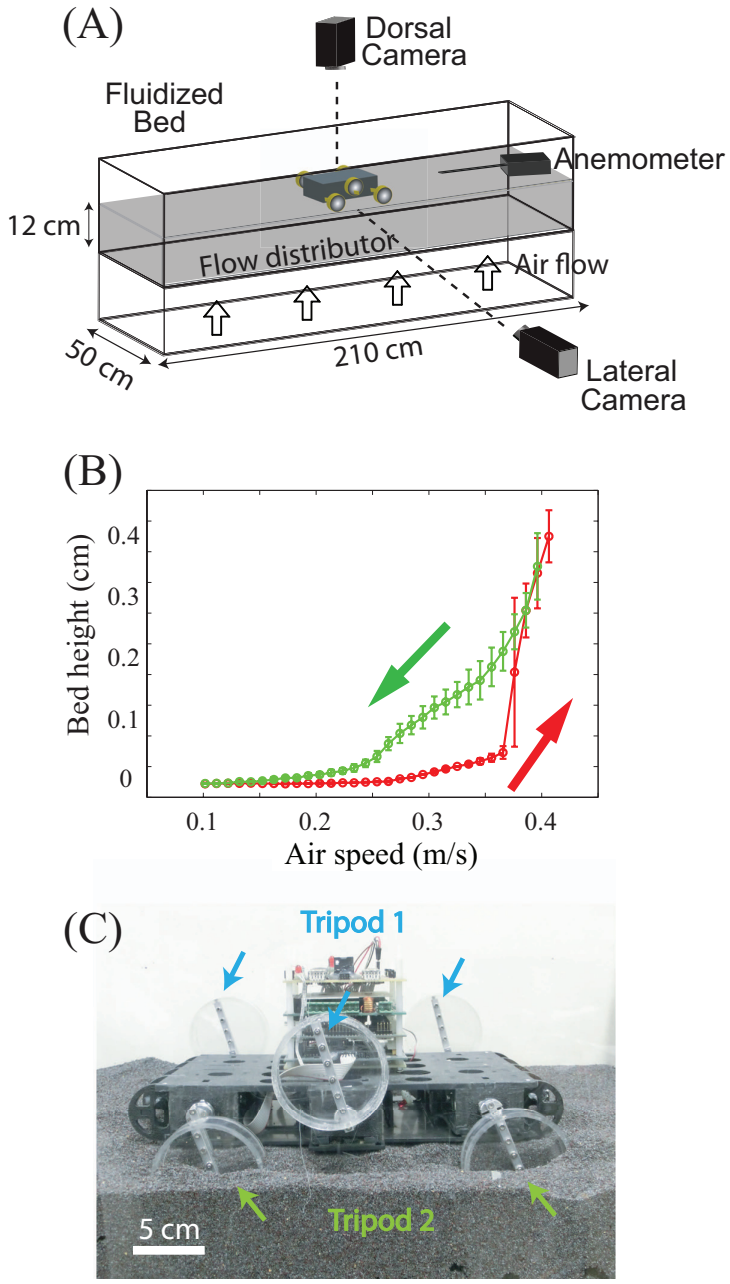

Figure 21: Apparatus to test principles of locomotion on flowable ground of variable penetration resistance. (A) Diagram of the air-fluidized bed trackway for SandBot locomotion testing. (B) Bed height vs. air flow speed, q. Red/green arrow indicates increasing/decreasing air flow. (C) SandBot, a small RHex-class hexapedal robot that uses a bio-inspired alternating tripod gait. Each tripod consists of three legs (the front and rear leg from one side and the middle leg from the other side) that move synchronously and π out of phase with the other tripod.

the granular media reduces the ground stiffness, but does not cause a significant lift force on the locomotors. Additionally, an air flow in the direction of gravity can produce penetration resistances greater than for the close packed compaction states reported previously [71]; we did not apply this technique in the current paper, but it could be of use for future studies which required stiffened substrates. In this study, we operated at flow rates below the bed fluidization transition so that the packing state remained constant ($\phi \approx 0.58$).

2.3.2 Physical model - a legged robot

Interactions between locomotor appendages and flowable terrains are challenging to model. We used a bio-inspired hexapedal robot, SandBot (a small RHex class robot [105]) as a simplified physical model to study such interactions and to develop theoretical hypotheses. SandBot is a 2.5 kg, cockroach-inspired robot with six cylindrical legs (Fig. 21C). Each 7.6 cm diameter cylindrical leg was attached to an axle at its circumference. Inspired by the alternating gaits of insects, SandBot's six legs function as two alternating tripods with the legs in each tripod rotating synchronously and with a half-cycle lag between the two tripods.

"Rotary walking" is a kinematic form of locomotion that can occur on granular media [71]. In rotary walking, robot legs penetrate the granular medium until the vertical ground reaction force matches the robot body weight plus the inertial forces required to accelerate the body. At this point the ground nearly solidifies and the legs rotate in place about their centers to propel the body forward. When ground penetration is large (weak ground or large inertial forces due to large stride frequency), SandBot's stride length decreases, its legs continuously encounter previously disturbed granular media, and it can no longer effectively perform rotary

walking via ground solidification. In contrast, lightweight legged locomotors [102] can utilize the inertial response of the granular substrate to achieve high performance despite sustained ground fluidization during foot contact.

The locomotor performance of the SandBot can be optimized for different ground conditions by adjusting gait frequency and intra-cycle timing parameters [70]. To analyze the effects of robot foot size and leg frequency on locomotor performance, we set the robot's intra-cycle timing parameters to the soft ground kinematics (SGK) values; these parameters produced effective legged locomotion on granular media [70]. In SandBot limb kinematics control, each leg rotation is composed of a fast phase and a slow phase. In SGK, the angular extent of the slow phase was set to be at 1.5 rad with its center at -0.5 rad (leg angles are measured clockwise about the axle and between the downward vertical and a diameter through the axle), and the duty cycle of the slow phase (i.e. fraction of the period spent in the slow phase) was set to 50% [70]. Two different widths of cylindrical legs ($w = 3.7$ cm and $w = 2.4$ cm) were tested, and we varied cycle-averaged leg frequencies ω between 2 rad s^{-1} and 8 rad s^{-1}. We chose cylindrical legs because their geometric symmetry facilitated the theoretical modelling of leg-ground interaction. Also, compared to the robot with 1.2 cm wide C-shaped legs (C-legs) used in our previous study [70], the wider cylindrical legs enabled the robot to move effectively over an extended range of air speed, up to 0.19 m s^{-1}, making it possible to test the general trend of robot performance across a wider range of substrate penetration resistances.

Robot kinematics were captured by two high speed video cameras (AOS X-PRI) mounted on the side and above the trackway, respectively. We recorded robot movement at 100 or 200 frames per second (FPS) for the 3.7 cm wide leg and at 80 FPS for the 2.4 cm wide leg.

2.3.3 Penetration test apparatus

To quantify the penetration resistance of the granular states generated by the air-fluidized bed trackway, we performed vertical penetration force measurements [42] (Fig. 22A) in a 24 cm long, and 22 cm wide fluidized bed. The depth of the bed was 16 cm, sufficiently deep as compared to the robot leg diameter (7.6 cm) to avoid boundary effects [117]. During each penetration test, a single SandBot cylindrical leg ($R = 3.8$ cm radius, $w = 3.7$ cm) was pushed into the ≈ 1 mm diameter poppy seeds by a linear motor actuator (Dunkermotoren ServoTube STA11), and the intrusion force was obtained from the motor current, whose linear relationship to the force was calibrated using a dynamic compression load cell (OMEGA DLC101-50).

When the cylindrical leg was pushed into the granular medium, the forces acting on it were recorded as a function of its depth. Since lateral forces were negligible during vertical penetration, only the vertical force was analyzed. In our robot locomotion study, the translational penetration speed of the leg during most of the stride (slow cycle) was small enough ($0.06 - 0.24$ m s^{-1}) that the effect of grain inertia was small and ground resistance force was insensitive to intrusion speed [116]. At low intrusion speed, the granular force exerted on the intruder is dominated by friction, and depends linearly on the penetration resistance of the granular media, k, the projected area of the intruder, A, and the penetration depth, d [38]. Therefore, we performed ground penetration resistance measurements at a constant intrusion speed of 0.08 ± 0.01 m s^{-1}.

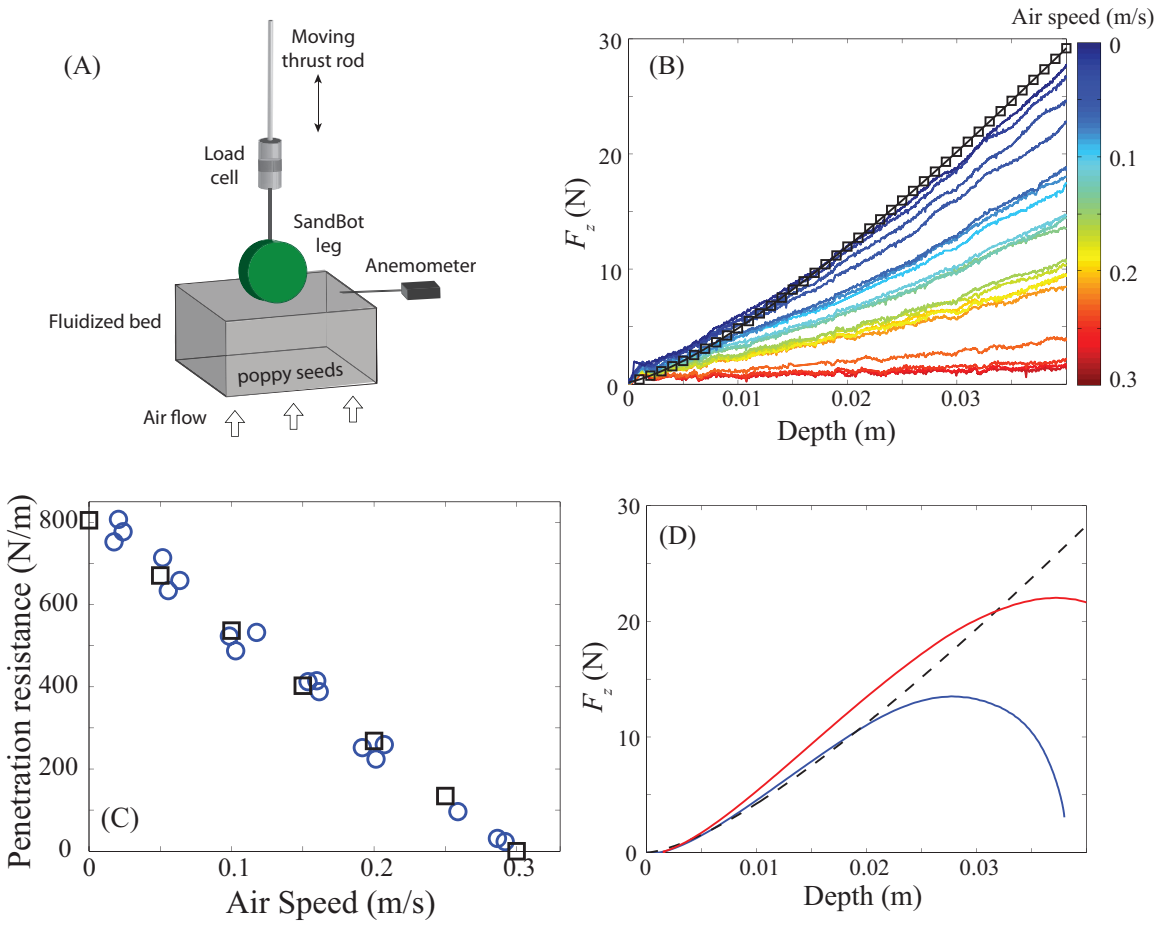

Figure 22: Experimental setup and force measurement for the penetration test. (A) Diagram of penetration experiment. (B) Vertical force on a $w = 3.7$ cm, $R = 3.8$ cm SandBot cylindrical leg vs. depth during penetration of ≈ 1 mm diameter poppy seeds at various air fluidization speeds from 0 m s^{-1} to 0.3 m s^{-1}. Colors represent air speeds. (C) Vertical penetration resistance, k, vs. air flow speed, q. Blue circles and black squares represent the slope of vertical force per unit depth from experiment measurement and RFT simulation, respectively. (D) RFT simulated rotational penetration force, F_z, vs. depth. Red curve: axle height = 2.5 cm; blue curve: axle height = 3.8 cm; black curve is the force from vertical intrusion, for comparison.

2.3.4 Animals and locomotion protocol

We measured the average straight line running speed and limb kinematics of five different animals (Fig. 23A) for varying ground penetration resistance achieved using the same air-fluidized bed technique, which was parameterized by the volumetric flow rate, Q. The volumetric flow rate was measured using a flowmeter connected in series between the compressed air source and the fluidized bed, and Q is proportional to the superficial air speed through the fluidized bed. All five animals contend with low-resistance ground in their natural habitats: a desert dwelling generalist lizard, *Callisaurus draconoides* (N=5, mass=11.3 ± 5.1 grams, Fig. 23A blue label); a sand-specialist Mojave fringe-toed lizard, *Uma scoparia* (N=5, mass=20.2 ± 6.9 grams, red label); an arboreal and ground dwelling gecko, *Pachydactylus bibroni* (N=5, mass=13.4 ± 2.6 grams, purple label); a generalist lizard, *Sceloporus olivaceus* (N=4, mass=19.3 ± 7.8 grams, green label); and the fastest land invertebrate, the sand-specialist ghost crab, *Ocypode quadrata* (N=3, mass=27.4 ± 6.4 grams, black label).

We tested all animals in a longer 300 cm by 40 cm wide trackway (Fig. 23B) filled with small glass spheres (mean $\pm$ s.d. diameter = 250 ± 30 μm) to a depth of 20 cm. We maintained the temperature of the trackway between 35 and 40 °C. The center section of the trackway (29 cm long $\times$ 18 cm wide) was a fluidized bed which allowed local control of the ground penetration resistance by application of upward air flow as for the robot trackway. The onset of fluidization for 250 μm diameter glass beads occurred at $Q_0 \approx 160$ LPM. We also measured locomotor performance on a rigid substrate (labeled 'hard' and made of a rigid board covered by fine grit sandpaper) and a closely packed granular bed (labeled 'CP' and with $\phi \sim 0.62$) as controls.

For all animal tests, we recorded synchronized videos using two cameras positioned for dorsal and lateral views. The lateral camera recorded the foot kinematics,

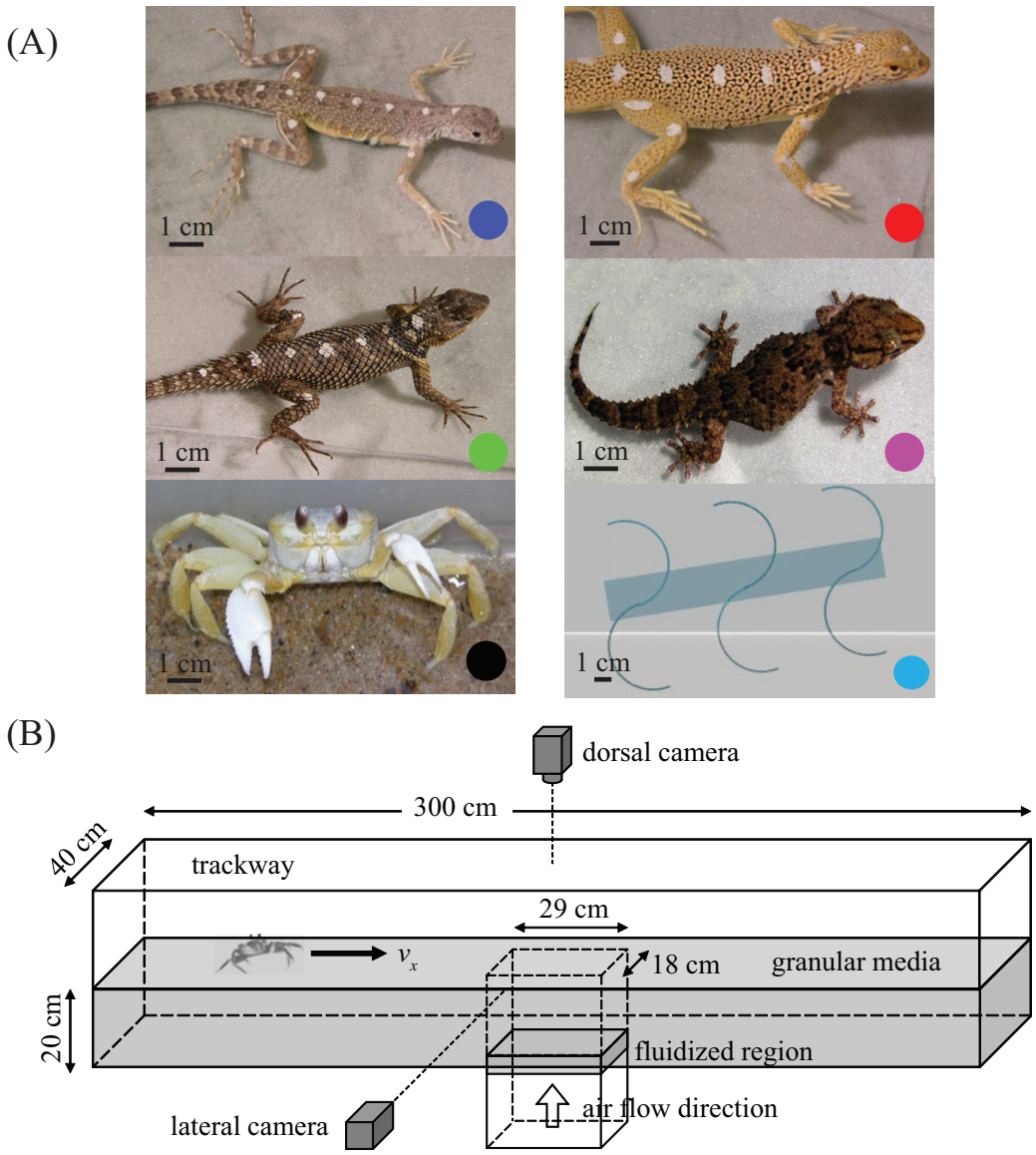

Figure 23: Small locomotors tested on granular media of different penetration resistance. (A) Five organisms studied in experiment (colored circles indicate corresponding symbols in Figs. 28, 29, 30 and 31) – *Callisaurus draconoides* (blue), *Uma scoparia* (red), *Sceloporus olivaceus* (green), *Pachydactylus bibroni* (purple), *Ocypode quadrata* (black), and the Xplorer robot (cyan) studied in simulation. (B) The trackway for the animal experiments contained a fluidized bed in the center which was used to vary the penetration resistance of the granular medium (250 ± 30 μm diameter glass particles).

and from the dorsal video we tracked circular reference markers placed on the dorsal surface of the animal to obtain the velocity of the estimated center of mass (CoM) as the animal crossed the fluidized section. To enhance accuracy in performance comparison of average speed, we accepted trials that met the following criteria: Animals had masses between 5 and 40 grams, and ran across the trackway without contacting sidewalls or stopping in the fluidized section. With these criteria, we collected 334 trials with at least three runs per individual per granular state.

We used analysis of variance (ANOVA) and analysis of co-variance (ANCOVA) for statistical analysis. We used a Tukey′s honestly significant difference (HSD) test for post hoc testing as needed. All statistical tests were performed using JMP (SAS Institute, Cary, NC, USA).

2.3.5 Numerical simulation

We used an experimentally validated terradynamics model of the granular media [72] to study the penetration resistance and the locomotor performance of the SandBot. The simulation model is based on the resistive force theory (RFT). By assuming that the frictional granular force on intruders is a linear superposition of independent surface element forces (Fig. 24B), we can compute the net intruding force for complex geometries like limbs. Here we did not attempt to simulate the complex morphologies and gaits of all organisms, but instead searched for general principles that governed legged locomotion on flowable substrates. Therefore, to facilitate comparison among small-scale runners, we also simulated the locomotor performance of a small (15 cm long), lightweight ($40 - 270$ g in simulation) robot, Xplorer (equipped with 1.5 cm radius, 1 cm wide C-legs [72], Fig. 23A). The simulated Xplorer robot used the same alternating tripod gait as SandBot, but is similar in size to the animals tested in this

study. Using the terradynamic simulation, the dynamics of Xplorer was successfully predicted in [72], and hence only simulations ("virtual" experiments) of its performance were performed here.

2.4 Results and Discussion

Using continuous air flow, we varied the ground resistance per unit area from 0 to 1.6 N/cm^3, and systematically tested SandBot and animal locomotor performance as a function of ground penetration resistance. We characterize the effect of leg frequency and foot size on locomotor performance, and develop a theoretical model that captures normalized locomotor speed on low resistance ground regardless of variation in morphology and gait.

2.4.1 Ground penetration resistance

The measured vertical penetration force, F_z, as a function of the penetration depth, d, (defined as the vertical distance from the granular surface to the lowest point on the cylinder) is plotted for various air flow speeds (Fig. 22B). For all q, F_z increased superlinearly for small depth ($d < 0.01$ m) due to the increasing projected area of the cylinder in contact with the substrate. For $d > 0.01$ m, F_z increased linearly with d. Therefore, linear regressions were performed for $d = 0.01 \sim 0.05$ m to obtain the penetration resistance, which is defined as the slope of the linear fit $k = F_z/d$. The penetration resistance measured in experiment (Fig. 22C, circles) decreased linearly with increased air flow speed, and this dependence was repeatable. At $q = 0.3$ m s^{-1} the air speed reached the onset of fluidization, and ground resistance was zero for larger flow rates.

We also characterized the penetration resistance in simulation. We first validated

the RFT using the vertical penetration force as the SandBot leg was vertically pushed into the granular media at $q = 0$. Since the ground resistance decreased linearly with the air speed in our experiments, we modeled the air flow effect with a single force scaling factor:

$$\lambda = 1 - \left|\frac{dk}{dq}\right| \frac{q}{k(q=0)}, \tag{1}$$

where dk/dq is the slope from the linear regression of the experimental penetration resistance vs. air speed data. The vertical penetration force from the RFT calculation (Fig. 22C, squares) agreed well with the results from experiment.

Since the ground penetration resistance displays sensitive angular dependence [72] and SandBot's legs rotated into the granular media (instead of penetrating vertically) during locomotion, we also calculated the rotational penetration force, and used the effective penetration resistance (defined as $F_z/\Delta d$, where Δd is the depth at which F_z is maximum) in our theoretical model to predict robot locomotion performance. The rotational penetration force is defined as the granular resistance force exerted on the robot leg when it rotated in the granular medium about a fixed, horizontal axle. We calculated the rotational penetration force exerted on a cylindrical leg rotated about an axle at various fixed heights above the surface. Fig. 22D shows the rotational penetration force for two different axle heights, 2.5 cm (red curve) and 3.8 cm (blue curve). The effective penetration resistance calculated from the rotational penetration was ≈ 400 Nm^{-1}, significantly smaller compared to $k = 800$ Nm^{-1} obtained from the vertical penetration measurements.

2.4.2 SandBot locomotion kinematics and performance

When navigating on granular media, SandBot kinematics can be approximated by a rotary walking model [71] (Fig. 24A). The model assumes that each leg of a tripod

equally supports one-third of SandBot's weight ($mg/3 = 8.14$ N) and interacts with the granular substrate as an isolated vertical intruder. The vertical penetration force in the model is assumed to be hydrostatic-like so that it increases proportionally with depth (i.e., $F_z = kd$). During locomotion, the tripod penetration depth is determined from the force balance $kd = m(g + a)$, where ma is the contribution from the robot inertia. The cylindrical leg stops translating at this depth and begins to rotate about its geometric center. The body is then propelled kinematically.

Our experiments showed that SandBot's forward speed was sensitive to ground penetration resistance. At a fixed leg angular frequency, ω, SandBot's average forward speed, v_x, decreased with increased air flow (i.e., reduced ground resistance). At $\omega = 8$ rad s^{-1}, when the air speed was low ($q = 0.03$ m s^{-1}, Fig. 25A top blue curve), SandBot's locomotor performance was relatively high with $v_x = 0.5$ bodylength s^{-1}. Leg penetration depth d (averaged over a tripod) was small (30% of the leg length/-diameter), and the robot's ventral surface was above the granular surface during the entire stance. As q increased and k decreased, SandBot's locomotor performance decreased. At $q = 0.19$ m s^{-1} (Fig. 25A, bottom purple curve), v_x decreased by nearly a factor of 3 to 0.17 bodylength s^{-1}. We observed that d also increased to 83% of the leg length ($2R$), and the robot's ventral surface experienced frictional drag during the entire locomotion trial. SandBot's accelerations became significantly smaller, indicating that leg generated thrust was only slightly greater than drag on SandBot's ventral surface.

We also noticed that when the penetration resistance was relatively high (Fig. 25B, cyan and blue curves), SandBot's forward speed increased with increasing leg frequency (0 rad s^{-1} to 8 rad s^{-1}) and the highest performance corresponded to the maximum leg frequency, similar to the rigid ground case. As the ground weakened

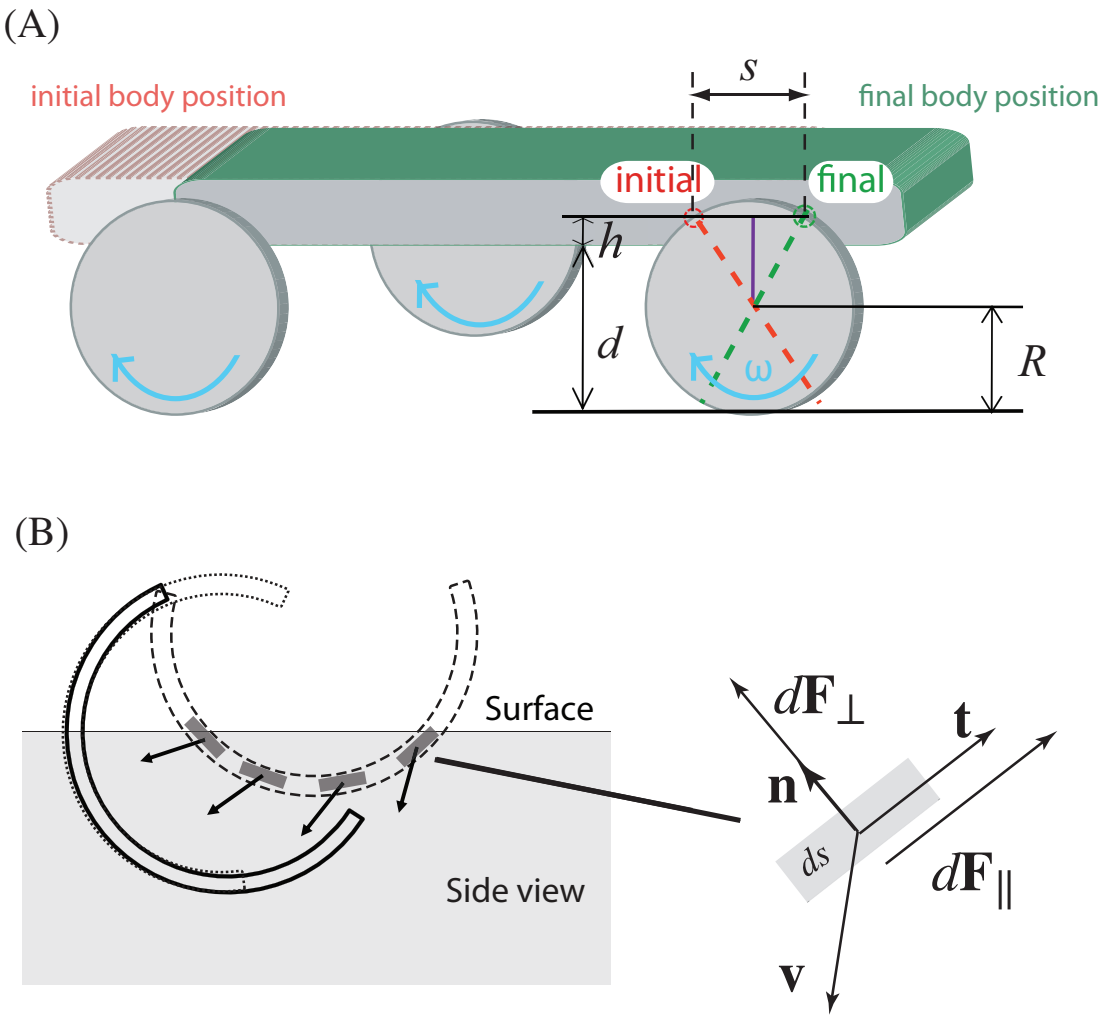

Figure 24: Diagrams of models discussed in the text. (A) Rotary-walking model [71]. R is the radius of the cylindrical legs, s is the stride length (forward displacement per cycle), d is the penetration depth and h is the hip height. Red circle indicates axle positions at the onset of rotary walking, green circle indicates axle positions at the end of rotary walking. (B) Resistive force theory (RFT) "terradynamics" [72] schematic for legged locomotion in the vertical plane. The leading surface of the leg is decomposed into small flat-plate segments. The forces $d\mathbf{F}_{\perp,\parallel}$ on each infinitesimal segment ds is determined from its normal direction $\hat{\mathbf{n}}$ (or tangential direction $\hat{\mathbf{t}}$) and velocity $\mathbf{v}$.

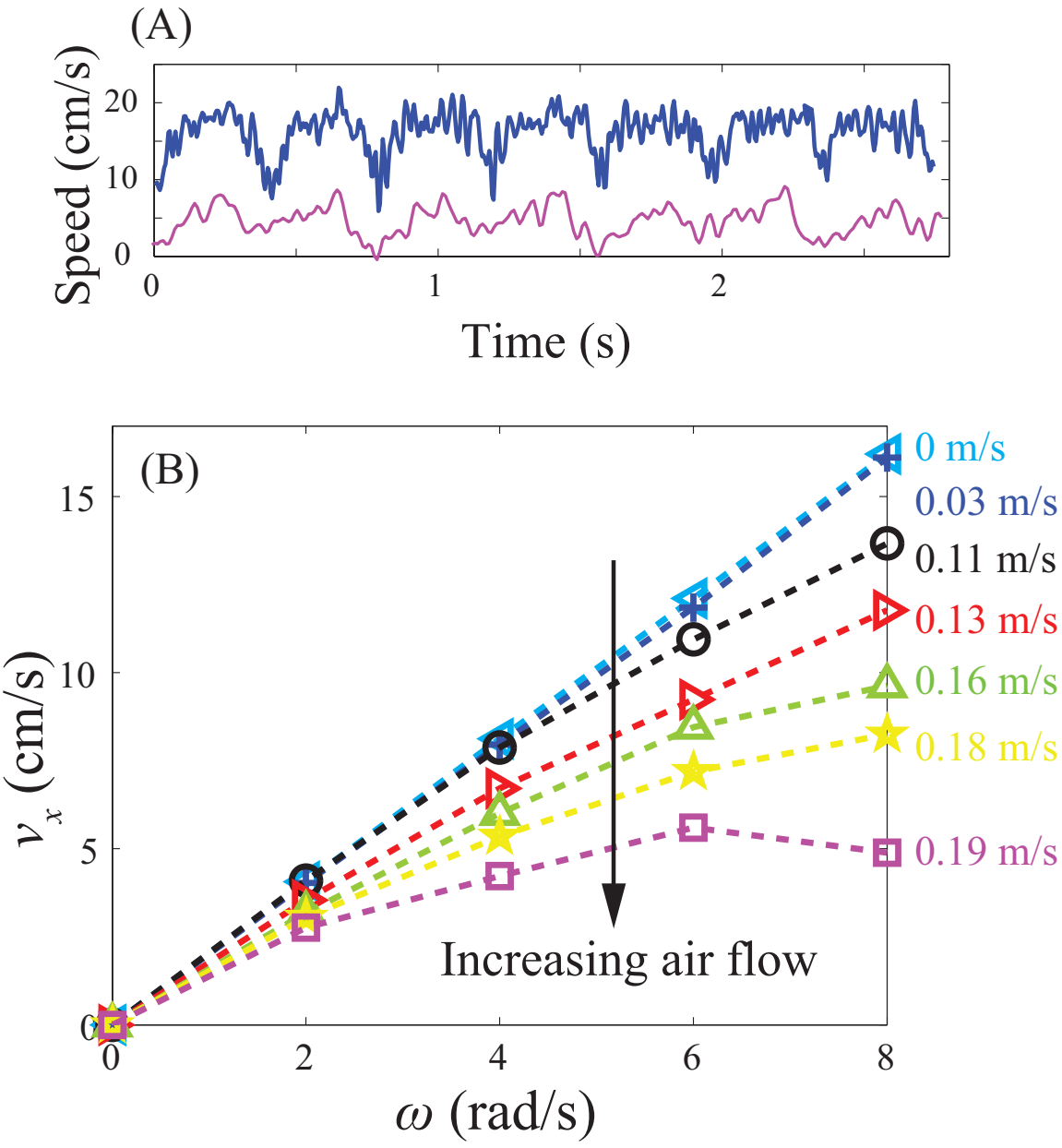

Figure 25: Kinematics of SandBot locomotion on flowable ground with different q. (A) Speed vs. time for different q (Blue: $q = 0.03$ m s^{-1}; Purple: $q = 0.19$ m s^{-1}) at $\omega = 8$ rad s^{-1}. (B) Average forward speed vs. gait frequency for various q (Purple: 0.19 m s^{-1}; yellow: 0.18 m s^{-1}; green: 0.16 m s^{-1}; red: 0.13 m s^{-1}; black: 0.11 m s^{-1}; blue: 0.03 m s^{-1}; cyan: 0 m s^{-1}).

with increased q (Fig. 25B, black, red, green and yellow curves), average speed increased monotonically with leg frequency, but exhibited a sub-linear trend, and was significantly lower than for $q = 0$. For highly weakened ground (Fig. 25B, purple curve), we observed a slight decrease in forward speed at the highest frequency ($\omega = 8$ rad s^{-1}).

To predict SandBot's speed on substrates with different penetration resistances, we used the RFT model [72], an approach that, when combined with the multibody dynamic solver MBDyn [28], predicted well the performance of the Xplorer robot [72]. We simulated SandBot using the parameters from the experiments (i.e., mass, leg geometry, SGK) and compared its performance directly with the experiments (Fig. 26). The model predictions for SandBot speed (curves) also agreed well with the experiments (symbols) for all tested leg frequencies and ground properties, even when the media was near the onset of fluidization ($q \approx 0.2$ m s^{-1}). The RFT predicts that when air speeds are low ($q < 0.10$ m s^{-1}) v_x does not vary significantly with increased q. However, for $q > 0.15$ m s^{-1} the increased wheel sinkage reduced the step length, and the ventral surface of SandBot contacted the ground which caused increased frictional drag, resulting in significantly decreased v_x.

2.4.3 Universal scaling

To generalize the locomotion model derived from SandBot to a larger variety of legged locomotors (e.g., different foot size, body weight, gait, etc.), we plotted the dimensionless average forward speed measured in experiment($\tilde{v}_x = \frac{v_x}{R\omega}$) against the dimensionless leg penetration depth ($\tilde{d} = \frac{d}{2R-h}$, where $2R - h$ is SandBot's effective leg length, i.e., the leg penetration depth when the ventral surface contacts the ground). All experimentally measured robot speeds for a wide range of ground penetration

resistances, leg frequencies, and two foot widths collapsed to a single curve (Fig. 27, filled markers), suggesting a universal scaling of locomotor performance that primarily depends on the locomotor leg penetration depth (we will refer to this as the "universal scaling model").

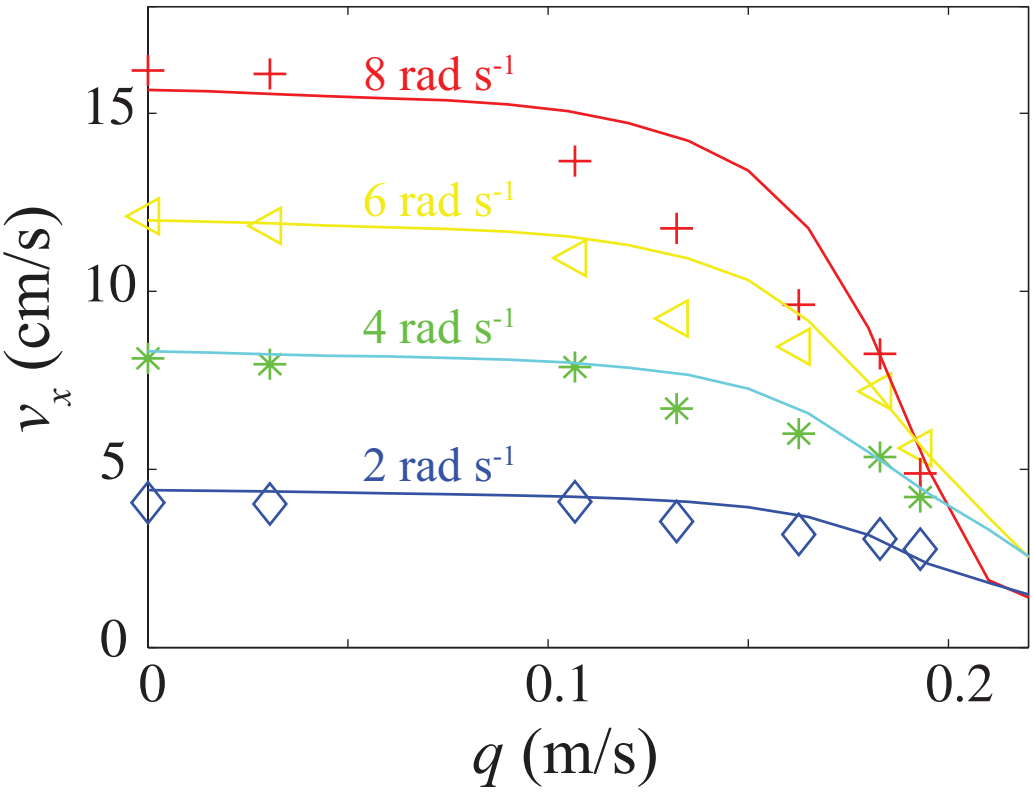

Figure 26: SandBot average speed vs. air speed (leg width 3.7 cm). Symbols represent experimental data and curves represent RFT model prediction [72]. Colors indicate different angular leg frequencies.

The experimentally validated terradynamics simulation, which facilitates rapid parameter variation, follows the same trend when plotted on the universal scaling curve (Fig. 27, unfilled markers). We further tested a wide range of masses ($m = 0.5$ to 4.7 kg) and leg angular frequencies ($\omega = 2$ to 20 rad s^{-1}) in simulation, and found that for a given leg frequency, $\tilde{v}_x$ for all robot masses also collapsed to a single curve, indicating that the locomotion is primarily kinematic. For all leg frequencies, the

locomotor performance of SandBot did not decrease significantly for $\tilde{d} < 1$ (the "insensitive region"). For $\tilde{d} \geq 1$ the robot's performance decreased substantially with increased leg penetration depth (the "sensitive region") due to drag of the ventral surface.

In the rotary walking model [71], the SandBot average speed is:

$$v_x = 2\omega R/\pi \sqrt{1 - \left(\frac{d}{R} + \frac{h}{R} - 1\right)^2}, \tag{2}$$

where $R = 3.8$ cm is the radius of the cylindrical leg, and h is the hip height (the distance between the axle and the ventral surface). Though the rotary walking model prediction (Fig. 27 black dashed curve) did not quantitatively follow the experiment and simulation data, as expected due to its assumptions of vertical leg intrusion and hydrostatic ground response, the model did capture the same qualitative behavior. We also noticed that at large leg penetration ratio ($\tilde{d} > 1.2$), the speed decrease in the experimental data exhibited a slower rate as compared to the RFT simulation which assumes a frictional resistive force. This is an indication of the effect of hydrodynamic ground response from leg-fluidized granular media [102].

The fact that $\tilde{v}_x$ decreased more slowly for small $\tilde{d}$ and significantly faster for large $\tilde{d}$ for all data in Fig. 27 suggested that despite different body weights, foot sizes and gait frequencies, the robot speed decrease rate can be significantly reduced if the robot maintains a low leg penetration ratio to stay within the "insensitive region". In other words, with sufficiently large foot area or small body weight, the robot can be passively "buffered" to changes in substrate properties and maintain effective performance as the substrate weakens.

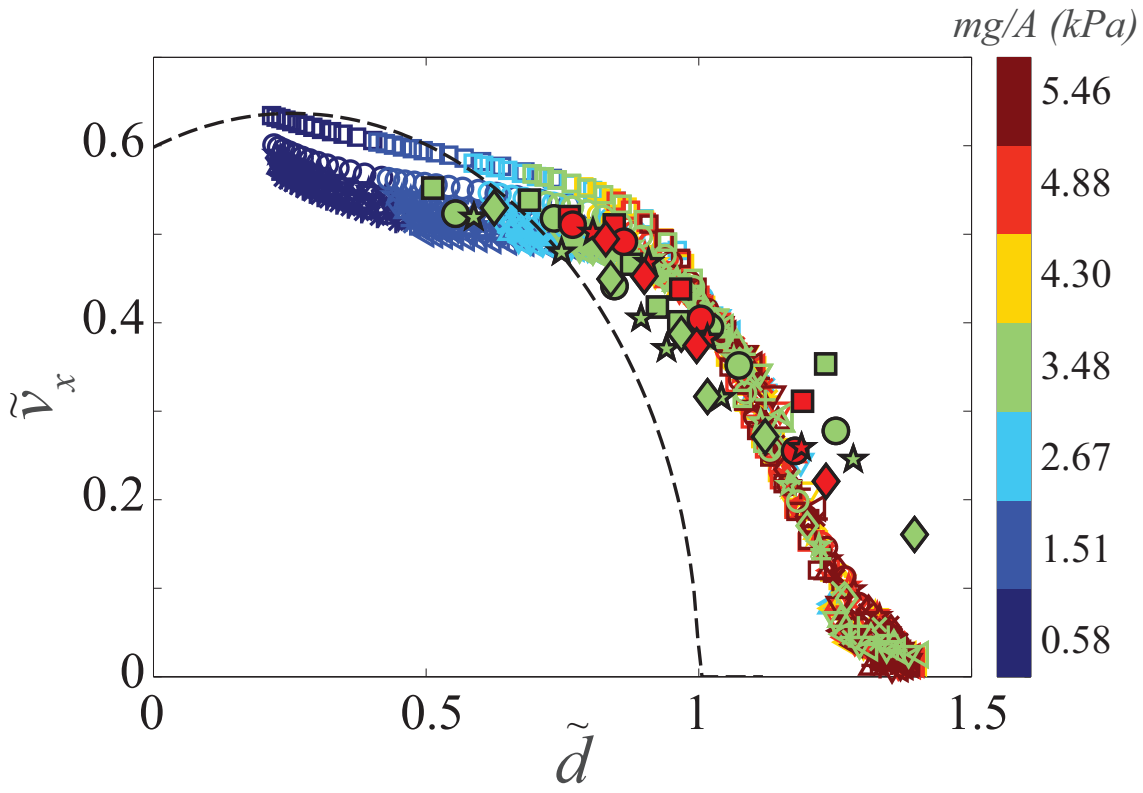

Figure 27: Universal scaling of SandBot performance. Dimensionless average forward speed vs. dimensionless leg penetration depth. Filled markers are data from experiments for 4 gait frequencies, 2 foot sizes and 7 ground stiffness, and unfilled markers are terradynamic simulation for 10 gait frequencies, 7 masses and 20 ground stiffness. Marker shape indicates gait frequency (square: 2 rad s^{-1}; circle: 4 rad s^{-1}; pentagram: 6 rad s^{-1}; diamond: 8 rad s^{-1}; cross: 10 rad s^{-1}; plus sign: 12 rad s^{-1}; upward-pointing triangle: 14 rad s^{-1}; asterisk: 16 rad s^{-1}; left-pointing triangle: 18 rad s^{-1}; right-pointing triangle: 20 rad s^{-1}). Color indicates the ratio of body weight to foot size as shown in the colorbar. The body weight, foot size and ground stiffness are also implied through different leg penetration ratio. Rotary walking model prediction is plotted as the black dashed curve.

2.4.4 Testing principles of foot and leg function in biological systems

Given the ability of the universal scaling model to rationalize SandBot performance over a wide range of substrate conditions and the idea that small leg penetration ratio buffers the locomotor against changes in substrates, we hypothesized that this same kinematic locomotion principle could be extended to help understand the performance of biological locomotors that walk in a non-rotary manner.

Kinematics and locomotor performance of animals

As mentioned in Section 2.3.4, we measured the average speed of *Callisaurus draconoides*, *Uma scoparia*, *Pachydactylus bibroni*, *Sceloporus olivaceus*, and *Ocypode quadrata* as they crossed the fluidized section of the trackway. The measured speeds of the five animals are plotted in Fig. 28 for hard ground (sandpaper), closely packed granular medium (CP, volume fraction $\phi \sim 0.62$), loosely packed granular media (LP, $Q = 0$, volume fraction $\phi \sim 0.59$), and granular states created by varying continuous air flow (0 to 200 LPM, normalized by the onset of fluidization at $Q = 160$ LPM) to the fluidized section of the trackway. We performed a two-factor ANOVA on velocity, with species and substrate state as fixed factors, and found both to be significant (Species: $F_{4,317} = 173$, $P < 0.0001$; Substrate: $F_{6,317} = 14$, $P < 0.0001$). Consequently, we explored the intricacies of the dataset with a series of ANOVAs and Tukey's HSD.

Tukey′s HSD *post hoc* test indicated that the generalists *C. draconoides* (ANOVA, $P = 0.0386$), *P. bibroni* (ANOVA, $P = 0.0036$), and *S. olivaceus* (ANOVA, $P = 0.0096$) were all significantly faster on hard ground than on closely packed ($\phi \sim 0.62$) granular media, while both sand specialists, *U. scoparia* (ANOVA, $P = 0.6075$) and

O. quadrata (ANOVA, $P = 0.2846$) were not statistically different in speed on hard ground than on closely packed granular media. For air-fluidized granular media, we found that animal speed decreased with flow rate (ANCOVA, $P < 0.0001$), and the slope of speed decrease depended on the species (ANCOVA, $P < 0.0001$). Whereas *C. draconoides* showed no drop in speed as the material was weakened (ANOVA, $P = 0.6291$), all other animals showed a decrease in average speed as the substrate strength was reduced to the point where the ventral area of many of the animals contacted the surface. The speed decrease was significant for *O. quadrata* (ANOVA, $P < 0.0001$) and *P. bibroni* (ANOVA, $P < 0.0001$).

On hard ground, animals can store and return energy gravitationally (walking) or elastically (running). Pendulous energy exchange can save energy during walking, while, during running, loading and unloading of elastic elements can store and return energy, thus aiding speed and stability. On rigid substrates, limits to performance are entirely dictated by physiological limits, including the maximal force that can be applied by muscles to accelerate the body at each step, the operating speeds of muscle (leg frequency and swing and stance duration), and morphological features like leg and toe lengths [25][50]. In our study, the speed of *C. draconoides* was nearly twice that of *P. bibroni*. This is in part due to the length of the leg and toes that contact the ground in a digitigrade posture and extend the stride length considerably. These effects appear most significant in *C. draconoides* which seems to "spring" over curled toes [25][50]. We observed that *U. scoparia* has difficulty running on hard ground, with frequent slips of its hind legs.

The situation is quite different during walking and running on deformable ground. When the ground becomes deformable and dissipative, energy [62] can be transferred to the ground and this can affect locomotor style and performance. Weyand [129]

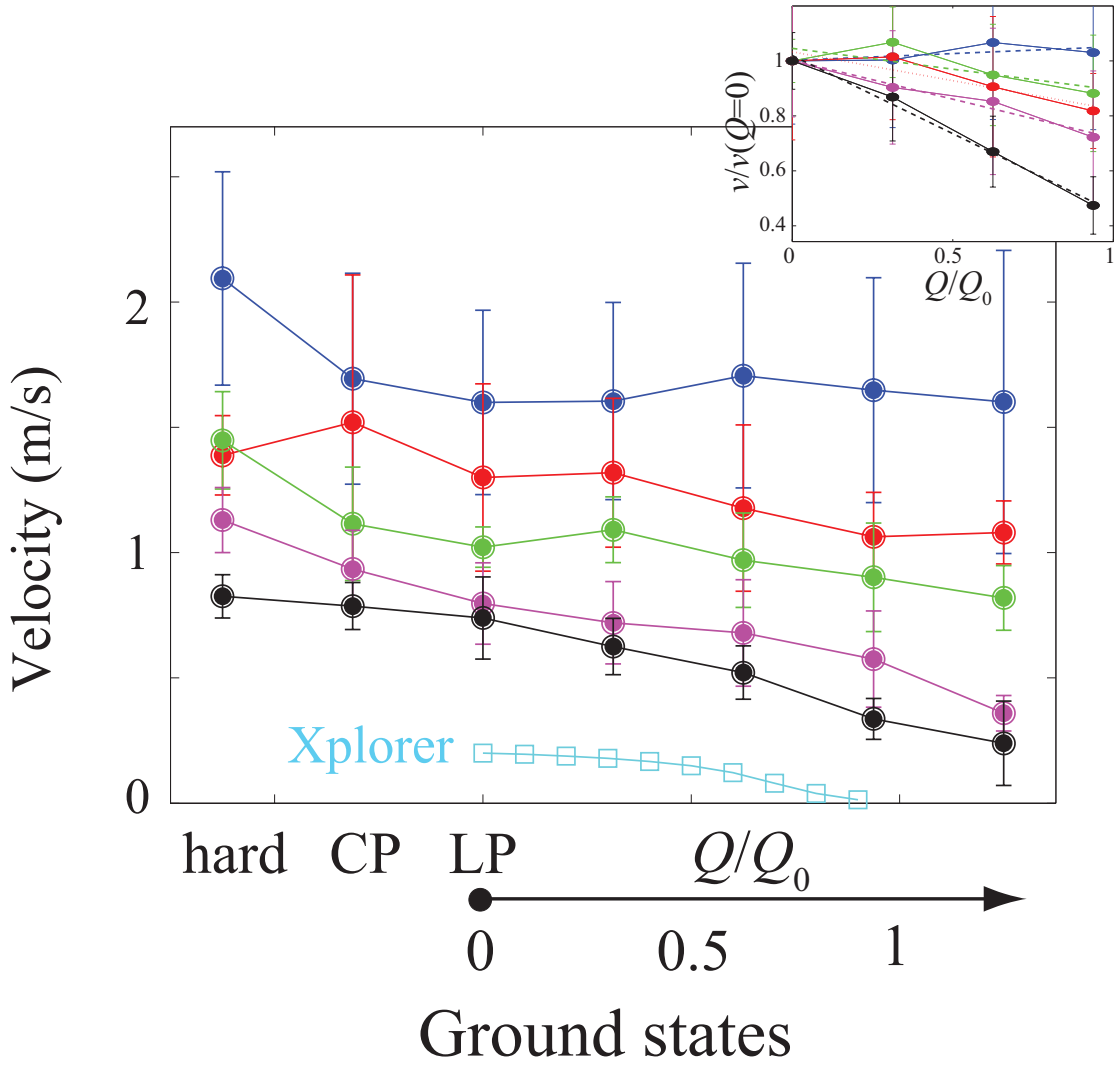

Figure 28: Average speed vs. air flow rate for the organisms and Xplorer shown in in Fig. 23A with the same color convention. The abscissa states are hard board (hard), glass beads closely packed (CP) to a high volume fraction ($\phi \sim 0.62$), glass beads in a loosely packed state ($\phi \sim 0.59$) with an increasing flow rate Q from $Q = 0$ to $Q = 200$ LPM. The volume fraction remains fixed from $Q = 0$ to $Q = 160$ LPM above which the system becomes fluidized. The plotted flow rate is normalized by the onset of fluidization $Q_0 = 160$ LPM. At least three runs were taken per individual and granular state. Error bars indicate one standard deviation. Inset: Normalized average speed vs. normalized flow rate for five organisms (filled circles) and the slope for each curve (dashed lines).

proposed that ground stiffness could account for running speed. Farley et al. [24] systematically varied the stiffness of a rubber track and found that locomotors adjusted leg stiffness to maintain running performance for different substrate stiffness. Spence et al. [114] investigated the kinematics of rapid insects on elastic surfaces, and found that they were able to maintain forward speed by lowering the CoM towards the compliant surface and thereby increase the period of double support. However, in these experiments the deformation of the substrate was relatively small compared to the leg length.

When moving on flowable granular substrates, small animals can penetrate a large fraction of their limbs and feet into the material at each step. After analyzing the *C. draconoides* foot kinematics, we observed that upon impact the hind foot vertically penetrated a small distance into the granular surface, then quickly stopped during the stance, at which point the animal began to rotate its ankle as the toes dug in the material, until the granular media reached a jammed state underneath the foot. The foot then withdrew from the granular substrate while the initially spread toes collapsed upon exit. This observation was consistent with a previous study on *C. draconoides* [68], where it was suggested that the larger hind foot of the *C. draconoides* reduced energy loss to the granular substrate. Consequently, we hypothesized that animals might actively modulate their gait frequencies to adapt to ground penetration resistance variation. However, the stride frequency on hard ground was ~ 10 Hz for all the lizards and ~ 7 Hz for the crab *O. quadrata*. On the granular substrate, gait frequency of *P. bibroni*, *U. scoparia* and *O. quadrata* decreased as the ground strength decreased (i.e., increased Q/Q_0), whereas *C. draconoides* and *S. olivaceus*'s frequency remained nearly constant. All animals had stance duty factors of approximately 0.5 on the granular substrate below onset of fluidization ($Q = 0$ to 160 LPM).

Therefore, although the active modulation of gait frequency could help the animals maintain relatively effective locomotion on weakened granular ground, the kinematic data suggests that the variation in gait frequency is not sufficient to explain the measured changes in speed. In particular, *C. draconoides* maintained nearly constant speed for the full range of flowable ground (Q/Q_0 from 0 to 1) without significant reduction in gait frequency. We speculate that in addition to the strategy of actively modulating their leg frequencies to achieve higher performance, there must also exist other possible mechanisms, like within-stride kinematics variation [70] or a "passive control" mechanism that enables effective locomotion on weakened substrates with minimum active control. We focus on the latter here based on the results from our robot model – we hypothesize that animals with large feet can maintain a small leg penetration ratio and stay within the range where their performance is "buffered" to substrate stiffness changes, and therefore passively maintain effective locomotion as the ground weakens.

Performance loss

To test the passive control and buffering hypothesis, we normalized the speed for the five animals by their speed on loosely packed granular media ($Q = 0$), and plotted the normalized speeds as a function of the normalized flow rate (flow rate normalized by the onset of fluidization). As seen in the inset of Fig. 28, there was a significant difference in the magnitude of speed decrease among different animals. To gain an intuitive sense of this difference, we compared the slope of the normalized speed vs. normalized flow rate for the five animals and the SandBot of two different foot size, as a measure of performance loss (Fig. 29A).

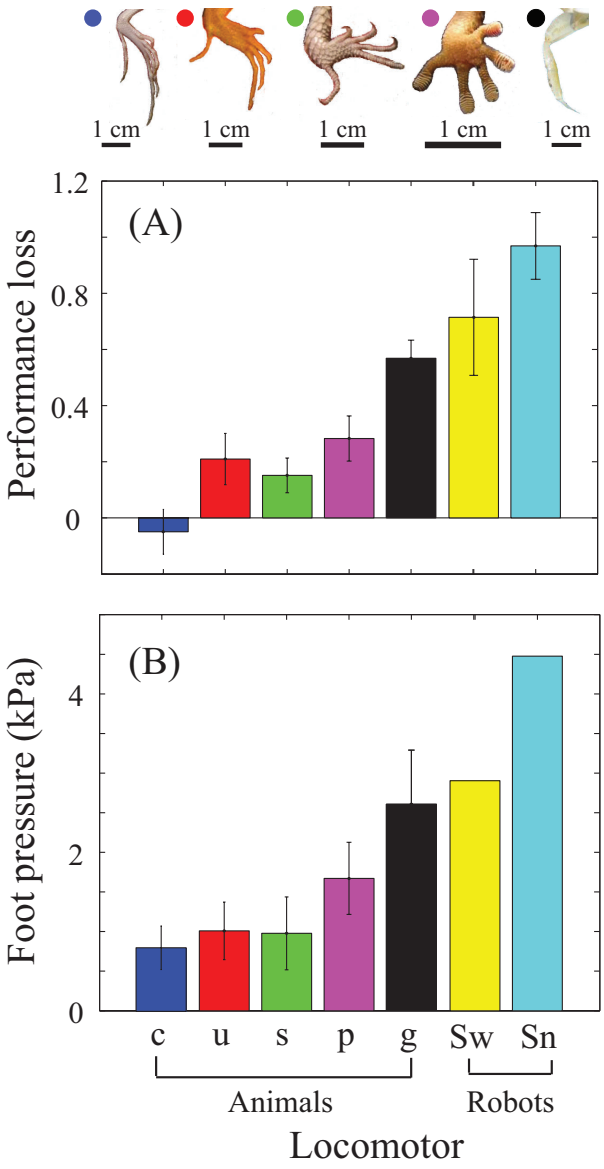

Figure 29: Performance loss and foot pressure for the five animals. (A) Performance loss (i.e. the slope of normalized speed vs. normalized flow rate from Fig. 28 inset) for the five animals: *C. draconoides* ("c"), *U. scoparia* ("u"), *S. olivaceus* ("s"), *P. bibroni* ("p"), *O. quadrata* ("g"), and the SandBot of two different foot size: $w = 3.7$ cm ("Sw") and $w = 2.4$ cm ("Sn"). Color convention for animals is the same as in Fig. 23A. For all locomotors, error bars of performance loss characterized standard deviation among different individuals and different trials, as well as standard deviation of the linear regression. For SandBot of both foot sizes, error bars also included deviation of 4 different leg frequencies ($\omega = 2$ to 8 rad s^{-1}). (B) Foot pressure for the five animals and robots. For all animals, error bars of foot pressure characterized deviation between individuals. Additional factors influenced the error bar size for some animals: for *C. draconoides* size difference between front foot and hind foot was considered; for *P. bibroni* changes in foot area between curled (0.3 cm^2) and spread (0.68 cm^2) were considered; for *O. quadrata* the deviation of mass distribution on the number of legs (3 and 4) used per alternating tripod were considered.

We found that locomotor performance loss was strongly correlated with the locomotor foot pressure (Fig. 29B). The foot pressure of each locomotor was estimated using $P = \frac{mg}{nA}$, where A is the projected animal foot size determined by tracing around the perimeter of the foot and toes, and n is the number of legs used per alternating gait ($n = 2$ for *C. draconoides*, *U. scoparia*, *S. olivaceus* and *P. bibroni*, $n = 3$ and 4 for *O. quadrata* (included in the error bars), and $n = 3$ for SandBot). Fig. 29 shows that *C. draconoides* had the smallest foot pressure and exhibited approximately zero loss of performance on the weakened ground. *U. scoparia* and *S. olivaceus*, with approximately twice the foot pressure as compared to *C. draconoides*, had an $\approx 20\%$ loss of performance when the ground was weakened from LP to the onset of fluidization. *P. bibroni* had more than a three-fold larger foot pressure relative to *C. draconoides* and exhibited a more pronounced performance loss of $\approx 30\%$, whereas *O. quadrata*, with the greatest foot pressure, exhibited the highest performance loss of more than $\approx 50\%$, which approached the performance loss of the robots. The SandBot with larger foot size had a performance loss of $\approx 70\%$, relatively lower compared to its smaller foot-size counterpart, which approached a total performance loss of $\approx 100\%$ before the onset of fluidization.

To test our hypothesis that larger foot size and light body weight could help locomotors reduce their performance loss rates by passively maintaining a small leg penetration ratio, we analyzed the relationship between normalized speed and leg penetration ratio for the five animals and the simulated Xplorer robot. The normalization factors for non-dimensional speed and leg penetration ratio were slightly different from Fig. 27 since the morphology and gaits of animals were more complicated and did not have explicit forms for parameters like R and h. Here the speed $\tilde{v}_x$ for all locomotors was normalized by their speed on loosely packed granular media

($Q = 0$), and the leg penetration ratio $\tilde{d}$ was calculated as the ratio of the leg penetration depth, d, to the total leg length, l. The leg penetration depth was obtained through vertical force balance $mg = kd$, and the limb length l was obtained from direct measurements (hip to ankle length for the lizards, and knee to dactyl tip length for the crab).

The plot of speed vs. leg penetration ratio (Fig. 30) shows that, despite differences in gaits and foot morphologies, the speeds of all tested animals were also correlated with the leg penetration ratio, as predicted by the universal scaling model derived from the SandBot data. Fig. 30 also reveals that for all locomotors tested, performance was minimally affected when the leg penetration ratio $\tilde{d}$ was small, but became sensitive to leg penetration ratio at larger $\tilde{d}$. The performance decay rate increased for larger leg penetration ratio.

This universal dependence of dimensionless speed on leg penetration ratio provides an explanation for the different speed decreases among the animals (Fig. 28 inset). From Fig. 28 inset we noticed that the normalized speed of *C. draconoides* remained nearly constant as the air flow rate increased. This is because with its large foot size and light body weight, the leg penetration ratio of *C. draconoides* was sufficiently low for all ground stiffness tested ($0 \leq Q/Q_0 \leq 1$). Therefore, all *C. draconoides*' performance data (Fig. 30, blue circles and blue dashed trend line) were located within the insensitive region where performance was minimally affected by leg penetration ratio. *S. olivaceus* and *U. scoparia*, as seen from Fig. 28 inset, maintained a nearly constant normalized speed for small air flow ($Q/Q_0 < 0.3$) where the performance was insensitive to leg penetration ratio (Fig. 30, two leftmost red and green circles), but became significantly slower as the ground was further weakened and the leg penetration ratio increased beyond the critical value (Fig. 30, two rightmost red and green

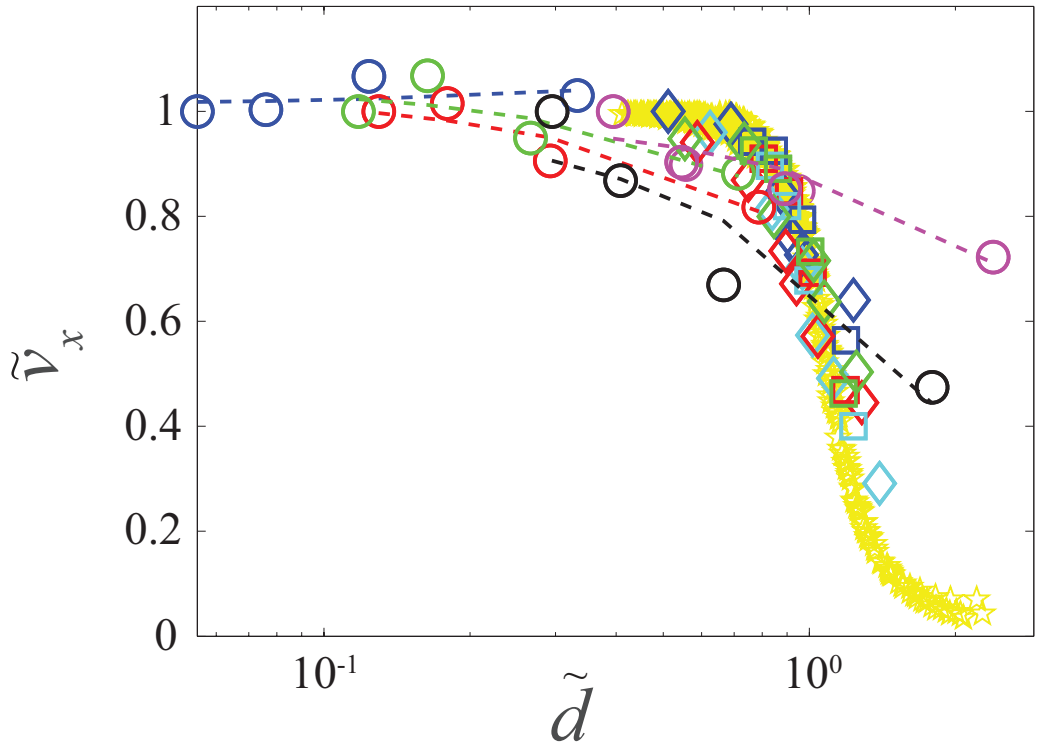

Figure 30: Normalized average speed vs. leg penetration ratio for five organisms (circles); SandBot of 2 leg widths (diamonds: w = 3.7 cm; squares: w= 2.4 cm), 4 different gait frequencies (blue: 2 rad s^{-1}; green: 4 rad s^{-1}; red: 6 rad s^{-1}; cyan: 8 rad s^{-1}) and 7 different air flow rates (Q/Q_0 between 0 and 0.64); and simulated Xplorer (yellow pentagrams) of 5 different masses between 40 and 90 g, 4 different gait frequencies between 2 and 8 Hz, and 20 different air flow rates (Q/Q_0 between 0 and 0.95). Dashed lines represent trend lines for each animal. Color convention for the five animals is the same as in Fig. 23A.

circles). Similarly, due to the large foot pressure, leg penetration ratio of *P. bibroni*, and *O. quadrata* were already relatively large (Fig. 30, purple and black circles and trend lines) and located within the sensitive region even without the air flow, and thus these two species exhibited significant performance loss as soon as the ground resistance began to decrease, and the average decay rates of performance loss were significantly higher compared to *C. draconoides*, *S. olivaceus* and *U. Scoparia*.

It is worth noting that although animals with larger foot pressures like the *P. bibroni* and the *O. quadrata* also exhibited significant performance drop for large leg penetration ratio (Fig. 30, $\tilde{d} \geq 1$), the rate of their performance loss at large penetration ratio was significantly smaller compared to the robots (i.e., SandBot and Xplorer). As seen from Fig. 28 inset and Fig. 30, animals can still maintain $\geq 50\%$ of their speed on fully fluidized ground, suggesting that they likely combine passive and active control to help maintain their locomotion performance on low stiffness substrates.

Critical flow rate analysis

To predict the effect of ground stiffness on locomotor performance, we derive an expression for the critical flow rate (defined as the point at which the locomotor speed begins to be affected significantly by leg penetration ratio) from the observed universal phenomenon, and compare to the measured values from experiment and RFT simulation.

Based on the rotary walking model, the leg penetration length is given by force

balance in the vertical direction:

$$d = \frac{m\left[g + a(\omega)\right]}{nk(Q)}, \tag{3}$$

where $k(Q)$ is the flow dependent limb penetration resistance and nk is the total resistance for the alternating gait. From the universal scaling shown in Fig. 27, non-dimensional SandBot speed began to decrease significantly with increasing leg penetration ratio at $\tilde{d} = 1$. In the $a \ll g$ limit, this gives the critical penetration resistance:

$$k^* = \frac{mg}{nl}. \tag{4}$$

Since the penetration resistance is a linear function of the flow (Fig. 22):

$$k^* = k(0)\left(1 - \frac{Q^*}{Q_0}\right) = k(0)\left(1 - \tilde{Q}^*\right), \tag{5}$$

where $\tilde{Q}^*$is the normalized critical flow rate. From Eqn. 4 and 5 we obtain:

$$\tilde{Q}^* = 1 - \frac{mg}{nlk(0)}. \tag{6}$$

For homogeneous granular media, $k = \alpha A$, and the ground resistance per unit area α is independent of the geometry of the intruder [72][2]. For loosely packed granular media with no air flow, $k(0) = \alpha_0 A$. Equation 6 can therefore be written as:

$$\tilde{Q}^* = 1 - \frac{P}{\alpha_0 l}, \tag{7}$$

where P is the foot pressure ($P = mg/nA$).

Equation 7 gives the theoretical prediction of the critical flow rate, which we compare to our experiment and simulation results. To obtain the critical flow, we fit the normalized locomotor speed vs. normalized flow rate data from experiment and simulation (Fig. 30) using stretched exponentials:

$$\tilde{v_x} = e^{-(\gamma \cdot \tilde{Q})^\beta}, \tag{8}$$

[2]To a certain degree and subject to further study.

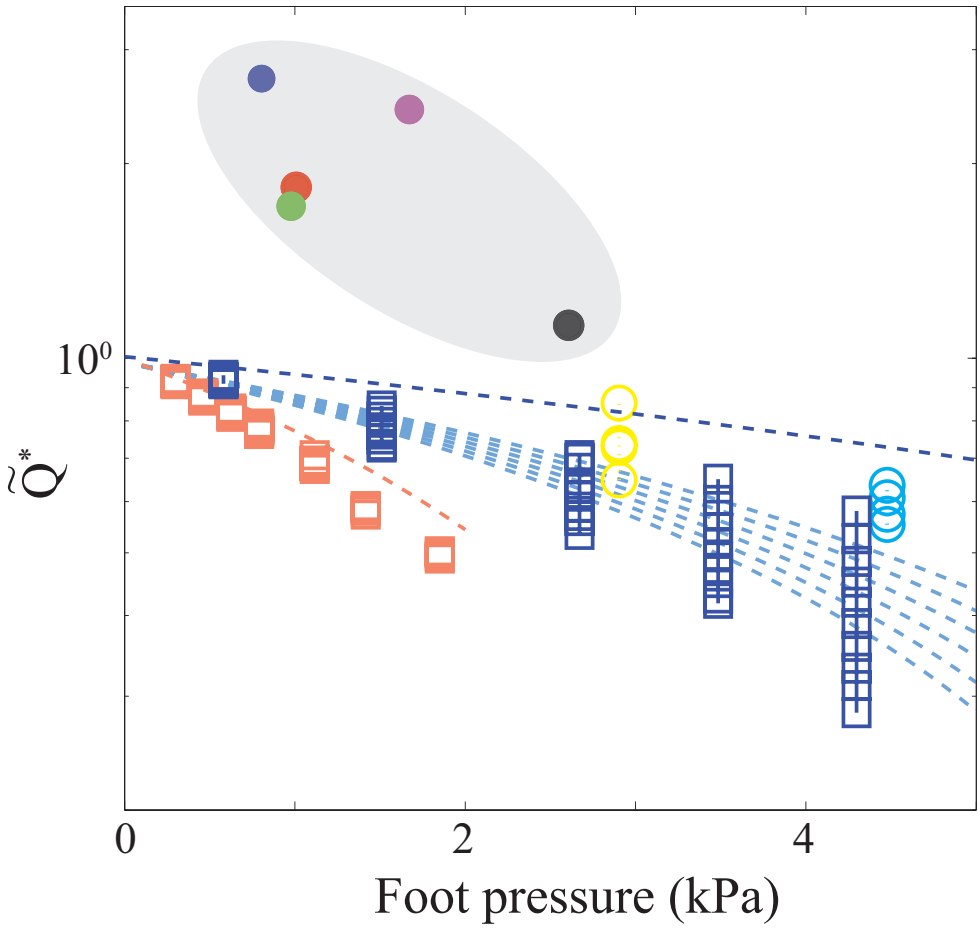

Figure 31: Normalized critical flow rate $\tilde{Q}^*$ vs. foot pressure. Filled circles represent five animals (color convention is the same as in Fig. 23A). Yellow and cyan unfilled circles represent data from SandBot experiment for two foot sizes (yellow: SandBot wide leg, $w = 3.7$ cm, "Sw" in Fig. 29; cyan: SandBot narrow leg, w= 2.4 cm, "Sn" in Fig. 29; leg frequencies are 2, 4, 6 and 8 rad s^{-1} from top to bottom markers for both foot sizes). Blue unfilled squares represent SandBot simulation (leg frequencies between 2 and 20 rad s^{-1}); Orange unfilled squares represent Xplorer simulation (leg frequencies between 2 and 16 rad s^{-1}). Top to bottom markers represent increasing body inertia. Blue and orange dashed curves represent model calculations for SandBot and Xplorer simulations with negligible body inertia, respectively. Top to bottom light-blue dashed curves represent model predictions for increasing SandBot body inertia.

where $\tilde{Q} = Q/Q_0$ is the normalized flow rate, $\tilde{v_x} = v_x/v_x(Q = 0)$ the normalized CoM average speed, and β the stretching parameter. The fitting parameter β is between 2 and 3 for almost all trials and will not be discussed here. γ is the performance loss rate under the effect of air flow, and its inverse has a direct physical meaning: $1/\gamma$ gives a normalized flow rate at which the speed has decreased significantly (to $1/e^{\beta}$). If our hypothesis is correct, the value of $1/\gamma$ obtained from the data should be close to the critical flow predicted by Eqn. 7.

Fig. 31 is a plot of the critical flow as a function of foot pressure for all locomotors studied. The model-predicted critical flow rate for Xplorer (orange dashed curve) and SandBot (blue dashed curve) with negligible body inertia agreed well with the $1/\gamma$ value obtained from both terradynamic calculation (top unfilled squares) and experimental data (top unfilled circles). Robots with increasing leg frequency and body inertia suffered significant performance loss at a smaller flow based on our model (top to bottom light blue dashed curves), which is consistent with the trend observed in our simulation (top to bottom markers).

For animals, our critical flow model qualitatively captured the trend of their performance on low stiffness ground as well as how this trend was affected by foot pressure. Like the robot model, animal performance also depends sensitively on ground stiffness, and having a large foot and a light body (i.e., smaller foot pressure) can help a locomotor passively minimize leg penetration ratio and stay insensitive to ground stiffness change. Fig. 31 reveals that animals with larger foot pressure also suffered significant performance loss at a smaller flow due to the increased sensitivity to ground stiffness change. However, our model did not capture the slower decay rate of animal performance at large leg penetration ratio (also noticeable in Fig. 30). According to our quantitative model, the normalized critical flow should always be

less than 1, because at $\tilde{Q}^* = 1$ (the onset of fluidization) the hydrostatic resistance of the ground decreases to zero, and locomotors would be unable to move forward at all if the ground reaction force was entirely due to the hydrostatic resistance [92] as the model assumes. However, the critical flow rates obtained from animal experiment were always greater than 1, which means animals can still manage to maintain relatively effective movement even on fully fluidized granular substrates with zero frictional resistance. Therefore, additional forces such as hydrodynamic granular response [102], or an added mass effect [126][2], must exist to enable the animals to maintain their locomotor performance in the "granular fluid".

2.5 Conclusion

We developed a technique to control the ground resistance over a wide range using a continuous upward air flow through a granular bed trackway. A penetration test verified that the granular substrate resistance created using this method was repeatable, and could be reduced below the loose compaction limit and reach zero resistance upon the onset of fluidization. This new ground control technique makes it possible to emulate a wide variety of natural complex terrains for locomotion studies and is especially useful in testing robot and animal locomotor limits and preparing robots for challenging environments. Using a legged robot, SandBot, as a physical model, we systematically studied how substrate properties, limb kinematics and foot size affected locomotor performance on low resistance granular ground. A resistive force theory based terradynamics simulation previously developed for GM with zero air flow successfully captured locomotor performance for all low resistance granular states with $Q > 0$. From experiment and simulation, we developed a universal scaling model which suggested that robot speed was primarily determined by the leg penetration ratio. Further locomotion experiments in five animals indicated that this

principle, derived from SandBot, can be generalized to locomotors with different leg morphology and kinematics. Analysis of animal foot pressure pointed to surprising similarities in the mechanisms used by a diversity of biological locomotors to maintain performance as the substrate property varies. It further revealed that locomotors with small foot pressure can passively minimize their leg penetration ratio as ground was weakened, and therefore maintain relatively effective performance on low resistance ground. Quantitative characterization of the critical flow rate for both robots and animals also suggests that animals likely combine passive and active control to achieve greater effectiveness on flowable substrates.

There are at least two important immediate avenues which could yield benefits to help generalize and explain our results. The first is that (as noted) there are certain aspects of the animal performance that cannot be explained using our model. We expect these are related to the vastly more complicated morphological and control elements employed by animals. As a first step toward understanding how these play a role, future studies should examine muscle activity in the limbs [115] to look for neuromechanical control principles and how they can help animals take advantage of the frictional and hydrodynamic [102][2] aspects of material response. The second avenue involves changes in particle shape and heterogeneity. Our study used model granular substrates, which were more regular in shape as compared to natural substrates, to facilitate comparison between experimental results and numerical simulations. But as previously measured in intrusion tests, these model granular substrates behaved similarly to natural sand [72]. We therefore expect that the results obtained using model granular substrates can be applied to more complex flowable terrains. Regarding substrate heterogeneity, we expect our recent robotic studies of locomotion in granular "boulder fields" [99] can provide hypotheses for templates for locomotion control when feet encounter large asperities, common in natural environments.

CHAPTER III

EFFECT OF SUBSTRATE RESPONSE ON TERRADYNAMIC PERFORMANCE FOR HOMOGENEOUS GRANULAR GROUND

3.1 Summary

We study the locomotor mechanics of a small, lightweight robot (DynaRoACH, 10 cm, 25 g) which can move on a granular substrate of 3 mm diameter glass particles at speeds up to 5 body length/s, approaching the performance of certain desert-dwelling animals. To reveal how the robot achieves this performance, we used high speed imaging to capture its kinematics, and developed a numerical multi-body simulation of the robot coupled to an experimentally validated simulation of the granular medium. Average speeds measured in experiment and simulation agreed well, and increased nonlinearly with stride frequency, reflecting a change in propulsion mode. At low frequencies, the robot used a quasi-static "rotary walking" mode, in which the substrate yielded as legs penetrated and then solidified once vertical force balance was achieved. At high frequencies the robot propelled itself using the speed-dependent fluid-like inertial response of the material. The simulation also allows variation of parameters which are inconvenient to modify in experiment, and thus gives insight into how substrate and robot properties change performance. Finally, our study reveals how lightweight animals can achieve high performance on granular substrates; such insights can advance the design and control of robots in deformable terrains [1].

[1]This Chapter is a paper by Feifei Qian, Tingnan Zhang, Chen Li, Pierangelo Masarati, Paul Birkmeyer, Andrew Pullin, Aaron Hoover, Ronald S. Fearing, and Daniel I. Goldman, *Robotics: Science and Systems (RSS)* [102]

3.2 Introduction

There is an increasing need for robots to traverse a diversity of complex terrain. Platforms have been developed that can effectively run on fractured rigid ground [105], [109], crawl within concave surfaces [133], and climb on walls [57]. However, relative to biological organisms [68], manmade devices often have poor locomotor ability on granular substrates like sand and gravel. For example, in wheeled and tracked vehicles, wheel slippage and sinkage can cause significant performance loss [82].

Granular media are collections of particles that interact through dissipative, repulsive contact forces [49]. Forced granular media remain solid below the yield stress but flow like a fluid when the yield stress is exceeded [91]. The solid-fluid transition presents great challenges for terrestrial devices moving on granular media. For example, previous studies [71] demonstrated that a bio-inspired RHex-class legged robot, SandBot (30 cm, 2.3 kg), walked effectively at up to 1 body length/s on granular media at low to intermediate stride frequencies, where the granular material behaved like a yielding solid. The granular material yielded as the legs penetrated until vertical force balance was achieved. The granular material then solidified under the legs while the body lifted and moved forward, as if the robot were walking on a solid. At high stride frequencies, however, because the legs encountered previously disturbed ground, the granular material around the legs became continuously fluidized, and the robot "swam" forward slowly ($\sim$ 0.01 body length/s) using drag on the legs to overcome belly drag.

In contrast, a variety of animals live in the deserts and move rapidly across granular surfaces. For example, the zebra-tailed lizard (*Callisaurus draconoides*, $\sim$ 10 cm,

$\sim$ 10 g) can run at speeds over 100 cm/s (10 body length/s) on sand. Unlike SandBot which must penetrate a large portion ($> 70\%$) of its limbs to move on granular media, the lizard is light enough that even while running it only penetrates a small portion ($< 30\%$) of its limbs to generate force [68]. This suggests that a small, lightweight body may confer advantages for locomotion on deformable surfaces such as granular media.

Recent advances in the technique of smart composite microstructures (SCM) [132] have enabled the development of small, lightweight robots ($\sim$ 10 cm, $\sim$ 20 g) [41] [12] like DynaRoACH (Fig. 32A). These robots are similar in size to the zebra-tailed lizard (among other myriad desert vertebrates and invertebrates [89], [17]) and can achieve performance approaching animals ($\sim$ 10 body length/s) on solid surfaces. Therefore, in addition to advancing locomotor capabilities of devices on complex terrain [70], these lightweight robots provide promising physical models to study how effective legged locomotion can be achieved on granular substrates in small, high-performing animals.

A challenge for studying locomotion on granular media is the lack of comprehensive force models at the level of the Navier-Stokes equations for fluids [124]. Recently an experimentally validated discrete element method (DEM) simulation (described below) of a model granular medium (3 mm diameter glass particles) was developed and successfully captured the locomotor mechanics of a sand-swimming lizard moving within granular media [79]. The DEM simulation provides a tool to obtain accurate, detailed information such as forces and flow fields of the media during intrusions relevant to locomotion. Such information is challenging to obtain in experiments, since force platforms [10] and 3D particle image velocimetry (PIV) techniques are not yet developed for deformable opaque ground.

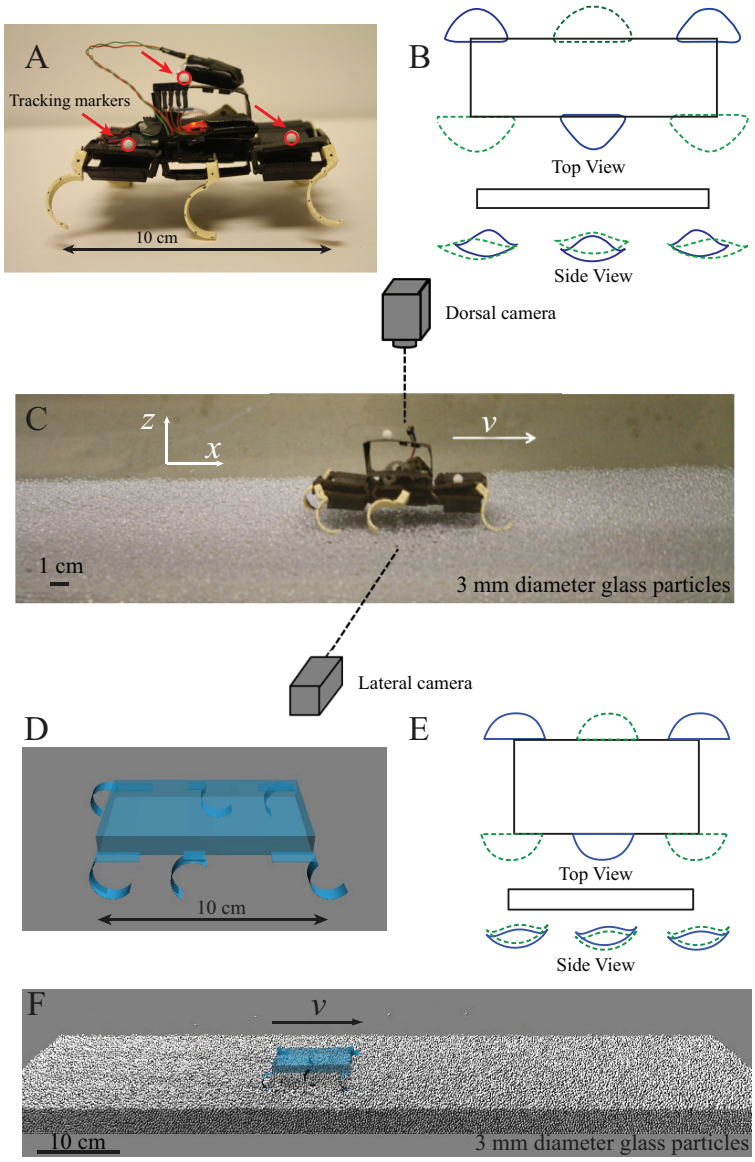

Figure 32: Locomotion experiment and simulation. (A) The lightweight, hexapedal DynaRoACH robot resting on a bed of 3 mm diameter glass particles. (B) Leg tip trajectories from top view and side view. Blue and green trajectories denote the two alternating tripods. (C) High speed video experimental setup. (D) Simulation of the robot using MBDyn (E) Leg tip trajectories in simulation. (F) Simulation of the robot running on a bed of 3 mm particles.

In this paper we reveal basic principles of movement of lightweight locomotors on granular media using a combination of laboratory experiment and computer simulation. We perform studies of DynaRoACH on a medium of small glass particles. To obtain estimates of ground reaction forces that result in high performance, we integrate the DEM simulation with a multi-body dynamic simulation of the robot. Our study reveals for the first time that qualitatively different propulsion mechanisms exist for low and high frequency movement on granular media. While the low frequency locomotion of DynaRoACH can be understood using a previously introduced "rotary walking" model, at higher frequency, the robot utilizes the hydrodynamic response of the granular medium to achieve high performance through sustained fluidization of the ground. Furthermore, we use the simulation to systematically vary parameters like friction (particle-particle and particle-leg) that are inconvenient to modify in experiment, and demonstrate performance and stability limits. We also demonstrate that limb size of the robot modifies the walk-run transition. We expect that the mechanics discovered here and the tools we have developed should be applicable to other devices and provide a starting point to understand biological locomotion and develop robot designs on more complex deformable substrates, like leaf litter and mud.

3.3 Materials and Methods

3.3.1 Experiments

Robotic platform

The DynaRoACH robot used in this study (Fig. 32A) is a small, lightweight (10 cm, 25 g), bio-inspired hexapedal robot [41]. It has six c-shaped legs (radius 1 cm) and uses an alternating tripod gait. All six legs are driven by a single motor through body linkages. The motor is controlled by a centralized controller mounted close to

the center of mass (CoM) of the robot. Control parameters like stride frequency, running time, and PID control gains are set on a PC and communicated to the controller through a Bluetooth wireless interface.

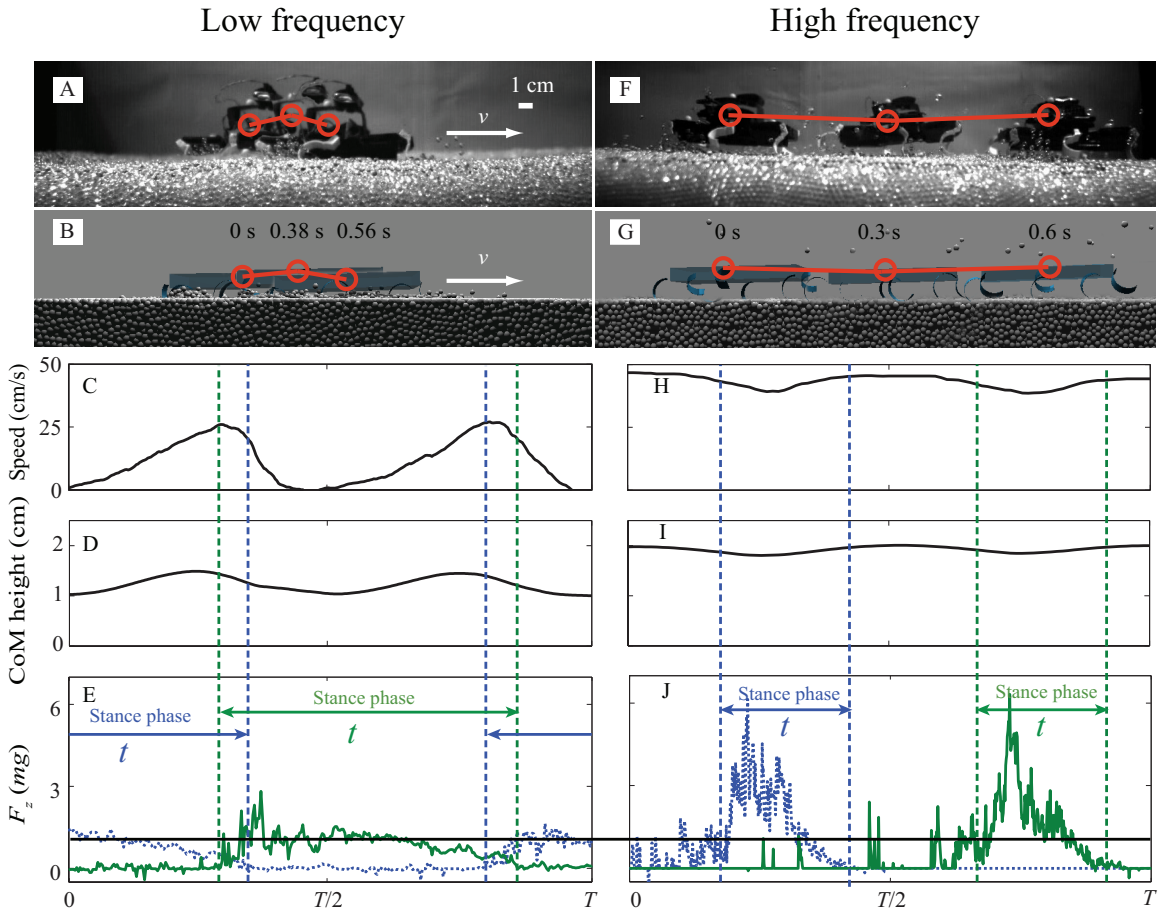

Figure 33: Two locomotion modes observed for the robot moving on granular media. (A-E) Walking at low frequencies (e.g., 3 Hz). (F-J) Running at high frequencies (e.g., 11 Hz). (A, F) Sideview of the robot in experiment. (B, G) Sideview of the robot in simulation. (C, H) Instantaneous forward speed vs. time. (D, I) Body height vs. time. (E, J) Vertical ground reaction force on a tripod vs. time. Dashed blue curve and solid green curve are for the two alternating tripods. Black horizontal line indicates body weight (mg). In (A, B) and (F, G) the three time instants shown are the start, middle, and end of three different stances. In (C-E) and (H-J) data are shown for simulation only. Duty factor is stance duration t divided by stride period T.

Model granular media

We used 3.0 ± 0.2 mm diameter glass particles (density = 2.47 g/cm^3) as the granular medium (see Fig. 32C). The large size of the particles reduces computation time in the simulation portion of the study, facilitating a direct comparison between experiment and simulation. While these particles are larger than most natural sand grains, they have similar qualitative behavior in response to intrusion; a previous study [79] also demonstrated that these particles were a good model for studying locomotion (swimming) within granular media.

In nature, granular media exist in a range of compactions, measured by the volume fraction ϕ (the ratio between the solid volume and the occupied volume). For dry granular media, ϕ can vary from $0.57 < \phi < 0.64$ [20], although this range is influenced by particle friction [52]. The yield strength of a granular medium generally increases with ϕ [71], [34] and affects locomotor performance on the granular medium [71]. In our study, we prepared the granular medium into a closely packed state ($\phi = 0.63$). However, we found that our results did not qualitatively change for different ϕ (e.g., robot speed was insensitive to ϕ), likely because the robot penetrated its legs into the granular medium to depths of only a few particle diameters and the range of achievable ϕ was small ($0.61 < \phi < 0.63$) in the low friction 3 mm particles.

Locomotion experiments

We ran the DynaRoACH robot on a 75 cm long, 30 cm wide trackway filled to a depth of 6 cm (Fig. 32C). We pressed the particles bed using a flat plate before each trial to prepare the particles to a closely packed state. Running kinematics were captured by two high speed video cameras (AOS X-PRI) from both top and side views at a frame rate of 200 fps. One high contrast dorsal marker was bonded above the robot

center of mass to obtain average forward speed; two lateral markers were bonded on the front and rear of the robot body to obtain CoM height (approximated by the average vertical position of the two markers). Stride frequency was determined from the videos.

Leg trajectories

To capture prescribed leg trajectories, the robot was suspended in the air and the trajectories of the leg tips were recorded as the motor rotated. During a cycle, each leg rotated backward about the hip (retraction), lifted-up sideways, and swung forward (protraction) (Fig. 32B). Leg kinematic parameters such as the fore-aft swing angle and lateral lifting angle were determined by tracking the markers on the legs and used to guide tuning of leg trajectories in simulation. We define a stride period T as the time between the start of two consecutive retraction phases, and stance as when the leg generates ground reaction force (determined from simulation).

3.3.2 Simulation

Discrete element method to model contact forces

To investigate locomotion of DynaRoACH in more detail, a simulation of the robot was developed and coupled to a granular media simulation. This granular simulation used the discrete element method (DEM) to compute the particle-particle and particle-leg interaction for the 3 mm diameter glass particles. As in previous work [79], the DEM simulation was validated by matching the forces on intruders moving in the granular medium (e.g., a rod dragged horizontally) with experimental measurements.

In the DEM simulation, the normal contact force between an interacting pair of

particles is given by a standard force law [46], a Hertzian repulsion and a velocity dependent dissipation (to account for a coefficient of restitution):

$$F_n = k\delta^{3/2} - G_n v_n \delta^{1/2}; \tag{9}$$

the tangential contact force is modeled as Coulomb friction:

$$F_s = \mu F_n \tag{10}$$

where δ is the deformation (virtual overlap) between contacting particle pairs or particle-leg pairs, v_n the normal component of relative velocity, $k_n = 2 \times 10^6$ kg $\cdot$ s^{-2} $\cdot$ m$^{-1/2}$ and $g_n = 15$ kg $\cdot$ s^{-1} $\cdot$ m$^{-1/2}$ the contact stiffness and viscoelasticity dissipation coefficient, and $\mu_{\{pp,pl\}} = \{0.1, 0.3\}$ the particle-particle and particle-leg friction coefficients. The restitution and friction coefficients were experimentally measured and validated in a rod drag experiment [79]. Once the parameters were set in the DEM simulation, the robot locomotion could be accurately predicted over a wide range of conditions. The simulated granular bed (3×10^5 particles) was 60 PD (particle diameter) in width, 15 PD in depth, and 290 PD in length, and had frictionless boundaries (Fig. 32F). At low frequencies we used a shorter granular bed (90 PD) containing 1×10^5 particles to save computation time.

Dynamic simulation of the robot

To model the robot we used a multi-body dynamic simulator, MBDyn [8], which allows time domain simulation of multi-body mechanical systems from first principle equations. MBDyn features a full 3D simulation with six translation and rotation degree-of-freedoms. This is essential for locomotion on the surface during which pitch, roll, and yaw are often present [70].

In the dynamic simulation, the robot was constructed with similar body and leg geometries as the actual robot (Fig. 32D). The simulated robot was composed of 13

individual rigid parts: one box-shaped body, six c-shaped legs, and six linking plates between legs and body. The legs of the actual robot were not perfectly rigid but experimental observations showed little leg deformation during locomotion on granular media. The joints between the link plates and c-legs allowed front-back swing of the legs while the plate-body joints allowed sideway lifting of the legs. Tuning kinematic parameters for the joint movements produced leg trajectories that resembled experimental measurements (Fig. 32E) without mimicking the internal linkage of the actual robot.

Integration of DEM with dynamic simulation

We combined MBDyn with the DEM code to simulate robot locomotion on granular media via a communication interface (a UNIX socket using C++). At each time step, MBDyn integrated the equations of motion for the robot combined with the force and torques calculated from the DEM code. The updated kinematics including position, orientation, velocity, and angular velocity of each part of the robot were then passed back to the DEM code to compute the force and torque on all interacting elements at the next time step. The time step was 1 μs set by the particle collision time in DEM.

In addition to the kinematics during locomotion (e.g., CoM position and velocity, stride length, limb penetration depth), the dynamics during locomotion (e.g., net ground reaction force on each limb and tripod) were also determined from the simulation.

Kinematic predictions based on previous work

Because the small DynaRoACH robot has similarly shaped c-legs to the larger SandBot, we use the rotary walking model developed for SandBot [71] to make two kinematic predictions for the locomotion of the DynaRoACH robot on granular media. We will then test these predictions in both experiment and simulation.

First, we predict that both the body height and forward speed will increase during stance and decrease between stances. For walking at low frequencies, leg intrusion speeds will be small enough that granular forces will be dominated by friction, and therefore independent of speed, increase with depth (hydrostatic-like) [4], [38]. As a result, during each step, the legs will initially slowly penetrate into granular medium while the body rests on the surface. As the legs penetrate deeply enough for the lift on the legs to balance the weight and vertical inertial force of the body, the legs should stop penetrating and rotate atop solidified granular media, lifting the body and kinematically propelling it forward. As the legs withdraw from the granular medium, the body should fall and forward speed will decrease to zero. We refer to this as rotary walking in SandBot, and expect to see these features in the small robot.

Second, based on the rotary walking model, we predict that stride length should decrease with stride frequency. In the quasi-static rotary walking mode, stride length is inversely related to leg penetration depth by geometry. As stride frequency increases, because the inertial force of the body during body lift-up increases, the legs should penetrate more deeply, and therefore the stride length will decrease. In addition, the transition from walking to swimming should be triggered by the reduction in stride length—at high enough stride frequency, stride length should become small enough that the legs will encounter previously disturbed material during each step.

3.4 Results and Discussion

3.4.1 Kinematics

The time-averaged forward speed of the robot measured in both experiment and simulation (Fig. 34A) agreed well, and increased monotonically with stride frequency. At the highest stride frequency (12 Hz) tested in experiment, the robot reached a speed of 50 cm/s (5 body length/s), comparable to slow runs of the zebra-tailed lizard. Calculated stride length (Fig. 34B) decreased with stride frequency from low ($0-3$ Hz) to intermediate frequencies ($4-6$ Hz) but increased with stride frequency at high frequencies ($7-12$ Hz). Duty factor (the percentage of the total stride period during which the limb is in contact with the ground) measured in simulation (Fig. 33E, J) fell below 0.5 at intermediate frequencies of ~ 6 Hz (Fig. 34C), indicating the onset of aerial phases. Closer examination of the kinematics revealed that the robot displayed a transition in locomotor mode as stride frequency increased:

Walking at low stride frequencies

At low stride frequencies (e.g., 3 Hz, Fig. 33A−E), as predicted, the DynaRoACH robot used a quasi-static rotary walking locomotor mode, where forward speed increased sub-linearly with stride frequency (i.e., stride length decreased; Fig. 34B). Instantaneous forward speed also increased from 0 to 25 cm/s during most of stance and then dropped to zero (Fig. 33C). Vertical position of the CoM tracked in simulation (Fig. 33A, B, D) showed that average body height was 1.28 ± 0.03 cm during stance, increased by 0.46 ± 0.03 cm (38% of the standing body height 1.2 cm) during most of stance, and then decreased by the same amount.

The observed decrease in stride length with stride frequency, increase in body height and forward speed during most of stance, and decrease in body height and

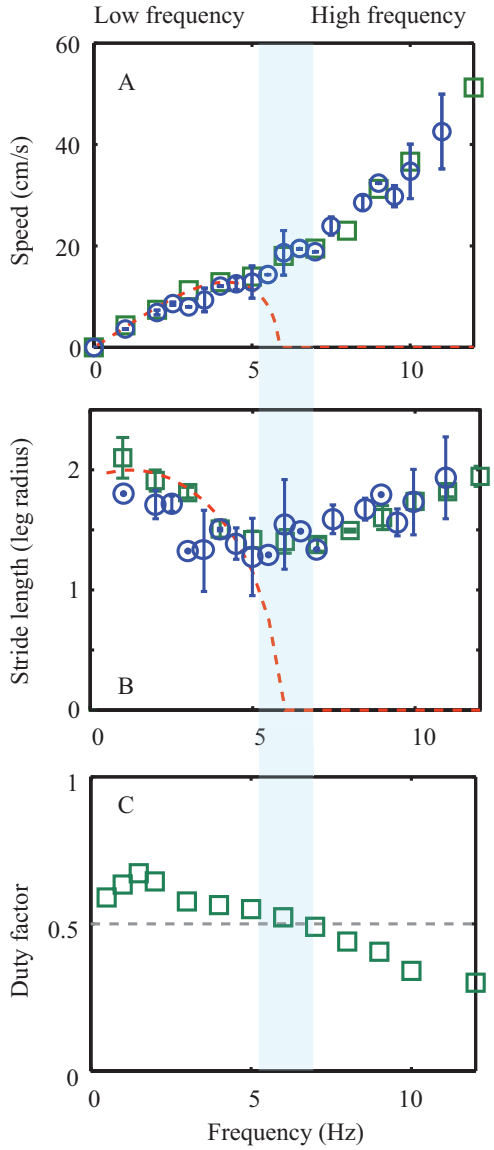

Figure 34: Performance and gait parameters. (A) Average forward speed vs. stride frequency (blue: experiment; green: simulation). (B) stride length vs. stride frequency (blue: experiment; green: simulation) (C) duty factor vs. stride frequency (simulation only). Dashed red curves in (A, B) are predictions from the rotary walking model [71]. Error bars indicate standard deviation.

forward speed between stances were in accord with the rotary walking model [71] (Fig. 34A, B, red curve). This suggests that like SandBot, the small DynaRoACH robot also rotary-walked on solidified granular media at low frequencies.

The decrease in body height and forward speed occurred at the start of stance; however, this does not contradict the rotary walking model, but is a consequence of the different leg trajectories of the small robot and SandBot. Because SandBot rotates its legs in circular trajectories, its body must rest on the surface between two tripods, resulting in stance phase that begins during the retraction phases of legs. The small DynaRoACH robot instead uses protraction-retraction leg trajectories, which result in stance phases that begin during protraction phases of the legs.

Running at high stride frequencies

At high stride frequencies (Fig. 33F−J, 11 Hz) the DynaRoACH robot exhibited a different locomotor mode than predicted by the rotary walking model. The forward speed of DynaRoACH increased super-linearly with stride frequency (i.e., stride length increased; Fig. 34B). Instantaneous forward speed was always greater than zero and decreased during the first half of stance. It then increased during the second half of stance (Fig. 33H). The average body height measured in simulation was 1.86 ± 0.02 cm above the surface (Fig. 33F, G, I), which was 0.58 cm (48% of the standing body height 1.2 cm) higher than that at low frequencies. Body height decreased by 0.19 ± 0.02 cm (16% of the standing body height 1.2 cm) during the first half of stance and increased by the same amount during the second half of stance. Simulation revealed that grains around the intruding legs remained fluidized throughout the stance phase.

While these kinematics were different from those predicted by the rotary walking model (Fig. 34A, B, red curve), they also differed from the slow surface swimming which SandBot used at high stride frequencies [71], in which the body height remained constant while the belly lay on the surface and forward speed was small ($\sim$ 1 cm/s). The decrease in body height and instantaneous forward speed during the first half of stance, the monotonic increase of average forward speed with stride frequency, and the aerial phases observed in the small robot at high stride frequencies resembled those observed in the zebra-tailed lizard running on granular substrates [68], which follows a spring-loaded inverted pendulum (SLIP) model [13]. This suggested that unlike SandBot but like the zebra-tailed lizard, the small robot used a SLIP-like running mode at high frequencies.

3.4.2 Vertical ground reaction force

To understand the mechanism of the transition in locomotor mode from walking at low frequencies to running (but not swimming) at high frequencies, we examined in simulation the vertical ground reaction force, F_z, on a tripod of legs. For animals and legged robots moving on deformable or yielding substrates such as the surface of water [29] or granular surfaces [68], [71], it is critical to generate sufficient F_z to balance the weight and inertial force of the body before legs sink too deeply into the substrate. Averaged over a cycle, lift must equal the body weight, i.e., $\frac{1}{DT}\int F_z dt = mg$, where mg is the body weight of the robot, T the cycle period, and D the duty factor defined as the stance duration divided by T.

At low stride frequencies (e.g., 3 Hz), because duty factor was greater than (but close to) 0.5, the F_z on both tripods was close to the body weight for most of the cycle (Fig. 33E). As duty factor decreased below 0.5 with increasing stride frequency,

the F_z on both tripods no longer overlapped, and the magnitude of F_z on each tripod increased. The peak of F_z increased from $\sim 1\ mg$ at 3 Hz (Fig. 33E) to $\sim 6-7\ mg$ at 12 Hz (Fig. 33J). Peak torque on a tripod about the hips measured in simulation at 12 Hz was 10 mN-m; this was less than the stall torque of the motor-gearbox system.

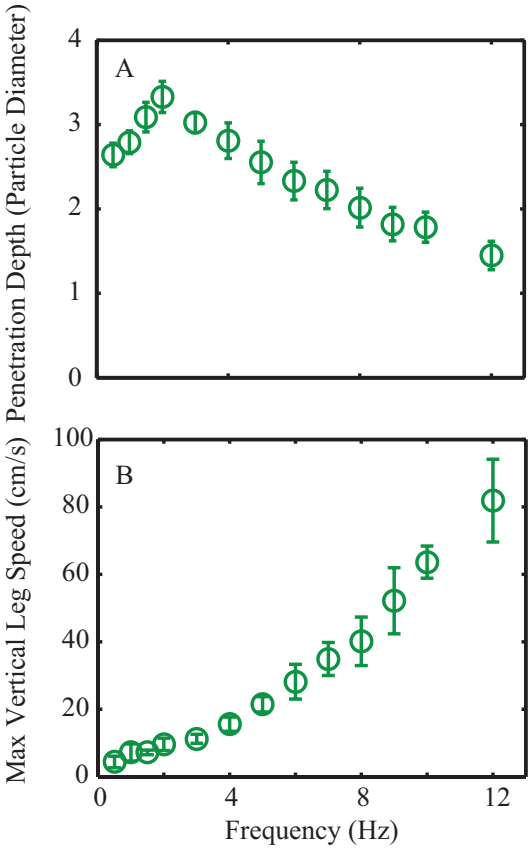

Figure 35: Limb penetration and intrusion speed measured in simulation. (A) Maximal leg penetration depth (measured in particle diameters) vs. stride frequency. (B) Maximum leg vertical penetration speed vs. stride frequency. Error bars indicate standard deviation.

The large increase in F_z at high frequencies was likely a result of a material response to leg intrusion and differed from the friction-dominated yielding observed in the SandBot study. This is because the SandBot walking model based on the friction-dominated hydrostatic-like forces could only explain the mechanism governing the increase in F_z at low frequencies. At low frequencies (< 3 Hz), the granular force was

friction-dominated, and therefore was assumed to be independent of intrusion speed and to increase with penetration depth. As stride frequency increased, this depth dependent granular force increased due to the increasing inertial force associated with lifting of the body [71], resulting in an increasing penetration depth (Fig. 35A). At high stride frequencies (> 3 Hz), however, the measured leg penetration depth decreased instead (Fig. 35A), counter to the rotary walking model prediction. In this case, the walking model predicted a decrease in the lift force on the legs, contrary to observations (Fig. 33E, J).

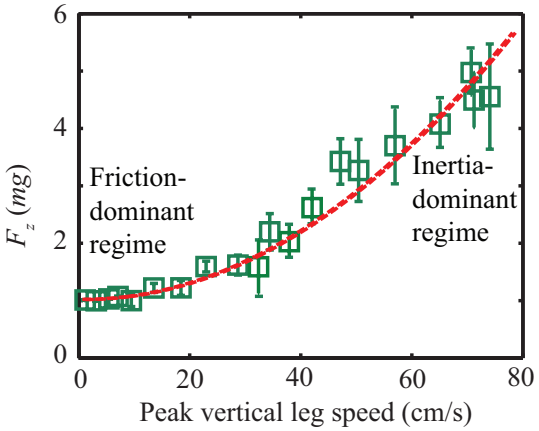

Figure 36: Vertical ground reaction force vs. peak leg penetration speed. Dashed red curve indicates quadratic fit $F_z/mg = \alpha v^2 + 1$ with fitting parameter $\alpha = 5.7 \times 10^{-3}$ cm^{-2}s^2 and with non-zero intercept at mg. Error bars indicate standard deviation.

This discrepancy suggests that there must be additional contribution to the force at high frequencies. Examination of leg kinematics in simulation revealed that the vertical penetration speed of the legs increased with stride frequency and reached nearly 1 m/s at 12 Hz (Fig. 35B). It is known that the granular forces during high speed impact are hydrodynamic-like and increase quadratically with impact speed [55], [30]. Our data of lift vs. vertical leg penetration speed (Fig. 36, green squares) can be described approximately by a quadratic with a non-zero y-intercept (Fig. 36, red curve),

due to the finite yield stress of the medium. We hypothesize that as the vertical leg penetration speeds increased, the inertial force of the grains being accelerated by the legs becomes important and contributes significantly to the vertical ground reaction force. In other words, at high frequencies, instead of swimming, the robot runs on the granular material that behaves like an inertial fluid, much like the basilisk lizard (*Basiliscus*), the so-called "Jesus Christ lizard" that runs on the surface of water [29].

We used previous intrusion studies in granular media to estimate the transition frequency for the DynaRoACH robot. Studies of horizontal drag and vertical impact in granular media [4], [55], [30] suggest that inertial effects become important for intrusion speeds beyond $v_c \sim (2gd)^{1/2}$, where d is the particle diameter and g the gravitational acceleration. For 3 mm glass particles, $v_c = 25$ cm/s. This indicates that hydrodynamic-like force should become significant as the vertical leg penetration speed increases beyond $\sim$ 25 cm/s, or as stride frequency increases past $\sim$ 6 Hz (Fig. 35B). This matches the observed transition in locomotor mode around 6 Hz (Fig. 34). We posit that this transition of the propulsion mechanism from low frequency (i.e., low vertical penetration speed) walking on yielding ground to high frequency (i.e., high vertical penetration speed) running on fluidizing ground is generic to locomotion on granular media. However the frequency at which the walk-to-run transition occurs should depend on parameters associated with the granular media as well as the robot morphology and kinematics.

The capability of the small robot to run rapidly at high frequencies on granular media by using hydrodynamic-like forces, in contrast to SandBot's slow swimming, suggests that lightweight locomotors have an advantage when moving on granular surfaces. Indeed, the small robot's legs are relatively large (~ 1.4 cm^2) compared to its

body weight (25 g) (each leg applies a pressure of 800 Pa when standing), and can generate enough hydrodynamic-like lift by paddling its legs rapidly to maintain the body well above the surface. By contrast, SandBot's legs are relatively small ($\sim$ 5 cm^2) compared to its body weight (2300 g) (each leg applies a pressure of $\sim 1.5 \times 10^4$ Pa when standing), and cannot generate enough hydrodynamic-like lift to support the body before the legs sink deeply enough to encounter previously disturbed material over steps and trigger swimming. This may explain why the zebra-tailed lizard, the highest-performing among desert lizards of similar size, has the largest hind feet [68].

3.5 Conclusion

Inspired by the high performing desert animals moving on granular media, we studied the locomotion of a lightweight, bio-inspired, legged robot on a granular substrate and developed an experimentally validated computer simulation of the locomotion. Kinematics measured in simulation matched experiment and enabled examination of ground reaction forces responsible for the high locomotor performance. The small robot displayed a transition in locomotor mode from walking at low frequencies to running at high frequencies. At low frequencies, hydrostatic-like forces generated during the yielding of the granular material ultimately led to solidification of the material, and the robot moved as if it were walking on a solid surface. At high frequencies, however, the inertia of the grains being accelerated became important and forces became hydrodynamic-like. In this regime the robot ran rapidly by paddling legs on fluidized granular material.

Our results reveal that lightweight robots can achieve high locomotor performance on granular media by exploiting fluid properties of the granular material. This locomotion mode is distinct from previously observed low frequency yielding walking

strategy, and provides a better understanding of fundamental locomotive modes for a broad class of granular substrates. The simulation of the lightweight robot platform enables detailed examination of legged locomotion, and provides likely the best model to date of a robot running on granular media. In addition, the simulation tool we have developed can be used to systematically test the effect of both locomotor and substrate properties on locomotor performance, which can guide the design, control and power consumption estimates for high-performing multi-terrain robot platforms.

Finally, we note that while experiment and simulation allow detailed investigation of mechanics of movement on granular media, a complementary approach is needed, that of low order dynamical models that can be used to gain insight into the critical mechanics of dynamical running. In our future work, we will investigate if a dynamic force law that describes the hydrodynamic-like forces during high speed leg intrusions can be obtained from measurements in DEM simulation. We posit that a generalized locomotion model similar to the Spring-Loaded Inverted Pendulum (SLIP) [13] can be developed based on the force law, and can extend our current study to more generalized conditions. This generalized model will shed light on the locomotor dynamics of legged animals and robots on granular media, as well as guide development for analytically tractable low order models.

CHAPTER IV

TERRAIN CREATION AND LOCOMOTION TESTING FOR LEGGED LOCOMOTION ON HETEROGENEOUS GRANULAR GROUND

4.1 Summary

Particulate substrates like deserts or Martian terrain are often composed of collections of particles of different sizes and shapes. While much is known about how robots can effectively locomote on hard ground and increasingly on homogeneous granular ground, the principles of locomotion over heterogeneous granular substrates are relatively unexplored. In this study we test the locomotion performance of an open-loop controlled legged robot (Xplorerbot, 15 cm, 150 g) in a trackway filled with 3 mm diameter glass fine grains, with two parallel lines of eight 25.4 mm diameter large glass "boulders" embedded within. In both experiment and simulation, we observe three distinct modes of robot leg-ground interaction which influence locomotion performance, and a chaotic dynamics in robot trajectories which sensitively depended on initial conditions. To systematically investigate how heterogeneity distribution and robot initial conditions affect the interaction modes and robot trajectories, we develop an automated system which can vary the properties of the heterogeneous granular substrate, as well as record robot locomotion performance. The system allows collection of $\sim$ 200 runs/day, facilitating systematic parameter exploration and comparison to simulation [1].

[1]This Chapter is a paper by Feifei Qian, Tingnan Zhang, Kevin Daffon, and Daniel I. Goldman, *in Proceedings of the International Conference on Climbing and Walking Robots (CLAWAR)* [99]

4.2 Introduction

Substrates that are rocky and loose are often found in environments that field robots must traverse; such terrains can contain granular media (GM) with particle sizes spanning multiple orders of magnitude (Figure 37b). When small robotic locomotors like PackBot or RHex (Figure 37a) travel across these flowable types of terrain [72], they exhibit characteristic failure modes (slips, unstable foot-holds, impassable barriers, or a limb/tread fluidization of a thin layer of smaller particles), which significantly affect robot stability, trafficability and power consumption. A major challenge in creating the next generation of mobile robots is expanding the scope of terramechanics [7][130] from large tracked and treaded vehicles on homogeneous ground to arbitrarily shaped and actuated locomotors moving on and within complex heterogeneous terrestrial substrates. However, in typical heterogeneous environments, the force fluctuations introduced by heterogeneities during intrusion and drag can be largecomparable in size to the average force, making the applicability of continuum terramechanics [7][130] unclear. Currently, most terrestrial vehicles (including mobile robots) are tested on substrates made of standardized homogenous media (e.g. Ottowa sand [86], lunar simulants [37]).

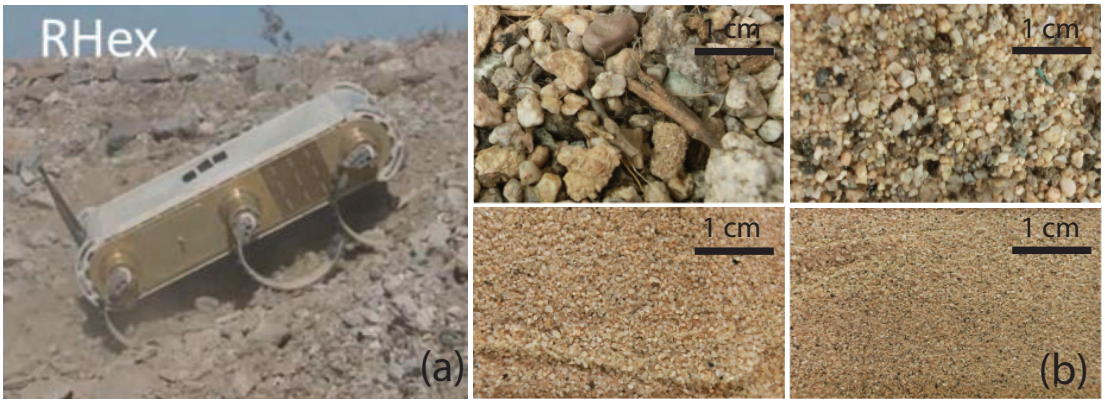

Figure 37: Natural heterogeneous terrain. (a) RHex robot traveling across heterogeneous gravel substrate (photo courtesy Alfred Rizzi, Boston Dynamics). (b) Sieved Mojave desert GM.

4.3 Experimental robot locomotion test and numerical modeling

To gain insight into robot locomotion on heterogeneous ground, in this paper we extend techniques from our previous studies [71, 98] to create repeatable states of GM with controlled heterogeneity. We used a hexapedal locomotor: an open-loop controlled small legged robot (Xplorer, 15 cm, 150 g, Figure 38a, b) to perform laboratory experiments. We initially tested the robot in a model desert-like heterogeneous terrain: a bi-dispersed granular test bed filled with 3 mm diameter small particles (simplified fine grains) with larger 25.4 mm diameter glass particles (simplified boulders) randomly embedded within (Figure 38c, d). The symmetrical geometry of the particles simplifies the leg-ground interaction, and makes it feasible to integrate experiment with our experimentally validated DEM simulations [102]. The kinematics of the robot were captured by two high speed cameras (AOS X-PRI) from both top and side views at a frame rate of 250 frames per second (FPS). High contrast dorsal markers were painted on the robot to obtain speed and trajectory information.

We extend our previous homogeneous granular media DEM simulation [102] for heterogeneous ground conditions. The granular bed in simulation ($\sim 2 \times 10^5$ particles) was 60 particle diameters (PD) in width, 15 PD in depth, and 180 PD in length, and has frictionless boundaries (Figure 38d). In addition, we introduced heterogeneity to the sand bed by generating $10 \sim 20$ randomly distributed glass boulders (25.4 mm diameter). To model the Xplorer robot, as in [102] we use a multi-body dynamic solver (MBDyn) and coupled it with our particle simulation(Figure 38b). By integrating the equations of motion using the force computed from DEM, we could reconstruct the locomotion of the robot on both homogeneous and heterogeneous GM.

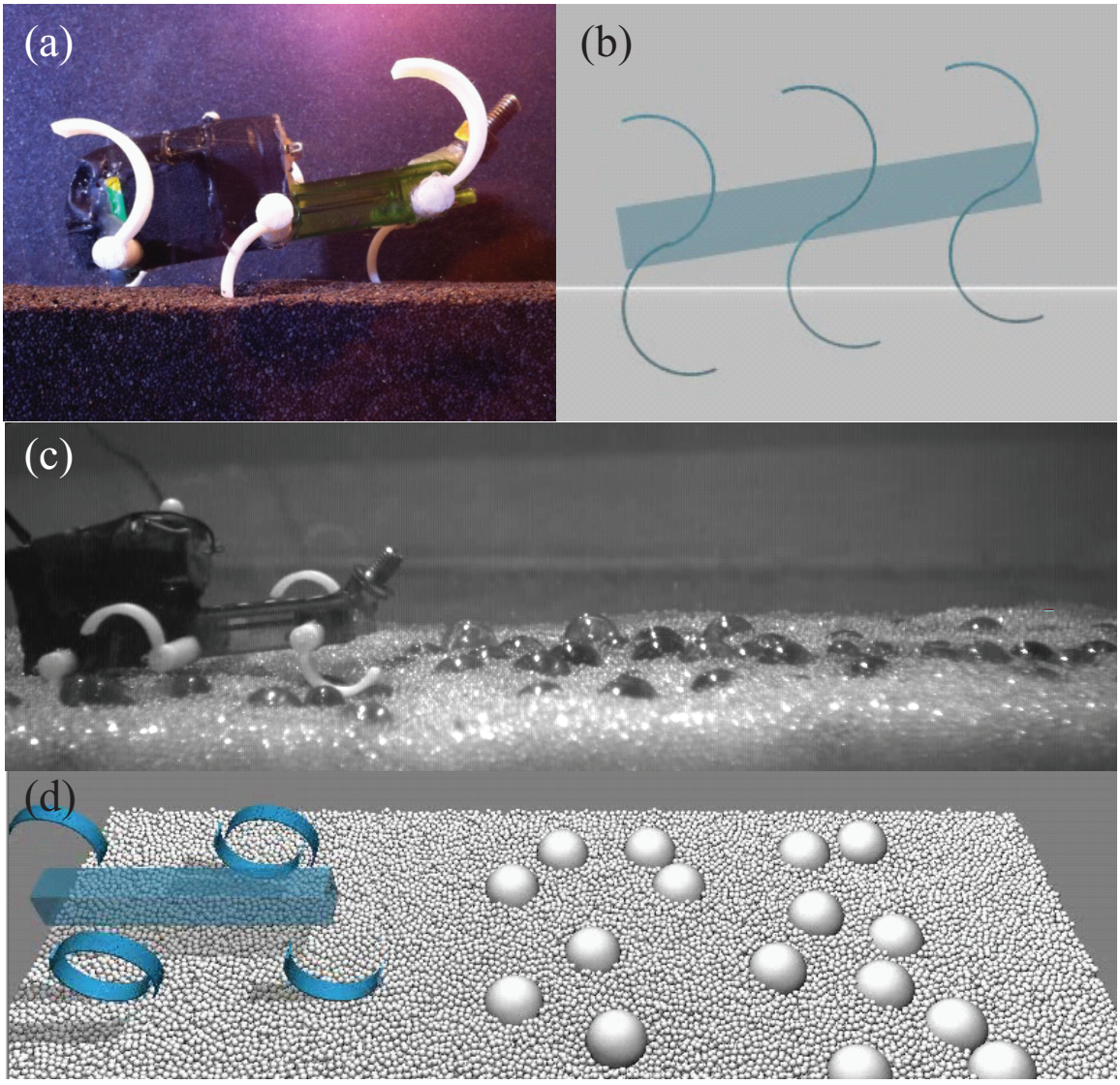

Figure 38: Robot experiment and simulation. A C-legged hexapedal robot, Xplorer, standing on homogeneous fine grains (1 mm poppy seeds). (b) The Xplorer robot in simulation constructed using MBDyn. (c) Xplorer traveling across model heterogeneous ground (bi-dispersed granular substrate as a randomized mixture of 3 mm fine grains with 25.4 mm larger glass boulders embedded within). (d) Xplorer traveling across model heterogeneous granular ground in DEM simulation.

4.4 Chaotic dynamics in robot trajectories

In both experiment and simulation on the random boulder field, we observed complex dynamics involving pitch, roll and yaw of the robot during transit. To simplify the problem and to make our system amenable to systematic study we next investigated locomotion on a boulder lattice. We arranged eight 25.4 mm diameter glass boulders into a 4×2 lattice (Figure 39a, c), and we measured robot CoM trajectories on the horizontal plane from both experiment and simulation (Figure 39b, d). We found that the robot legs and body began to collide with the boulders after a few steps, and the direction of the robot altered after each contact. Starting from similar initial conditions, the robot CoM trajectories eventually diverged for different runs, much like that of electron beam scattering in a lattice (from a classical point of view) [85].

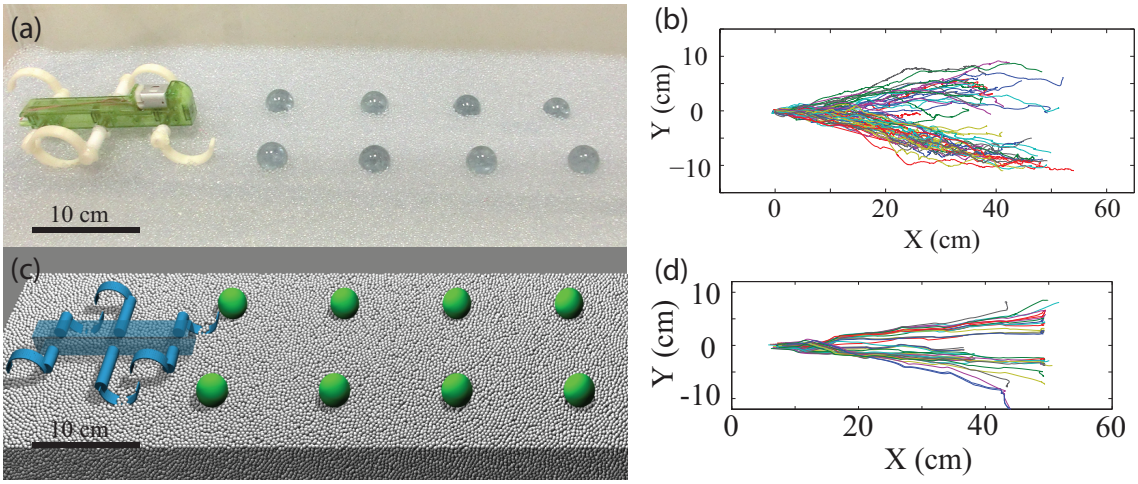

Figure 39: Experiment setup and sample trajectories. (a) Experiment setup of Xplorer running over 4×2 large boulder field; small particles are 3 mm diameter glass spheres. (b) Xplorer horizontal plane CoM trajectories measured in experiment. (c) Numerical simulation of Xplorer running over 4 x 2 large boulder field. (d) Xplorer horizontal plane CoM trajectories measured in DEM simulation.

Closer investigation in simulation suggested that the robots CoM trajectory was sensitive to initial conditions. Figure 40 shows an example of two simulation runs where the Xplorers CoM initial position varied by 0.5 cm in both x and y directions

(Figure 40a), while all other initial conditions were identical (e.g., the robot body axis was initialized to be parallel to the x-axis, the c-legs initial phase was kept the same, and the boulders were distributed to the same locations and depths). For a short time, the two robot trajectories remained similar. After 0.3 s, however, the middle left leg of the robot impacted boulder 1 at a different attack angle, resulting in two different leg-boulder contact modes. In the top trajectory, the leg forced the boulder to slide forward, and thus, the robot orientation was not significantly affected. In the bottom trajectory, the leg slipped off the boulder, generating a horizontal impulse that caused ~ 20 degree change in the yaw angle of the robot, and leading to a dramatically different trajectory (Figure 40b). This sensitivity to the initial condition indicates a signature of chaotic dynamics [118]. We intend to perform Lyapunov exponent analysis [75] in our future work to predict how nearby trajectories separate, and to explore the existence and type of attractors generated by these dynamics.

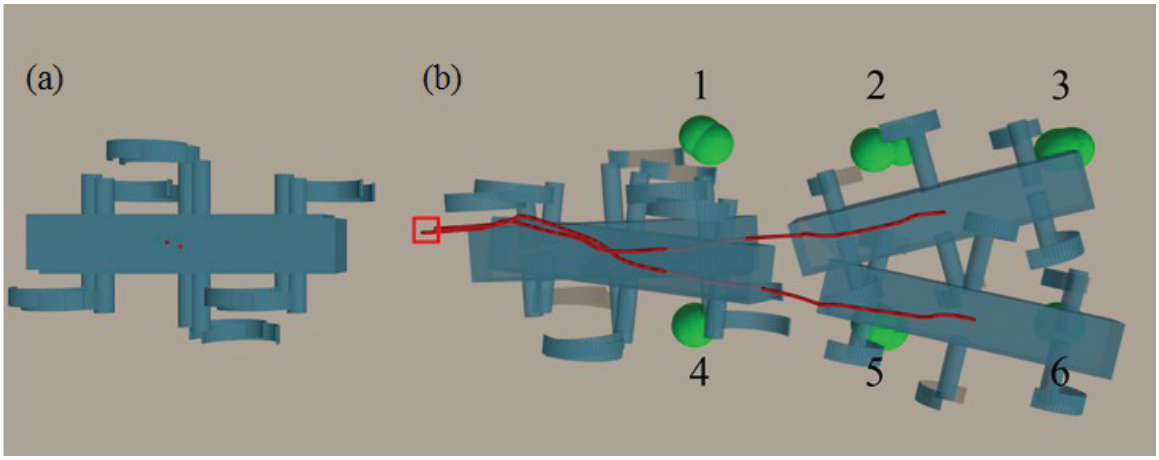

Figure 40: Two simulation runs with the CoM of the robot placed 0.5 cm apart initially. (a) Difference in the two initial locations. (b) Two trajectories. Red square indicates the robot initial position. Green filled circles indicate locations of 25.4 mm boulders. Gray background indicates 3 mm fine grains.

4.5 Leg-ground interaction modes

Based on our observations of locomotion sensitivity due to different limb-boulder interactions, we were inspired to characterize these interactions. We collected 67 locomotion runs on the boulder lattice ground, and 124 leg-ground interaction events were characterized. We observed three distinct modes (Figure 41) in both experiment and simulation:

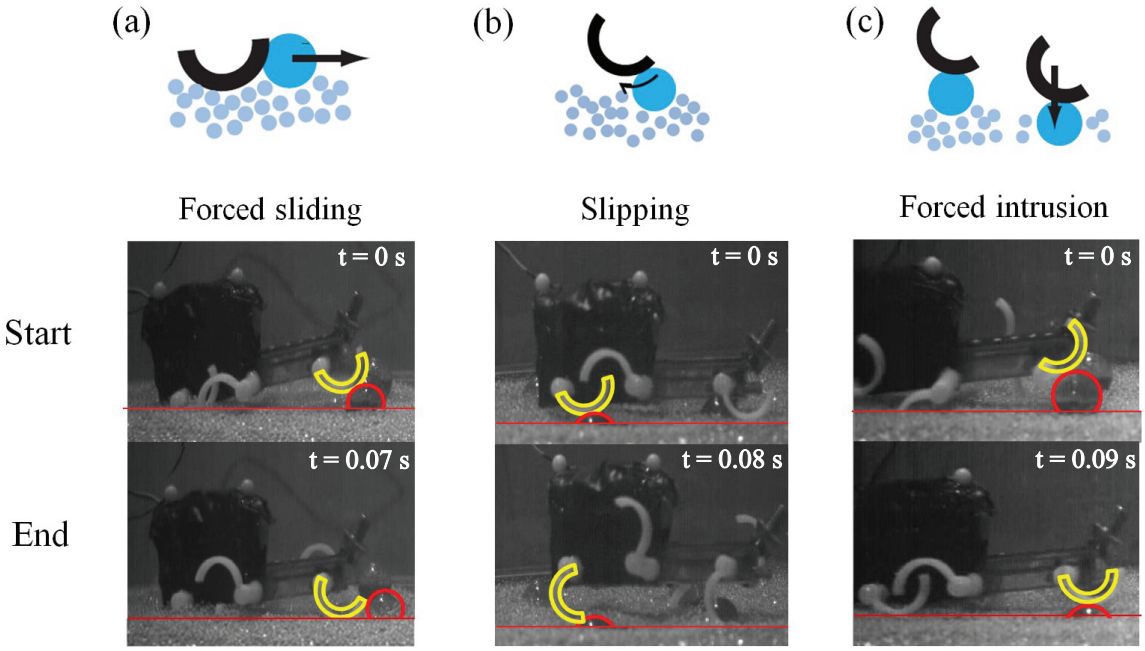

Figure 41: Three leg-ground interaction modes showing schematic (top row) and experimental data from side-view camera. (a) Forced sliding mode. (b) Slipping mode. (c) Forced intrusion mode.

4.5.1 Forced sliding mode

where the leg struck on the side of a slightly buried boulder, propelling the boulder forward or sideways (Figure 41a). The effect of this interaction on robot performance was small. We observed 53 cases when the robot exhibited this forced sliding mode (out of 59 cases where the robot leg struck on the side of the boulder), and the robot trajectories were not affected (yaw $<$ 10 degree) in 51 cases of those (98.1%).

4.5.2 Slipping mode

where the leg slid on the top of a deeply buried boulder, causing the robot to pitch/yaw/roll, while the boulder remained still or rotated against smaller grains(Figure 41b). Robot stability was significantly affected in this mode. We observed 28 cases when the robot exhibited slipping mode (out of 31 cases where robot leg struck on top of deeply buried boulders), and the robot trajectory was significantly affected (yaw $>$ 10 degree) in 23 cases of those (82.1%).

4.5.3 Forced intrusion mode

where the robot leg struck the top of the slightly buried boulder, forcing the boulder downward into the fine grains (Figure 41c). By taking advantage of the mobility of obstacles towards leg intrusion direction, the robot reduced the impulse of the collision and maintained its stability in this mode. We observed 17 cases when the robot exhibited the forced intrusion mode (out of 36 cases where robot leg struck on top of slightly buried boulders), and the robot trajectory was affected significantly (yaw $>$ 10 degree) only in 1 case (0.06%).

4.6 Automated terrain creation and locomotion testing system

To comprehensively investigate how different heterogeneities and robot initial conditions affect the locomotion performance and trajectories on heterogeneous granular media, we developed a fully-automated terrain creation and robot locomotion testing apparatus, the Systematic Creation of Arbitrary Terrain and Testing of Exploratory Robots (Figure 42), which allows precisely control and systematic variation of properties of heterogeneous multi-component substrates such as compaction, orientation, obstacle shape/size/distribution, and obstacle mobility within the substrate.

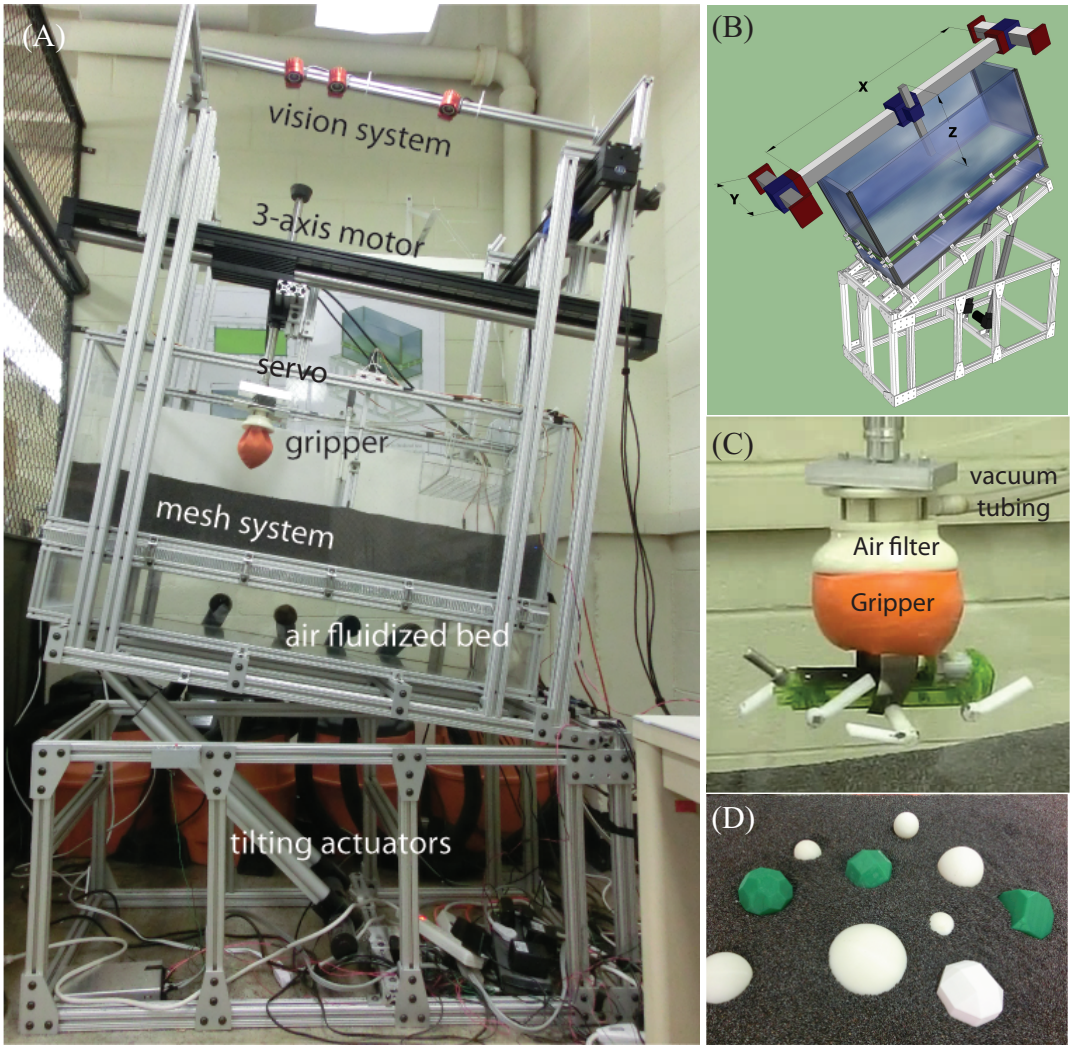

Figure 42: The SCATTER system. (A) The automated terrain creation and locomotion testing system, including the vision system, the 3-axis motor, the universal jamming gripper, the air fluidized bed and the tilting actuators. (B) Mechanical drawing of the automated system: a 3-axis motor mounted on a tiltable trackway. (C) The universal jamming gripper lifting the robot. (D) An example of controlled heterogeneity for systematic variation in boulder shape and size – 1mm poppy seeds (the "sand") with larger 3D-printed spherical and polyhedral "boulders" embedded within.

The central structure of the SCATTER system consists of a 122 cm long, 51 cm wide air fluidized bed trackway (Figure 42B). Four vacuums (RIDGID, 16 gallon) are connected below the trackway, blowing air through a flow distributer (0.635 cm thick, 50 μm pore size porous plastic) to evenly fluidize the fine grains in the trackway, allowing control of the compaction and creation of repeatable homogeneous granular states of the fine grains. We used 1 mm diameter poppy seeds as the model fine grains in this study, but this ground stiffness control technique can be applied to a large variety of granular media, with sand particle diameter ranging from hundreds of microns to a few millimeters. The resistance of the granular substrate created using this method is highly repeatable, and could be varied over a large range, from greater than close packed compaction states [71] to a zero resistance state [98]. Also, as previously measured in intrusion tests, the results obtained using these model granular substrates can be applied to more complex natural sand composed of grains with greater polydispersity and angularity [72].

The entire trackway is supported by an aluminum tiltable support framing actuated by two linear actuators (Firgelli, 454 kg load, 61 cm stroke), such that the trackway can tilt to create inclined/declined granular environments. By controlling the extruded length of the linear actuator, the substrate inclination angle could be varied to more than 40°, exceeding the maximum angle of stability [33] for most granular media used in locomotion studies [81][72].

To generate states of arbitrary heterogeneity, a 3-axis motor system (Copley,

STA25, STB25, XTB38) was installed above the trackway, enabling the motor end-effector to move in three dimensions, driving a universal jamming gripper [14] (Figure 42C) to programmed locations, creating arbitrary distributions of multi-size granular particles. The customized gripper assembly includes a balloon filled with granular material (a "universal jamming gripper" [14]), a support frame, and a HI-TEC servo motor (HSR-5980SG). The 3D-printed support frame connects the gripper to vacuum tubing through an air filter, enabling the granular material in the gripper balloon to switch between fluid-like and solid-like properties. The fluid-like property of the granular media inside the balloon (when suction is off) allows the gripper to deform around the robot or boulders, while the solid property of the granular material (when suction is applied) enables the gripper to reach a jammed state, resulting in a rapid gripping of objects of complex shapes.

The gripper can handle objects with large variation in geometries (spheres, polyhedrons, cylinders, etc.), sizes (as long as the gripper membrane could reach sufficiently around the sides of the target [14], $\approx 50\% \pm 20\%$ balloon diameter), and weights (up to 0.2 kg for the size of our gripper). Using the universal jamming gripper, a large variety of ground heterogeneities (boulders, rocks, logs, etc.) as well as small scale robots can be automatically distributed and retrieved to produce different heterogeneous ground configurations and locomotor initial conditions. The gripper support frame also provides an attachment from the gripper balloon to the servo disk, enabling the gripper assembly to adjust the heterogeneity and robot orientation for each test.

Kinematic information of the robot, including the x, y, z center of mass (CoM) position as well as the yaw, pitch, and roll angle, was obtained by tracking 3 IR-reflective markers attached to the robot using three top-view cameras (Naturalpoint,

Flex13, 120 FPS). The cameras also monitored the location of the robot and the boulders before and after each test. This information was communicated to the motor system, so that the gripper could retrieve both the robot and boulders. The system also recorded dorsal and lateral high speed reference videos that synchronized with the tracking data.

All functions of the SCATTER system were controlled by a single integrated LabVIEW program. This terrain creation and robot locomotion testing system can currently take more than 200 locomotion tests in one day, without human intervention, allowing comprehensive and systematic exploration of effects of arbitrary heterogeneity and spatial distribution on interaction modes and performance.

Using SCATTER, we can investigate a variety of terrain and locomotor parameters, including sand resistance, boulder geometry/texture/orientation, heterogeneity distribution, substrate inclination, as well as robot leg shape, foot size and gait frequency, etc. Fig. 42D demonstrates a sample heterogeneous substrate created by SCATTER – a granular test bed filled with small diameter spherical particles (the simplified "sand") and larger objects of various shapes (the simplified "boulders" and "rocks") embedded within. The relatively simple geometry and configuration of the model terrain makes it feasible to create repeatable states of granular media with controlled heterogeneity, and facilitates systematic exploration of heterogeneous ground properties.

4.7 Conclusion

In this study, we explored an open-loop controlled legged robots locomotion performance on heterogeneous granular ground, and characterized leg-ground interaction

modes. We extended previous DEM numerical simulation for heterogeneous ground application and revealed chaotic dynamics of the robot CoM trajectories caused by different types of leg-boulder interaction. We also designed and constructed an automated terrain-creation and locomotion testing system, the SCATTER, which enabled the creation of repeatable heterogeneous granular substrate and systematic locomotion testing with minimal human intervention.

CHAPTER V

UNIVERSAL SCATTERING IN LEGGED LOCOMOTION ON HETEROGENEOUS GRANULAR GROUND

5.1 Summary

Natural substrates are often composed of particulates of varying size, from fine sand to pebbles and boulders. Robot locomotion on such heterogeneous substrates is complicated in part due to large force and kinematic fluctuations introduced by heterogeneities. To systematically explore how heterogeneity affects locomotion, we study the movement of a hexapedal robot (15 cm, 150 g) in a trackway filled with ~ 1 mm "sand", with a larger convex "boulder" of various shape and roughness embedded within. Using a previously developed fully-automated terrain creation system, the SCATTER (Systematic Creation of Arbitrary Terrain and Testing of Exploratory Robots), we control the properties of the substrate and the initial conditions of the robot, and we investigate how the presence of larger boulder affects the robot's trajectory on granular media. Analysis of the robot's trajectory indicates that the interaction with a boulder can be modeled as a scatterer with attractive and repulsive features. Depending on the contact position on the boulder, the robot will be scattered to different directions after the interaction. The trajectory of an individual interaction depends sensitively on the initial conditions, but remarkably this dependence of scattering angle upon initial contact location is universal over a wide range of boulder properties. For a larger heterogeneous field with multiple "scatterers", the trajectory of the robot can be estimated using a superposition of the scattering angles from each scatterer. This scattering superposition can be applied to a variety of complex terrains, including heterogeneities of different geometry, orientation,

and texture. Our results can aid in development of both deterministic and statistical descriptions of robot locomotion, control and path planning in complex terrain [1].

5.2 Introduction

Rocky, loose substrates are common in environments that exploratory robots must traverse; such terrains can contain granular media (GM) with particle sizes spanning multiple orders of magnitude. When robotic locomotors travel across these "flowable" types of heterogeneous terrain, they exhibit characteristic failure modes (slips, unstable foot-holds, impassable barriers, course deviation, or a limb/tread fluidization of a thin layer of smaller particles), which significantly affect robot stability, maneuverabilitys and power consumption. One of the major challenges in creating the next generation of mobile robots is expanding the scope of terramechanics [7][130] from large tracked and treaded vehicles on homogeneous ground to arbitrarily shaped and actuated locomotors moving on and within complex heterogeneous terrestrial substrates, to create a "terradynamics" [72] (in analogy to hydro and aerodynamics which provide predictive power for aquatic and aerial vehicles) of locomotion on heterogeneous ground. However, in typical heterogeneous environments, the force fluctuations introduced by heterogeneities (gravels, rocks, boulders, etc.) during intrusion and drag can be large, which makes the applicability of continuum terramechanics [7][130] unclear. Currently, most terrestrial vehicles (including mobile robots) are tested on substrates made of standardized homogenous media (e.g. Ottowa sand [86], lunar simulants [37]), while robot locomotion on heterogeneous granular ground is relatively unexplored.

Modelling and controlling robot locomotion on heterogeneous granular terrain requires fundamental understanding of the complex interactions between the robot

[1]This Chapter is a paper by Feifei Qian and Daniel I. Goldman, *SPIE Defense + Security* [100]

and the heterogeneous ground. This interaction can be especially complicated when obstacles possess mobility relative to the substrates underneath (e.g., boulders/rocks can rotate, tilt, shift on or even sink into the fine sand). Multiple types of interactions – robot with the fine sand [72], robot with the multi-shaped boulders/rocks, as well as boulders/rocks with the fine sand – must be considered, and the mobility of the boulders/rocks can dynamically change the terrain profile during the interaction. Studying the response of a locomotor on heterogeneous granular terrain will generate a better understanding of such interactions, and provide guidance for obstacle-interactive navigation planning. Most traditional navigation planning methods involve finding a collision free path, which requires the robot to avoid obstacles. For example, the potential field method (PFM) [64] treats obstacles as repulsive potentials that repel the robot. This is legitimate for most wheeled/treaded robots which must circumvent obstacles, but for legged robots, traversing obstacles by stepping over or upon them [63] is often a more efficient option. This could be particularly important for time critical tasks like search and rescue. Allowing robots to interact with obstacles [9], or even, manipulating the locomotion environment [67], could significantly expand viable exploration space for obstacle-filled environments.

In addition to developing a deterministic understanding of robot-heterogeneity interactions, major advances in robot mobility will also require a statistical terradynamics framework for locomotion and control in which the deterministic models of obstacle-robot interactions function as important inputs. A statistical terradynamics will allow robots to evaluate obstacle traversability and predict the probability of outcomes (e.g., possible failure, trajectory deviation, etc.) of different locomotion modes. In this manner robots could choose locomotion maneuvers to traverse challenging terrain, and perform successful anticipatory control to avoid fatal failure and course deviation.

To initiate an effort to create a terradynamic framework for legged robot locomotion on heterogeneous flowable substrates, we previously designed and constructed a SCATTER system [99] (Systematic Creation of Arbitrary Terrain and Testing of Exploratory Robots) to automatically create heterogeneous granular ground conditions and perform robot locomotion tests, and we used SCATTER to study the robot's locomotion on a diversity of heterogeneities, searching for principles that will allow us to move toward a terradynamics of heterogeneous granular media. We find that the complex interaction between the robot and a single boulder can be modelled as a scattering process – each interaction will cause the robot to leave the boulder with a certain angle of trajectory deviation, as if the robot was scattered. The form of the scattering process is sensitive to initial conditions of the robot but is insensitive to boulder shape and texture. As an initial step toward the heterogeneous terradynamics, we largely focus on single localized scatterers, but discuss toward the end of the paper the applicability of these results to robot locomotion on more complex heterogeneous fields with arrays of scatterers.

5.3 Single boulder interaction analysis

Previous studies revealed that even on simplified bi-disperse heterogeneous granular ground robot locomotion exhibited chaotic dynamics and multiple robot-ground interaction modes [99]. The robot could slip on the top of a deeply buried boulder, push a lightweight boulder to yield towards the side or into the sand, get stuck on the top of a large boulder, or force a high-friction boulder to rotate in place. The complexity of observed interactions, even in the simplified substrates, prompted us to concentrate on an even simpler model system. Therefore we began with a single boulder interaction study to systematically analyze how different boulder properties,

robot kinematics, affected robot-boulder interaction modes and robot locomotion performance.

5.3.1 Experimental setup

We analyzed the interaction between the robot and a single boulder buried in the sand, and the resulting robot CoM trajectories. The boulder size was chosen to be $4-5$ cm in diameter, comparable with robot C-leg diameter ($3-4$ cm), such that the boulder had a significant effect on robot locomotion and had enough exposed area to distinguish leg-boulder contact positions, but was not a barrier too high for the robot to traverse. We tested robot interactions for different boulder properties varying boulder shape, orientation, texture. We also tested robot interactions with both immobile boulder (i.e., boulder was fixed at a certain burial depth) and free boulder (i.e., boulder was allowed to move during interaction). In all experiments, robot leg frequencies were kept small (< 0.3 Hz) such that the inertial effects were negligible.

At the beginning of each test, the gripper placed the robot at a different initial position relative to the boulder (Figure 43A). The fore-aft initial position (along the Y axis) of the robot was programmed to be within $1-2$ bodylengths away from the boulder, and increased by 1 cm increments each time.

After the interaction with the boulder, the robot continued moving for another $1-3$ bodylengths, to allow accurate characterization of robot CoM trajectory angle after the disturbance. Similarly, the lateral initial position of the robot CoM (along the X axis) was varied within $0-9$ cm, with 0 cm being robot centerline passing the boulder center and 9 cm being the robot no long in contact with the boulder along its trajectory. We define this lateral distance between the boulder center and

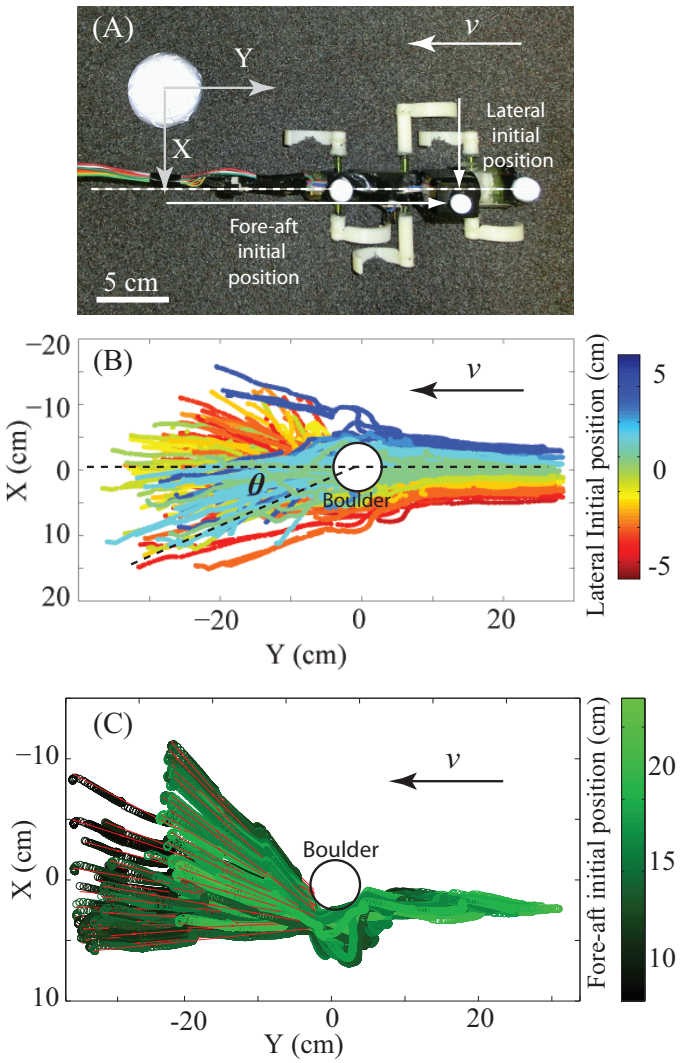

Figure 43: Single boulder scattering experiment. (A) Experimental setup. The center of the boulder is set as the origin. X and Y axis represents lateral and fore-aft direction. (B) Robot CoM trajectories for different lateral initial positions (i.e., different impact parameter). Data were collected from a free boulder experiment, where the boulder was initially placed at a burial depth of $\approx$ 1 cm, a quarter of the free boulder diameter. Trajectory color indicates different impact parameters. (C) Robot CoM trajectories for different fore-aft initial positions (i.e., different leg phase at contact). Data were collected from immobile boulder experiment, where the boulder was fixed at a burial depth of $\approx$ 1.25 cm, a quarter of the immobile boulder diameter. Red lines represents the linear fit of the robot's trajectories after boulder interaction, which was used to calculate the scattering angle θ. The white circles in (B) and (C) indicate boulder position.

the robot centerline as the "impact parameter", in analogy to the scattering theory in nuclear physics [85]. After the gripper placed the robot, the automated system performed a check on the robot's initial X and Y position as well as initial yaw angle, and re-positioned the robot if the error was larger than the pre-set threshold (position error > 1 cm and heading error $> 2°$).

5.3.2 CoM trajectory analysis for a spherical boulder

We collected ~ 1000 runs for a spherical boulder using the automated system, varying the robot's initial lateral and fore-aft positions. Figure 43B shows ~ 200 trajectories with robot lateral initial positions (the impact parameter) varied from -4 cm to 4 cm relative to a 4 cm diameter spherical boulder. All trajectories were plotted in the boulder frame (i.e., with the boulder located at the origin (0, 0)). The color of the trajectories represents different impact parameters.

We observed that the robot's trajectories were straight before the interaction with the boulder, then exited to different angles (depending on the initial conditions) after the interaction. Surprisingly, we noticed that for a significant number of runs, instead of being repelled by a repulsive obstacle potential as assumed in the PFM, the robot turned towards the boulder after the interaction, as if it was attracted to the boulder.

Closer analysis indicated that the interaction with the single boulder could be modelled using a set of attractive or repulsive scattering angles depending on the initial conditions. For each robot CoM trajectory, we fit two straight lines for before and after the boulder interaction, to characterize the trajectory angle change (the scattering angle, θ). The analogy to the scattering problem simplified the complex interaction, allowed systematic characterization of the effect of different boulder

properties on robot trajectory deviation, and provided a way to perform long term dynamics analysis for exploratory robot trajectories on a large scale heterogeneous field.

Figure 43C shows CoM trajectories with variation in initial fore-aft positions. The impact parameter was fixed, and the robot was programmed to start from each initial position with the same initial leg phase such that the leg contacted with the boulder at different leg phases. We noticed that the scattering angle depended sensitively on the initial fore-aft position, and this sensitive dependence was highly repeatable given the same initial fore-aft position. The sensitivity of robot trajectory to the initial conditions indicates that the effect of a given boulder on robot trajectory deviation can be expressed by a 2D scattering pattern with the X and Y axes representing the leg phase and impact parameter effect, respectively (Figure 44d). We investigate this scattering pattern for boulders of different properties, and search for the general principle that governs the robot-boulder interaction modes.

5.3.3 Robot scattering pattern for different boulder shape, orientation and roughness

To investigate how different boulder properties affected the scattering pattern, we studied the robot's interaction with a variety of boulder shapes, orientations and roughnesses. Boulder shapes were varied through 3D-printing (uPrint SE plus, Stratasys), and boulder roughness was varied by coating the boulder surface with different textures. We note that natural heterogeneous terrain comes in a huge variety of forms and it is obviously impossible to test all possible boulder configurations. In this study, as a starting point to initiate an effort in creating a terradynamics framework for legged robot locomotion on heterogeneous granular substrates, we use boulders with regular geometry like spheres and symmetric polyhedrons to simplify the interaction and facilitate the development of initial principles. However, we seek to develop key

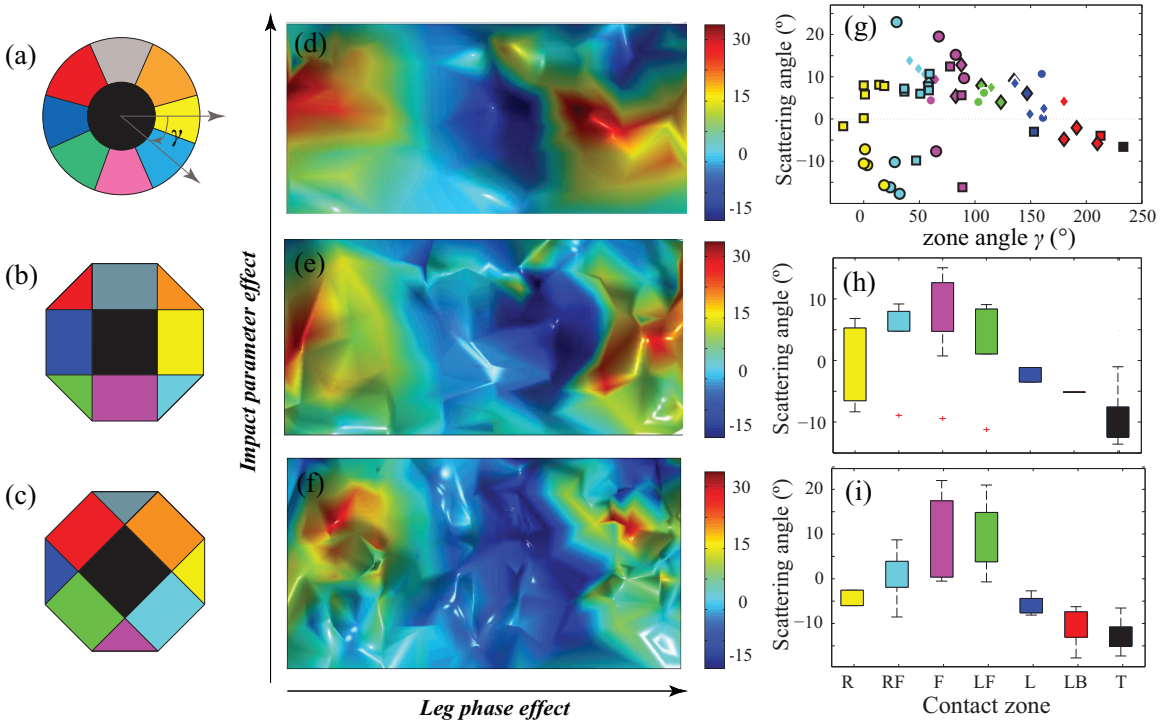

Figure 44: Scattering pattern and scattering angle dependence on contact position for boulders of different shapes and orientations. (a, b, c) Top view diagrams of the three boulders, including a sphere (a), a 90 degree oriented rhombicuboctohedron (b), and a 45 degree oriented rhombicuboctohedron (c). Different colors (yellow, cyan, purple, green, blue, red, black) corresponding to different contact zones (right, right-front, front, left-front, left, left-back, top), respectively. Among all the zones, it was relatively unlikely for the robot leg to struck on the B and RB zones due to the leg rotation direction and the experiment configuration (i.e., all tests were performed with robot initial lateral position on the left side of the boulder, since the scattering pattern was symmetric for both sides). Therefore statistical data were not compared for these three zones, and were only analyzed and plotted for a selective of boulders in Figure 45. For the 90 degree oriented rhombicuboctohedron (b) and the 45 degree oriented rhombicuboctohedron (c), the zones were divided using the edges of the polyhedrons; whereas for the sphere (a), the zones were divided based on the radius r and zone angle γ (right: $-20° < \gamma < 20°, r > 2$ cm; right-front: $20° < \gamma < 60°, r > 2$ cm; front: $60° < \gamma < 100°, r > 2$ cm; left-front: $100° < \gamma < 130°, r > 2$ cm; left: $130° < \gamma < 170°, r > 2$ cm; left-back: $\gamma > 170°, r > 2$ cm; Top: $r < 2$ cm. (d, e, f) 2D scattering pattern for 3 different boulders. The X and Y axes represent different robot fore-aft initial positions (i.e., the leg phase effect) and lateral initial positions (i.e., impact parameter effect), respectively. (g, h, i) Scattering angle vs. contact zone for three low-friction boulders. Lower and upper limit of the central box in boxplots (h, i) represent the 25% and 75% quantile of the data, respectively. Markers color convention in (g, h, i) is the same as (a, b, c). Marker shape (square, diamond, circle) represents front, middle, rear leg contacted with the boulder, respectively. Markers without outlines indicate robot leg shaft contact.

principles which are not limited to the select cases but can be expanded to a generalized form to provide a better understanding of the robot-heterogeneity interaction and its effect on locomotor performance.

We first tested and analyzed the scattering pattern for three low-friction boulders, including a 5 cm diameter glass sphere, a 3D printed 90 degree oriented 5.2 cm diameter ABS plastic rhombicuboctohedron, and a 3D printed 45 degree oriented 5.2 cm diameter ABS plastic rhombicuboctohedron (Figure 44a, b, c). The rhombicuboctohedron was chosen because its polyhedral faces were naturally separated into 9 zones – front (F), back (B), left (L), right (R), right-front (RF), left-front (LF), right-back (RB), left-back (LB) and top (T), which facilitated identification and analysis of the effect of leg-boulder contact positions. The spherical boulder, on the other hand, was chosen as the simplest example of a continuously varying boulder surface inclination angle, while the symmetric shape facilitated the interaction analysis and the generalization of our principles.

We observed that the scattering pattern exhibited similar characteristics for all three boulders (Figure 44d, e, f). The scattering angle varied sensitively along the fore-aft direction (between 30° and -15°) but was relatively uniform along the lateral direction. To explain this phenomenon we characterized the leg-boulder contact positions on the boulder using different contact zones. For the polyhedral boulders, we used the polyhedron faces to categorize the contact zones (Figure 44b,c), whereas for the spherical boulder, we used a polar coordinate system (the radial distance r and the zone angle γ) to describe the contact position on the boulder (Figure 44a). We analyzed the scattering angle dependence on contact zone for high-friction boulders as well (Figure 45) by coating the boulder surface with 120 grit sandpaper.

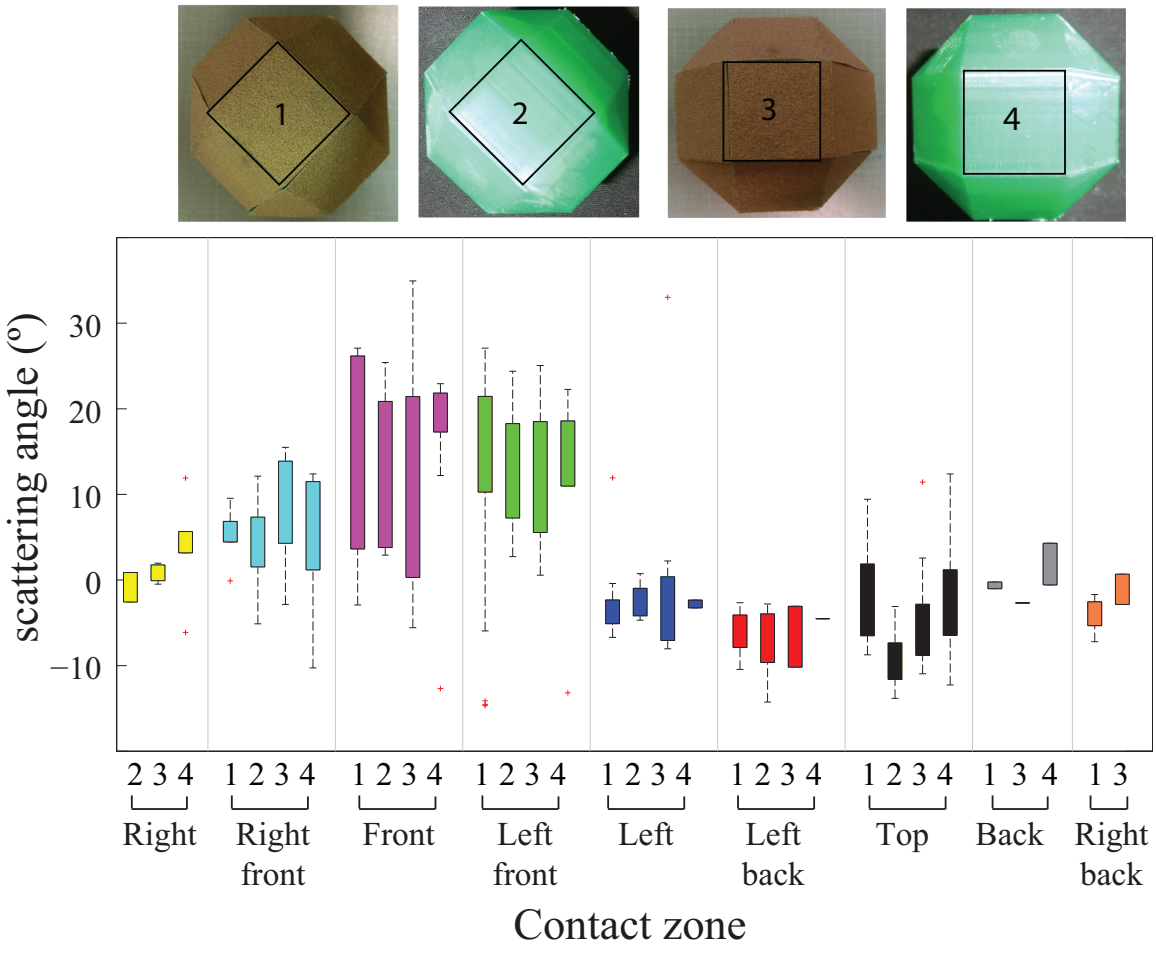

Figure 45: Scattering angle vs. contact zone for four boulders with differences in roughness and orientation, including a rough 45 degree oriented rhombicuboctohedron (1), a smooth 45 degree oriented rhombicuboctohedron (2), a rough 90 degree oriented rhombicuboctohedron (3), and a smooth 90 degree oriented rhombicuboctohedron (4). Colored groups represent different contact zones, and color convention is the same as in Figure 44b,c.

We found that despite variation in boulder shape (sphere vs. rhombicuboctohedron), orientation (45° shift) and roughness (low friction vs. high friction), the scattering angle vs. contact zone exhibited qualitatively similar dependence for all boulder types tested (Figure 44g, h, i; Figure 45). This universality of scattering angle dependence upon contact zone explained the similarity observed in the scattering pattern for different boulder shapes and orientation (Figure 44d, e, f), and suggested that the scattering angle can be modelled as a function of the boulder surface inclination angle at the contact point.

More interestingly, we noticed that most of the "attractive" zones were distributed on the front side of the boulder (Right front, Front, Left front), whereas most of the "repulsive" zones were distributed on the center or back side of the boulder (Left back, Top, Right back). We hypothesized that the fore-aft direction boulder surface inclination angle was largely responsible for the variation in the scattering angle. This also explains the more significant variation of scattering angle along fore-aft direction as compared to lateral direction (Figure 44d, e, f).

5.4 Scattering angle dependence on surface inclination at contact

To test our hypothesis of scattering angle dependence on boulder inclination, we characterized the fore-aft direction boulder surface inclination angle at the beginning of each leg-boulder interaction for a previous experiment [99] of robot locomotion on a 2×4 lattice boulder field. We found that, as hypothesized, the scattering angle depended sensitively on the fore-aft inclination (Fig. 46A), and this scattering angle vs. fore-aft inclination curve was closely related to the different interaction modes (Fig. 46B):

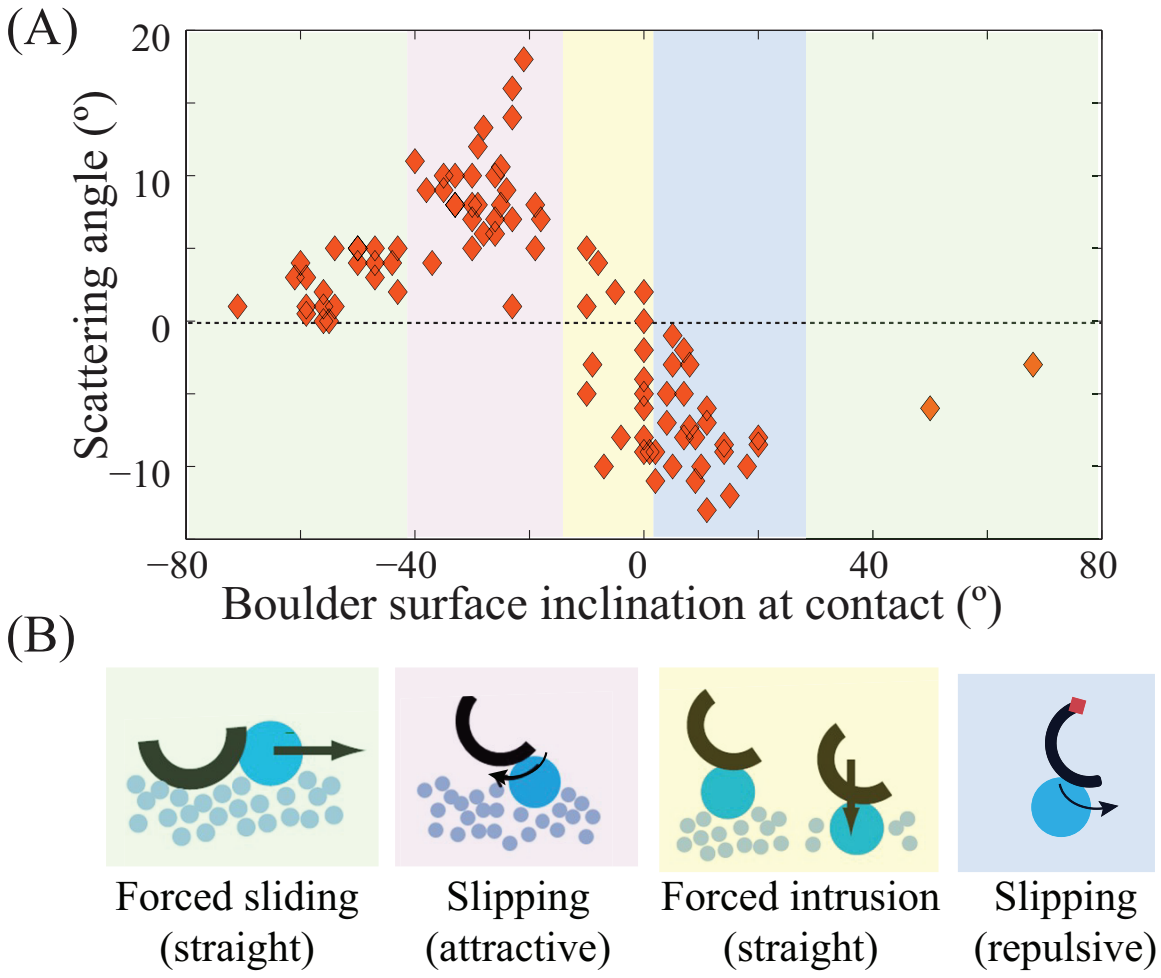

Figure 46: Scattering angle dependence on boulder inclination and the corresponding locomotion modes for different region. (A) Scattering angle of each leg-boulder interaction as a function of the fore-aft direction boulder surace inclination angle at the beginning of leg-boulder contact. Scattering angles were characterzied from robot locomotion experiment on a lattice boulder field, with eight 2.54 cm free boulder embedded in 3 mm glass beads. All boulders were free to move during the interaction. (B) Diagram of four different leg-boulder interaction modes observed in robot locomotion test in substrate with multiple, free boulders. Different color blocks of interaction modes corresponded to the same color shaded regions in (A).

a) Inclination $< -40^\circ$ or $> 30^\circ$ (Fig. 46A, green shaded region): forced sliding mode (Fig. 46B, green shaded block), where the leg struck on the side of boulder, propelling the boulder forward or sideways. The effect of this interaction on robot performance and trajectory was small (scattering angle $\leq 5^\circ$).

b) $-40^\circ <$ Inclination $< -15^\circ$ (Fig. 46A, pink shaded region): attractive slipping mode (Fig. 46B, pink shaded block), where the leg impacted near the top of the boulder and slid down towards the front of the boulder, causing the robot to turn toward the boulder, while the boulder remained still. Robot trajectory was significantly affected in this mode (scattering angle $5^\circ \sim 20^\circ$).

c) $-15^\circ <$ Inclination $< 5^\circ$ (Fig. 46A, yellow shaded region): forced intrusion mode (Fig. 46B, yellow shaded block), where the robot leg struck on top of boulder, forcing the boulder downward into the fine grains. The robot exhibited a passive stability when the leg impacted on this top region of the boulder, and the effect of this interaction on robot trajectory was relatively small (scattering angle normally within $\pm 5^\circ$). In mode a) and c), the robot reduced the impulse of the collision by taking advantage of the mobility of boulders relative to the sand.

d) $5^\circ <$ Inclination $< 30^\circ$ (Fig. 46A, blue shaded region): repulsive slipping mode (Fig. 46B, blue shaded block), where the leg hit beyond the top of a deeply buried boulder and slid down towards the back of the boulder, causing the robot to turn away from the boulder, while the boulder remained still. Robot trajectory was significantly affected in this mode (scattering angle $-5^\circ \sim -15^\circ$), similar to the attractive slipping mode.

We also characterized the scattering angle vs. inclination for different boulder sizes,

textures and mobilities, and found that the scattering angle vs. boulder inclination curves exhibited qualitatively similar characteristics among a variety of boulder properties. This universality in scattering angle dependence upon surface inclination of the heterogeneity allows us to further generalize our results to ground heterogeneities with different geometries, and in the future to statistically estimate the outcomes of the robot-heterogeneity interaction and perform anticipatory control.

5.5 Expanding the scattering principle to non-localized heterogeneities

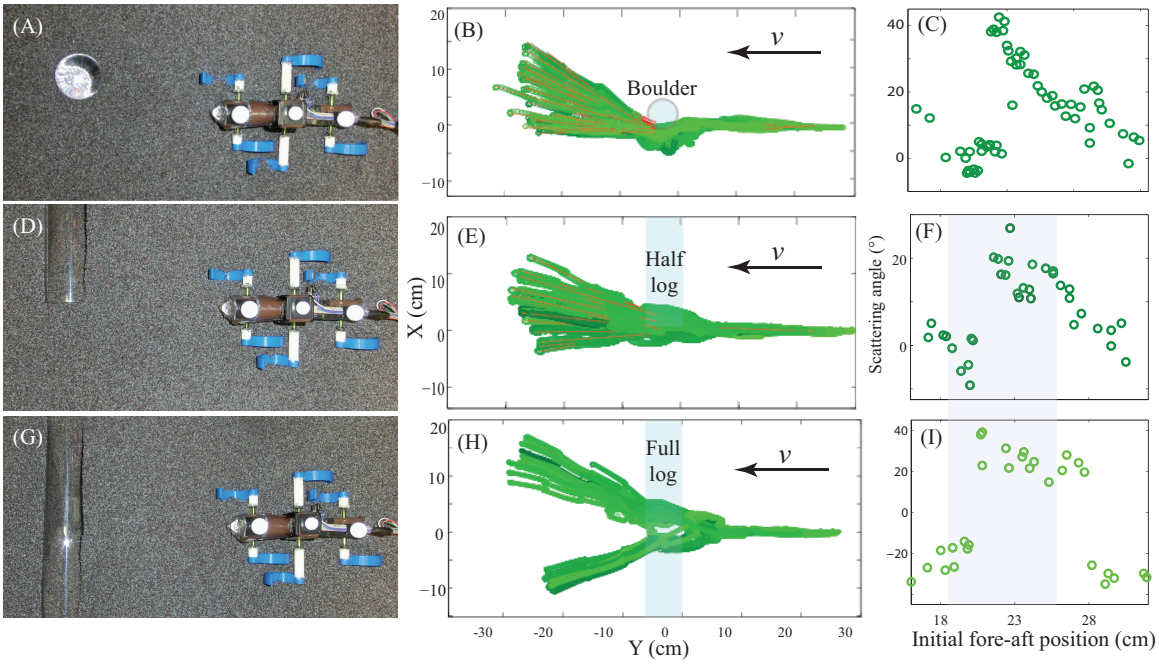

Figure 47: Robot trajectory and scattering comparison between boulder and log. (A, D, G) Robot scattering experimental setup for a 5 cm diameter spherical boulder (A), a 5 cm diameter cylindrical half log (D), and a 5 cm diameter cylindrical full log (G) embedded in 1 mm poppy seeds. (B, E, H) Robot trajectory for the boulder (B), the half log (E) or the full log (H). (C, F, I) Robot scattering angle as a function of initial fore-aft distance between robot and the boulder (C), the half log (F) or the full log (I).

To further validate our hypothesis that fore-aft boulder inclination mainly contributed to scattering angle variation, and further generalize the applicability of our scattering results, we tested robot locomotion as it traversed over a cylindrical "log" (5 cm diameter, Fig. 47D, G) fixed at a burial depth of ≈ 3.75cm, with a quarter of the log diameter protruding from the granular surface. We compared the scattering pattern from the cylindrical log with the result from a spherical boulder with the same diameter (Fig. 47A) and same burial depth. We first tested a "half log" (Fig. 47D), where only the legs on the right side of the robot body interact with the log, similar to the situation in the single boulder experiment. We found that the scattering pattern and the scattering angle vs. initial robot fore-aft position for the half log (Fig. 47E, F) was qualitatively similar to the scattering pattern of the spherical boulder (Fig. 47B, C). This was consistent with our hypothesis that the scattering angle depended mainly on the fore-aft boulder inclination, and this indicated another level of superposition in the scattering – the log can be viewed as a slice of the boulder and the boulder as a superposition of many thin logs of different heights stacked laterally. We suspected that the difference in magnitude of the scattering angle depended on the height of the log (i.e., where we "slice" the boulder), and in future work we plan to test different log heights. We note that the scattering superposition approach we propose for the heterogeneous granular ground is analogous to the granular Resistive Force Theory (RFT) terradynamics [72] which predicted locomotion performance on homogeneous granular ground by assuming forces exerted on the robot leg were approximated using a linear superposition of the resistive forces on infinitesimal leg elements.

We also tested a "full log" (Fig. 47G) where the legs on both sides of the robot body can interact with the log. Interestingly, the robot never travelled straight across the log, instead all trajectories were separated into two branches (Fig. 47H) with scattering angles greater than 15° (Fig. 47I). This was significantly different from the

pattern observed for the boulder or the half log, and was likely due to a "switching" of which side of the legs the dominant scattering mode occurred. For a robot with initial fore-aft position between 19 and 26 cm ($\approx$ 1/2 robot stride length), the interaction between the right-side legs and the boulder was causing a larger scattering angle (i.e., was dominating the scattering) as compared to the left-side leg interactions. Thus, the full log scattering pattern within this range (Fig. 47I, shaded region) was qualitatively similar as compared to the half log scattering pattern for right-side leg interactions within the same range (Fig. 47F, shaded region). For the other 1/2 robot stride length (Fig. 47I, un-shaded region), the left-side legs dominated the scattering, and therefore the full-log scattering pattern was "inverted" to a left-side half log scattering pattern.

5.6 Rationalizing sensitive dependence of trajectory on initial conditions

Our scattering superposition principle provides a framework to understand the previously observed chaotic dynamics [75][118] in robot trajectories on a large, multi-boulder field [99]. In our previous results, we noticed that the robot's trajectories were sensitive to initial conditions in both experiment and our multi-particle DEM simulation [102]. Fig. 48 visualizes an example of two simulation runs where the Xplorers CoM initial position varied by 0.5 cm in both X and Y directions (Fig. 48A), while all other initial conditions were identical (e.g., the robot body axis was initialized to be parallel to the X axis, the initial leg phase was kept the same, and the boulders were distributed to the same locations and depths). However, after the robot ran across a lattice boulder field (eight 2.54 cm boulders buried in 3 mm sand), the two trajectories deviated significantly (Fig. 48B). This sensitivity to initial conditions is a signature of chaotic dynamics [75, 118]. For a larger field with more boulders present, the long term dynamics of the robot will be even more complex.

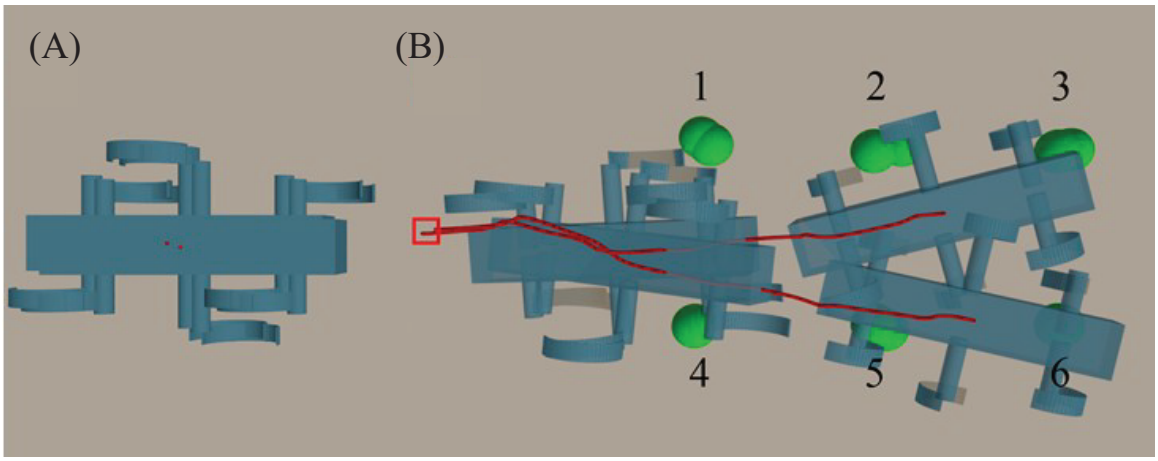

Figure 48: Two simulation runs with the CoM of the robot placed 0.5 cm apart initially. (a) Difference in the two initial locations. (b) Two trajectories. Red square indicates the robot initial position. Green filled circles indicate locations of boulders. Gray background indicates fine grains. Figure adapted from [99].

Using our single boulder scattering pattern and the superposition principle, the long term dynamics of robot trajectories on large, heterogeneous ground can be estimated. Based on the scattering superposition principle, each boulder can be modeled as a scatterer whose scattering direction and magnitude sensitively dependent on the fore-aft inclination at the contact point. Since the robot step length is fixed, two robots which begin 0.5 cm apart in the fore-aft direction will contact the first boulder (Fig. 48B, boulder 1) with a difference in fore-aft inclination of at least $20\,^\circ$, leading to a different scattering angle after the first collision. In the top trajectory, the leg forced the boulder to yield to the front (the forced sliding mode in Fig. 46B, green shaded block), and thus, the robot orientation was not significantly affected. In the bottom trajectory, the leg slipped off the boulder, generating a horizontal impulse that caused $\approx 20\,^\circ$ degree change in the yaw angle of the robot (the repulsive slipping mode in Fig. 46B, blue shaded block). This difference will lead to an even larger difference in boulder surface inclination at the next contact point, and become further amplified in the multiple collisions along the robot trajectories. For given ground

heterogeneities, the trajectory of the robot can be deterministically predicted using the characterized scattering pattern. In more general settings (with uncertainty in boulder property and mobility), based on the dependence of interaction modes upon local inclination at contact, our scattering superposition principle can be expanded to statistically estimate the robot locomotion and trajectory for complex heterogeneous terrains with different heterogeneities.

5.7 Conclusion

Using a previously developed system SCATTER, we systematically examined how the presence of ground heterogeneity affects the robot's locomotion and trajectory. Analysis of robot CoM trajectories revealed that the interaction with a single boulder could be modeled as a scatterer with attractive and repulsive features. The scattering angle depended sensitively on the fore-aft boulder inclination at the contact point, but remarkably this dependence was universal and relatively insensitive to boulder geometry, orientation, and texture. We demonstrated that different scattering modes could be inferred from the fore-aft inclination angles at the initial contact point. For a field with multiple boulders, robot long-time trajectories sensitively depend on initial conditions, and this can be explained using a superposition of the scattering feature. The analogy to the scattering problem provides a way to simplify the characterization of the heterogeneous ground effect on robot trajectory deviation, and allows for long term dynamics analysis for exploratory robot trajectories on large, complex heterogeneous fields.

CHAPTER VI

ANTICIPATORY CONTROL OF LEGGED LOCOMOTION ON HETEROGENEOUS GRANULAR GROUND

6.1 Summary

Legged robots must traverse complex terrain consisting of particles of varying size, shape and texture. While much is known about how robots can effectively locomote on hard ground and increasingly on homogeneous granular media, principles of locomotion over heterogeneous granular substrates are relatively unexplored. To systematically discover how substrate heterogeneity affects ambulatory locomotion, previously we investigate how the presence of a single boulder (3D printed convex objects of different geometries) embedded in fine granular media affects the trajectory of a small (150 g) six legged robot. Using an automated system to collect thousands of locomotion trials, we observed that trajectories were straight before the interaction with the boulder, and scattered to different angles after the interaction depending on the leg-boulder contact positions. However, this dependence of scattering angle upon contact zone was relatively insensitive to boulder shape, orientation and roughness[101]. Inspired by this insensitivity, here we develop an anticipatory control scheme which uses the scattering information in coordination with a tail induced substrate jamming. Our scheme allows the robot to "envision" outcomes of the interaction such that the robot can prevent trajectory deviation before the scattering occurs. We hypothesize that (particularly during rapid running or in the presence of noisy sensors) appropriate substrate manipulation can allow a robot to remain in a

favorable locomotor configuration and avoid catastrophic interactions [1].

6.2 Introduction

Legged locomotors in the biological world combine sensory information and prior knowledge to perform anticipatory obstacle negotiation on challenging heterogeneous terrains[96]. In particular, we are interested to understand how animals like the Zebra-tailed lizard (Fig. 49A) which live in heterogeneous granular terrain locomote so effectively in the presence of particulates of widely varying sizes (from micro-scale fine particles to rocks comparable to body height). While little is known about animal locomotion in such terrain, in the past ~ 10 years, there have been a number of biological studies that demonstrate that animals can use a combination of preflexive and "anticipatory" control (integrating muscle function, body dynamics and neuromuscular control) to achieve graceful locomotion on terrain possessing obstacles, gaps, etc.[11, 96, 18, 120, 115].

Among robotic locomotors, such anticipatory control schemes could be useful in traversing heterogeneous terrain. Such terrain is common in particulate substrates like deserts or Martian terrain (Fig. 49B,C) – these landscapes are often composed of collections of particles of different sizes and shapes. When even well controlled legged robotic locomotors, like the RHex shown in Fig. 49B, travel across these heterogeneous granular environments, they exhibit failure modes like slips, unstable foot-holds, impassable barriers, etc. Such terrain mismanagement significantly affects robot stability, trafficability and power consumption.

[1] This Chapter is a paper by Feifei Qian and Daniel I. Goldman, *Robotics: Science and Systems (RSS)* [101]

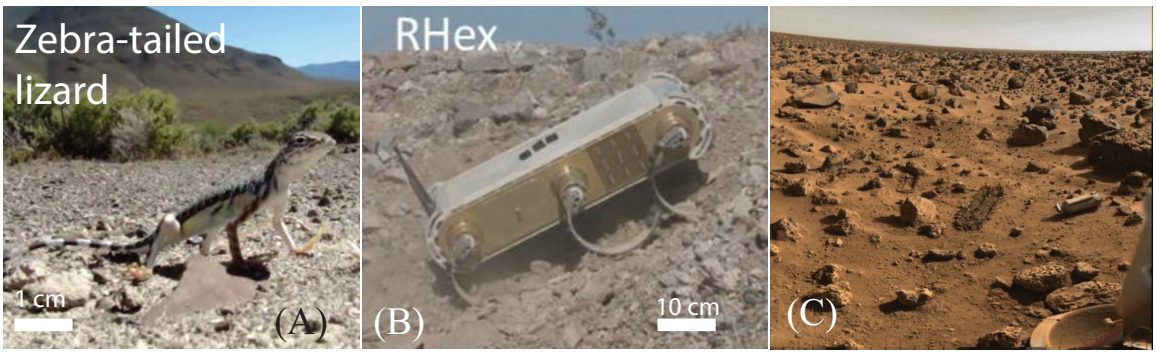

Figure 49: Natural heterogeneous granular terrain and locomotion challenges on such substrates. (A) The Zebra-tailed lizard (*C. draconoides*) runs rapidly over a diversity of such terrain (photo courtesy YouTube [1]). (B) RHex robot traveling across heterogeneous gravel substrate (photo courtesy Alfred Rizzi, Boston Dynamics). (C) A representative example of natural heterogeneous granular substrate, a view of the Martian terrain taken by the Curiosity Rover (photo courtesy NASA). As seen from the photo the substrate consists of multi-shape and multi-size particles, from fine sand and small gravel to large rocks.

Obstacle-interactive locomotion strategies are relatively unexplored for robotic locomotors. Currently, most terrestrial vehicles (including mobile robots) are tested on either hard ground or substrates composed of standardized homogenous media like Ottowa sand[86] and lunar simulants[37]. Many traditional navigation planning methods for navigation in obstacle environments involve finding a "collision free" path, which requires the robot to avoid obstacles. This is reasonable for most wheeled/treaded robots which must circumvent obstacles, but for legged robots, traversing obstacles by stepping over or upon them[63] can be a valid and possibly even a more effective option. Allowing robots to gracefully interact with obstacles[9] opens a new avenue for strategic navigation planning, and could significantly expand viable exploration space for obstacle-filled environments as well as aid robots in time critical tasks like search and rescue.

Development of obstacle-interactive legged robot locomotion control on heterogeneous granular terrain requires fundamental understanding of the complex interactions between the robot and the heterogeneous ground, which can be especially complicated when ground heterogeneities possess mobility relative to the substrates underneath. One of the challenges in creating the next generation of mobile robots is creating a discipline that can expand the scope of terramechanics [7, 130] from large tracked and treaded vehicles on homogeneous ground to arbitrarily shaped and actuated (e.g. limbs [71], flippers [84], body undulators [77, 81]) locomotors moving on and within complex heterogeneous terrestrial substrates; we refer to this generalizaton as "terradynamics". Both terramechanics and our recent terradynamic Resistive Force Theory models [72] can model locomotion on homogeneous substrates largely because interaction models are smooth and deterministic. However, in typical heterogeneous environments, the force fluctuations introduced by heterogeneities (gravel,

rocks, boulders, etc.) during intrusion and drag can be large, which makes the applicability of continuum based approaches like terramechanics [7, 130] and resistive force theory unclear.

To move toward a terradynamics of heterogeneous terrain, previously we designed and constructed the SCATTER system [99] (Systematic Creation of Arbitrary Terrain and Testing of Exploratory Robots) to automatically create heterogeneous granular ground conditions and perform robot locomotion tests within these environments. Using SCATTER, we investigated the locomotor dynamics during interaction with a single 3D printed convex objects of different geometries, textures, burial depths and mobilities [101]. Our study revealed that the complex interaction between a robot with a single boulder could be modelled as a scattering process – depending on the contact position on the boulder, the robot left the heterogeneity with a certain angle of trajectory deviation.

In this paper, we demonstrate that using the scattering information as prior knowledge, the robot can statistically estimate the outcomes of the interaction and thus perform an anticipatory correction to avoid catastrophic interaction modes and large course deviation. In particular, we rely on use of the solid-fluid transition in the granular media to effect a simple control scheme to manipulate the world: a deeply penetrated tail induces a granular media solidification, which enables a kinematically constrained body reorientation that corrects for the trajectory deviation caused by the scattering event. Our results thus indicate that the control of terrestrial locomotion can be simplified through manipulation of the environment.

6.3 Scattering angle dependence on leg-boulder contact position

In [99] , we developed a fully-automated terrain creation and robot locomotion testing apparatus, which we call the Systematic Creation of Arbitrary Terrain and Testing of Exploratory Robots (SCATTER, Fig. 42A). Using SCATTER, properties of heterogeneous multi-component substrates such as compaction, orientation, obstacle shape/size/distribution, and obstacle mobility within the substrate can be precisely controlled and varied to emulate a wide range of heterogeneous granular terrains.

Using the SCATTER system, we systematically studied how a single boulder (a localized heterogeneity) affected the robot's trajectory[101]. For example, we compare robot trajectories during interaction with a single spherical boulder fixed at different burial depths in the sand (Fig. 50A). The boulder diameter was chosen to be 5 cm, comparable with the robot C-leg diameter (4 cm). We tested the robot trajectory for two different burial depths, one is a quarter-buried "High boulder" (Fig. 50B left, with three quarters of the boulder diameter, ≈ 3.75 cm, protruding from the granular surface) and the other is a three quarters buried "Low boulder" (Fig. 50B right, with only a quarter of the boulder diameter, ≈ 1.25 cm, protruding from the granular surface).

We fixed the robot's initial leg phase and systematically varied the initial fore-aft position of the robot such that the robot contacted with the boulder with different leg phases. We observed that the robot's trajectory was straight before interaction with the boulder, then exited at different angles (depending on initial conditions) after the interaction (Fig. 50C, E), as if the robot was "scattered" by the boulder. Interestingly, most of the robot trajectories were "attracted" to the boulder after the interaction. We noticed that the average trajectory deviation with "attraction"

towards the boulder was significantly larger during high boulder interaction as compared to the low boulder interaction. When the robot contacted the high boulder, the interaction caused the robot to pitch and yaw significantly, in some cases the robot even flipped over backwards when the interaction occurred closer to the top region of the high boulder (lateral distance between robot centerline and boulder < 4 cm, with 0 cm being robot centerline passing through the boulder center). Therefore, in Fig. 50C $\sim$ F we only compare robot trajectories and scattering angle for initial lateral distances between 4 and 9 cm, with 9 cm being the point where the robot will no longer contact the boulder along its trajectory.

To quantitatively analyze the scattering effect of the boulder, we fit two lines to the trajectory, one before and one after the boulder interaction. These lines were used to characterize the trajectory's angular change (the scattering angle). We noticed that for both the high boulder and the low boulder the scattering angle depended sensitively on the robot's initial position. While the scattering magnitude upon the high boulder was significantly larger as compared to the low boulder, the dependence of scattering angle upon robot initial fore-aft position was similar (Fig. 50D, F).

This sensitivity of scattering angle to robot initial position was likely due to different leg-boulder contact positions (or the boulder surface inclination at contact). The difference between the scattering magnitude between the low boulder and the high boulder was likely caused by the different boulder surface inclination angle at the same contact position on the boulder. In [101] we characterized the scattering angle as a function of the contact zones for a variety of boulders with variation in shape, orientation and roughness (Fig. 51), and we found that despite variation in boulder shape, roughness and orientation, the scattering angle sensitively depended on the leg-boulder contact zones, and this dependence exhibited similar characteristics for

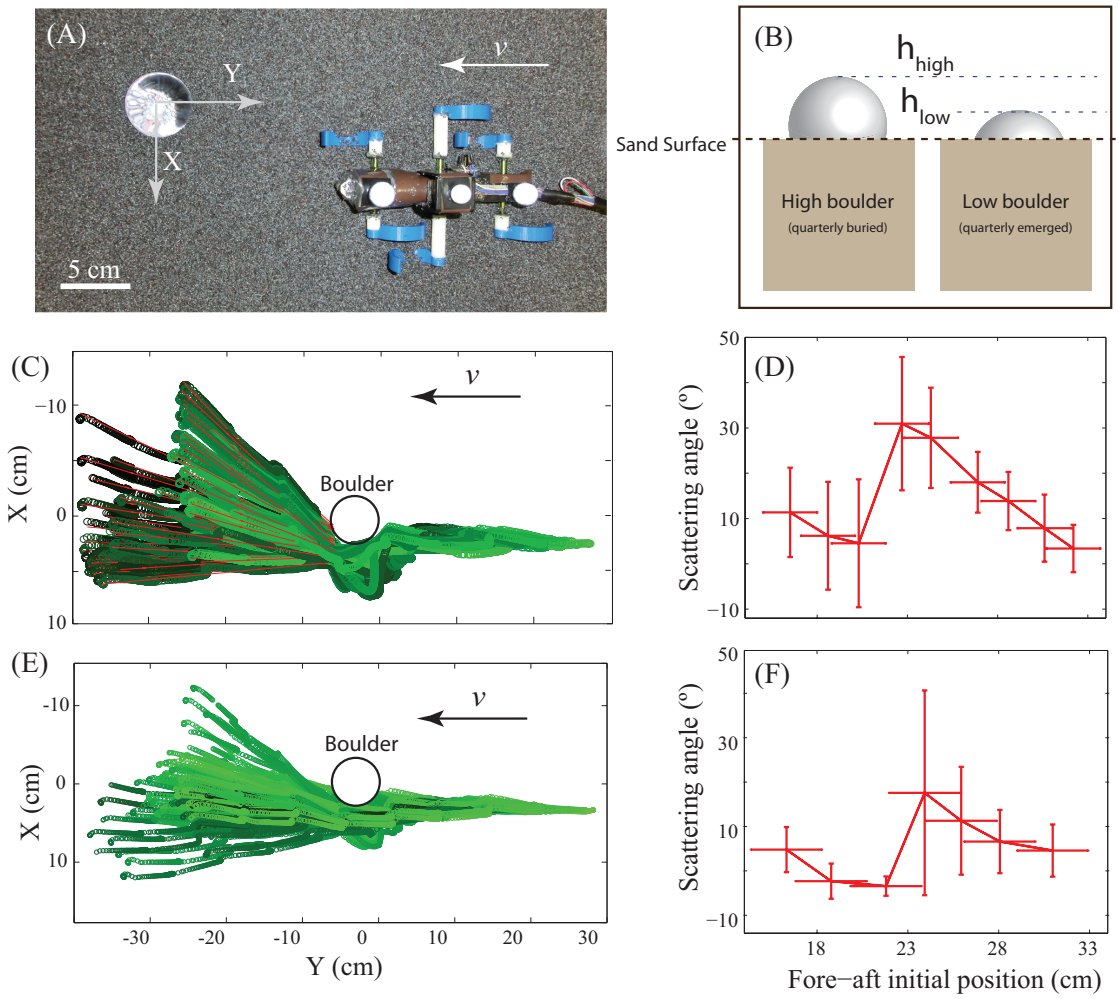

Figure 50: Robot interaction with single spherical boulder. (A) Experimental setup of the single boulder experiment. The center of the boulder is set as the origin. X and Y axis represents lateral and fore-aft direction. (B) Diagram of the two different boulder conditions tested here. The high boulder was slightly buried in the "sand" with three quarters of the boulder diameter (≈ 3.75 cm) protruded from the granular surface, whereas the low boulder was deeply buried with only a quarter of the boulder diameter, ≈ 1.25 cm, protruded from the granular surface. Both boulders were fixed at the burial depth and were not allowed to move during robot leg interaction. (C, E) Robot CoM trajectories for both high boulder setup (C) and low boulder setup (E). Trajectory color represents different initial fore-aft positions. Red lines are a linear fit of the robot's trajectories after boulder interaction, which were used to calculate the scattering angle. (D, F) Robot scattering angle after interaction with high boulder (D) and low boulder (F) as a function of the initial fore-aft distance between robot and the boulder. Postive scattering angle means that the robot turned to boulder (was "attracted") after the interaction and negative angle means the robot turned away from the boulder (was "repelled").

all boulders. We also noticed that most of the "attractive" zones were distributed on the front side of the boulder (Right front, Front, Left front), whereas most of the "repulsive" zones were distributed on the center or back side of the boulder (Left back, Top, Back, Right back). This is also consistent with our observation from the low boulder and high boulder experiment, and suggested that the fore-aft direction boulder surface inclination at contact was largely responsible for the sensitivity of scattering angle to robot initial positions (Fig. 50).

6.4 Anticipatory boulder negotiation using robotic tail

Based on the insensitivity in the scattering angle dependence upon contact zone among different boulder shape, roughness or orientation, we hypothesized that this general principle could be used as a prior knowledge to allow low-cost platforms to perform anticipatory control. This is especially important for rapid running on complex terrains, where the sensing signals are usually noisy and sometimes not fast enough for the feedback controller to adjust robot posture from large perturbations, which could compromise the performance of feedback controllers. With anticipatory control, the robot can statistically estimate possible outcomes of the interaction before the disturbance, and therefore remain in a favorable configuration close to its natural, preferred movement pattern thereby allowing the feedback controller to better adjust robot locomotion. Here we demonstrate this scheme using a simple, tail-assisted substrate solidification approach, and we use a touch sensor embedded in the boulder to facilitate contact zone characterization.

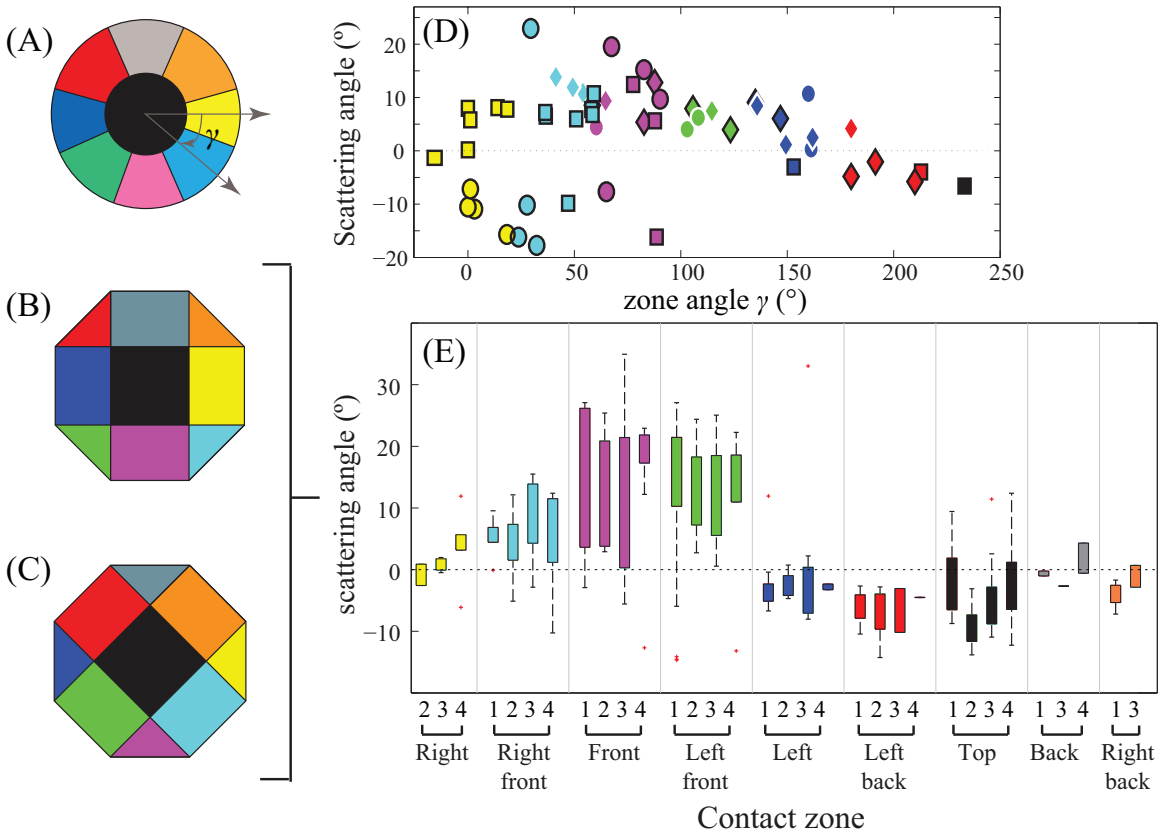

Figure 51: Scattering angle dependence on contact position for boulders of different shape, orientation and roughness. (A, B, C) Top view diagrams of the three boulder shapes and orientations, including a sphere (A), a 90 degree oriented rhombicuboctohedron (B), and a 45 degree oriented rhombicuboctohedron (C). For (B) and (C) we also tested two different roughness (plastic "smooth boulder" and sandpaper coated "rough boulder"). Different colors (yellow, cyan, purple, green, blue, red, black) corresponding to different contact zones (right, right-front, front, left-front, left, left-back, top), respectively. (D, E) Scattering angle vs. contact zone. (D) is spherical boulder and (E) are rhombicuboctohedral boulders with variation in orientation and roughness, including a rough 45 degree oriented rhombicuboctohedron (1), a smooth 45 degree oriented rhombicuboctohedron (2), a rough 90 degree oriented rhombicuboctohedron (3), and a smooth 90 degree oriented rhombicuboctohedron (4). Lower and upper limit of the central box in boxplot (E) represent the 25% and 75% quantile of the data, respectively. Color convention in (D, E) is the same as (A, B, C). Marker shape (square, diamond, circle) in (D) represents front, middle, rear leg contacted with the boulder, respectively. Markers without outlines indicate robot leg shaft contact. Figure adapted from [101] .

6.4.1 Boulder sensing and tail actuation

To detect leg-boulder contact positions, we embedded a capacitive touch sensor (Freescale MPR121, 12 channels) into the 3D-printed rhombicuboctahedron boulder. Wire leads of 9 channels were attached to all polyhedral faces on the top half of the rhombicuboctahedron boulder, and fixed by adhesive copper tape (Figure 52A, B) that covered the different contact zones. The convex surfaces of all 6 robot legs were also covered by copper tape (Figure 52E) and grounded to trigger the capacitive touch sensor. Touch signals were acquired using Arduino Uno and then sent to LabVIEW via serial communication. When one or multiple zones were touched, the corresponding bit in the 2-byte signal was set to 1. This signal was then processed by LabVIEW and used to trigger different tail control behaviors.

The robotic tail (Figure 52C, D) was actuated using two servo motors, one (HS-A5076HB) controlling the lateral swing of the tail, and another (HS-5055MG) controlling the vertical intrusion of the tail. Both servo motors were driven by a servo controller (Lynxmotion SSC-32) and controlled by pulse width modulation (PWM) in LabVIEW. The swing motor rotation was defined to be 0° when the tail was aligned with the robot body, and to be positive for clockwise (CW) rotation and negative for counterclockwise (CCW). The insertion motor rotation was defined to be 0° when the tail was horizontal, and to be positive for lifting upwards and negative for intruding downwards.

6.4.2 Trajectory control through tail induced substrate solidification

We implemented a simple control sequence (Figure 53A) to test the effectiveness of scattering correction using the tail. During the control sequence the tail moved in a rectangular trajectory in the sequential order of (1) Swing horizontally (CW/CCW)

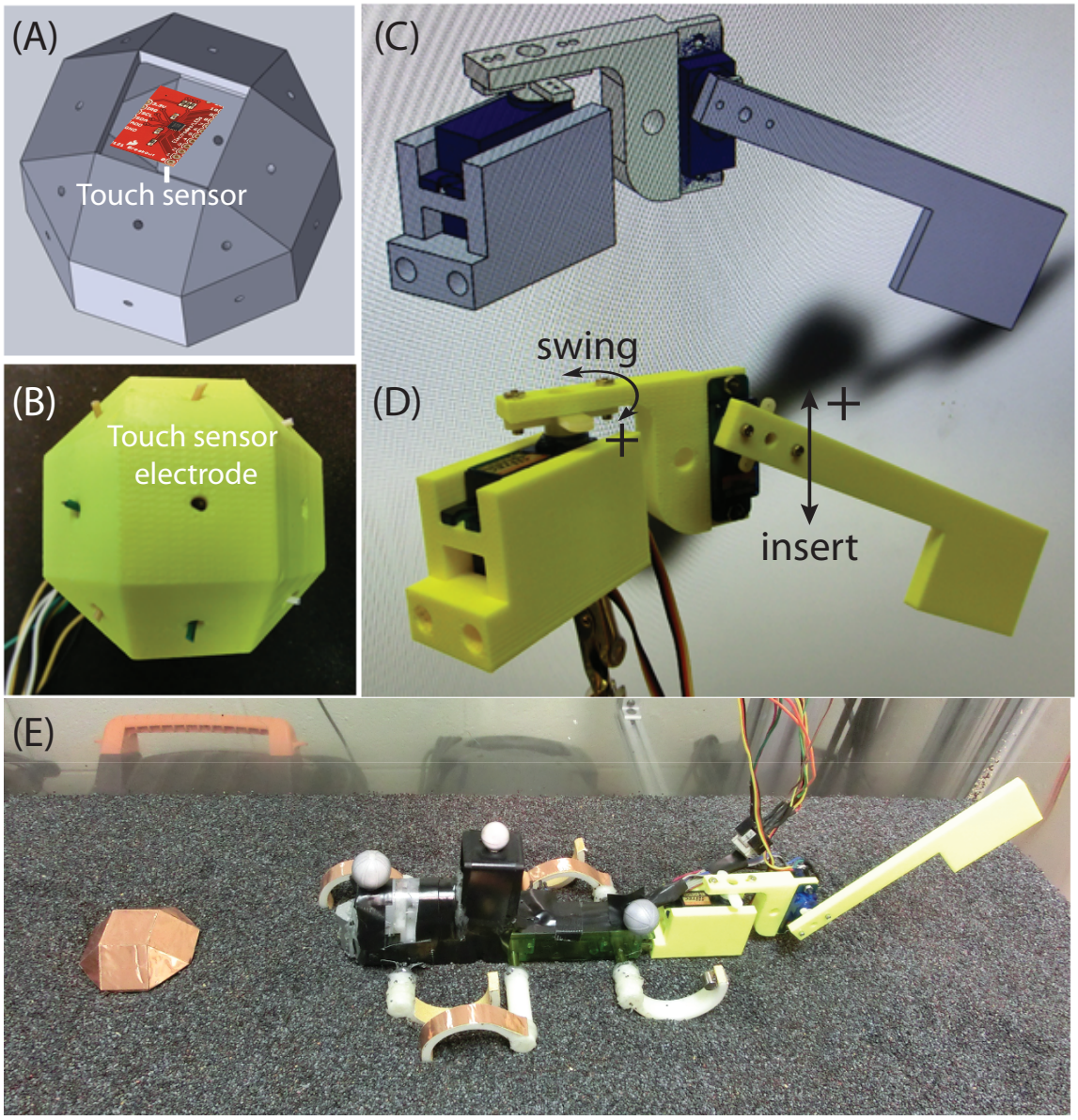

Figure 52: Boulder sensing and tail design in anticipatory control experiment. (A) Mechanical design diagram of a rhombicuboctahedron boulder with touch sensor embedded within. (B) 3D-printed "touch boulder" with electrodes from the embedded touch sensor wired to the boulder surface through 2 mm diameter holes. (C) Mechanical design of the robotic tail. (D) Integrated swing-insertion robotic tail controlled by two servo motors. (E) Experiment setup of the robot tail anticipatory control experiment. Touch sensor electrodes on each boulder zone were defined by copper tape. Robot legs were grounded to trigger touch sensor.

in air; (2) Insert vertically into sand; (3) Swing back horizontally within the sand; (4) Lift up. We characterized the resulting robot body turning angle β (Figure 53B, red squares) for a variety of tail motor swing and insertion angles, and surprisingly, we found that for all insertion angles that penetrated deeper than $-10°$, the body rotation angle mainly depended on tail motor swing angle and was insensitive to insertion angle.

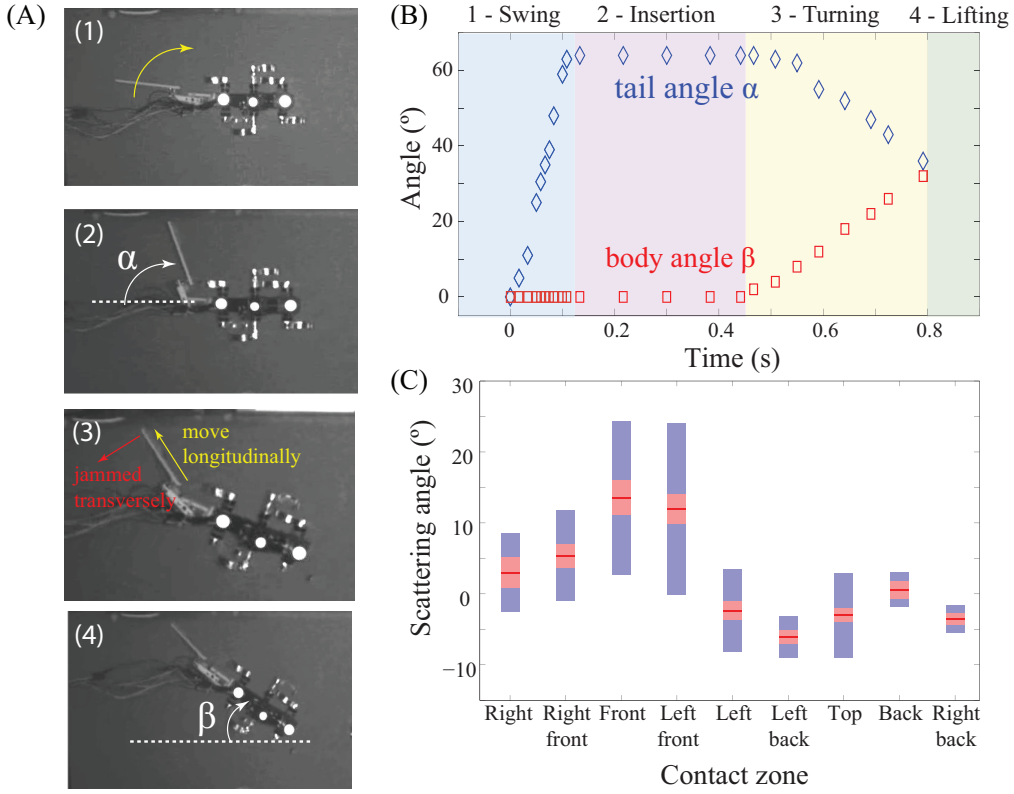

Figure 53: Tail control sequence and control signal that statistically estimated from scattering result. (A) Control sequence of the robotic tail. (1) Swing horizontally in air; (2) Insert vertically into sand; (3) Rotate back about swing motor axis, jamming the GM and constraint transversely to rotate the body; (4) After reorient the body, lift from the sand. (B) Tail angle (blue diamonds) and body angle (red squares) measured in world frame. (C) Statistical boxplot of the scattering angle vs. contact zone from experiment measurements shown in Figure 51E. Red line represents the mean of the scattering angle; pink box represents the 95% confidence interval; and blue box represents 1 s.d.. Non-overlapping confidence intervals indicate a significant difference at the chosen p-value of 5%. Tail control signal was set to be proportional to the mean scattering angle (red lines) but in opposite direction.

This independence of insertion angle is a result of the granular media reaching a jammed state. Granular jamming and solidification have been be used in robot and animal locomotion control to generate propulsion and achieve effective locomotion on granular substrates [71, 84, 81]. Unlike turning control in fluids where hydrodynamic response of the medium governs the turning dynamics, the solidification feature of granular material (i.e., the presence of a yield stress) provides a simple way to perform turning control, using the kinematically constrained relation between the robot body angle and tail swing angle. As shown in Figure 53A, during (3) the tail rotated about the swing tail motor axis, but due to the jammed granular media the tail could only extend longitudinally but not transversely. In this manner the resulting body rotation angle was kinematically constrained and could thus be controlled by only the initial tail swing angle. The tail swing angle, therefore, was set to be proportional, but in the opposite direction, to the average scattering angle for each contact zone (Figure 53C), to correct for the body rotation during the scattering event. The intrusion angle was kept the same ($-30°$) for all contact zones, since the course correction angle was insensitive to tail insertion angle given that the tail intruded deeply enough to prevent significant fluidization of the granular media.

6.4.3 Scattering angle reduction with tail assisted anticipatory control

As a proof of concept, we did not attempt to correct for every incident of boulder contact, but instead looked to use minimal control effort to reduce the trajectory deviation on heterogeneous terrain. Our tests demonstrated that even with this simplified tail control, the scattering angle of the robot trajectory could be significantly reduced.

Figure 54 shows an example of two experimental runs with the same initial and kinematics settings, one with tail anticipatory control and the other without. Before

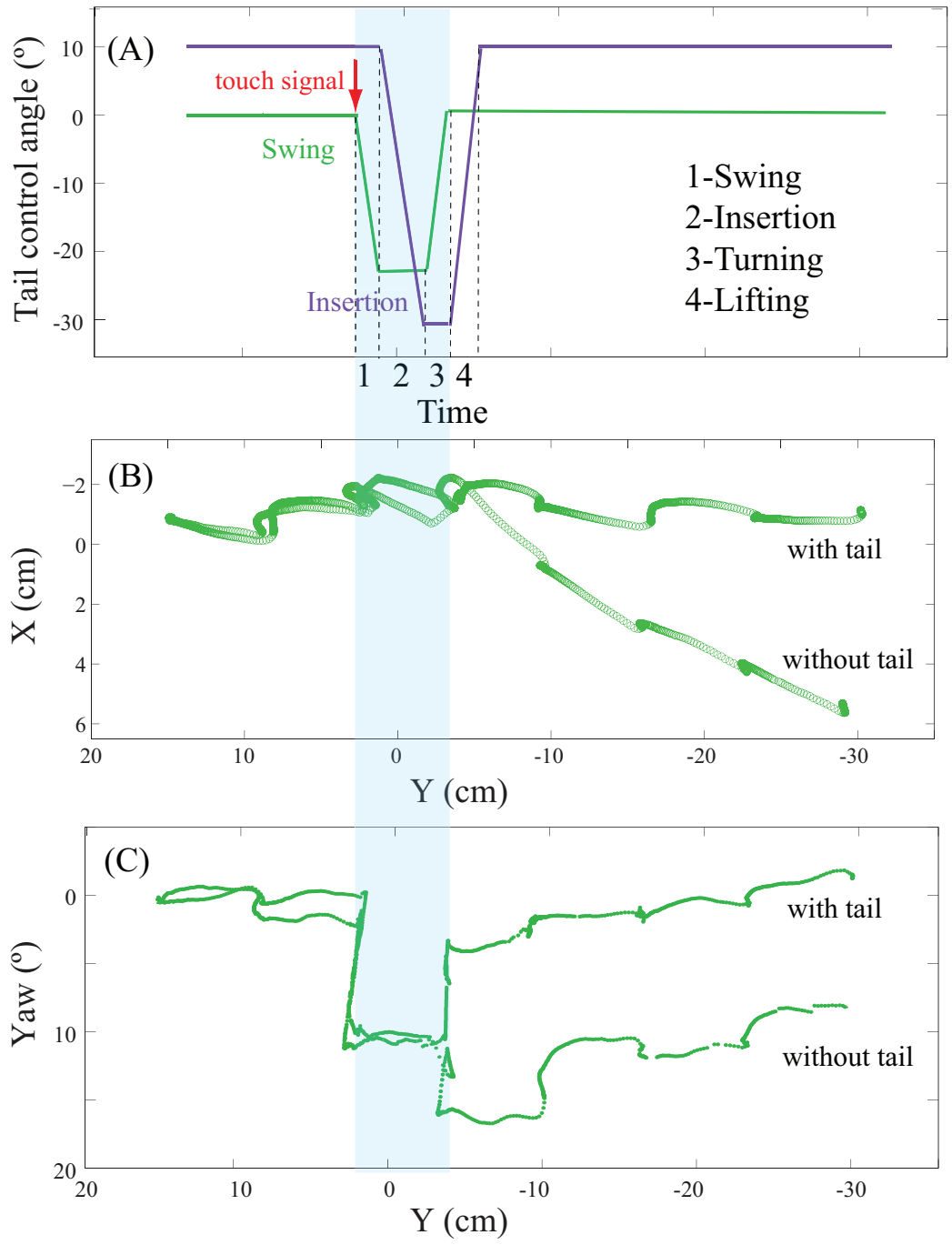

Figure 54: An example of two experimental runs with the same initial position and kinematics, one with tail anticipatory control and the other without. (A) Tail swing motor and insertion motor control signal. 1 - Tail rotated horizontally; 2 - Tail inserted $-30°$ into the sand; 3 - Tail rotated back to $0°$ in sand, jamming the GM to generate body rotation; (4) Tail lifted up to initial position. (B) Robot CoM trajectory comparison between open loop control and tail anticipatory control. (C) Robot body yaw angle comparison between open loop control and tail anticipatory control.

the robot started moving, the tail swing motor was set to 0° and the insertion motor angle was set to 10° (slightly lifted above the sand surface). For the tests with tail control enabled, upon the first leg-boulder contact (triggered by the touch sensor signal), as shown in Figure 54A, the tail rotated horizontally (1-Swing) to the prescribed angle based on the scattering angle predicted by the zone of contact, subsequentially descended into the GM (2-Insertion), then rotated back to 0° about the swing motor axis, while remaining transversely constrained in the jammed GM and generating a body rotation to reorient the robot (3-Turning). Following the body rotation, the tail was lifted from the GM (4-Lifting).

We see from Figure 54 that before the leg-boulder contact, the two robot trajectories were similar. However, as the robot leg contacted the boulder, the robot without tail control slipped off the boulder, generating a lateral impulse that caused $> 10°$ change in the yaw angle of the robot (Figure 54B without tail), and leading to a CoM trajectory that deviated from the initial direction (Figure 54C without tail). The tailed robot began the anticipatory control (Figure 54A) upon leg-boulder contact, and successfully reduced the scattering angle within the same step (Figure 54C with tail) resulting in a straight trajectory (Figure 54B with tail), similar to the robot trajectory on homogeneous granular ground.

Figure 55 shows the difference in scattering angle distribution between with and without tail anticipatory control over 300 runs. With anticipatory control, the scattering angle was significantly reduced from maximum values reaching $\approx 28°$ to $\approx 13°$, eliminating large attractive scattering angles and reducing the average trajectory deviation to close to zero. The $\pm 10°$ distribution of uncorrected scattering angles was a consequence of the simplified control scheme. That is, the tail performed anticipatory control only upon the first contact on the boulder, but there could be multiple

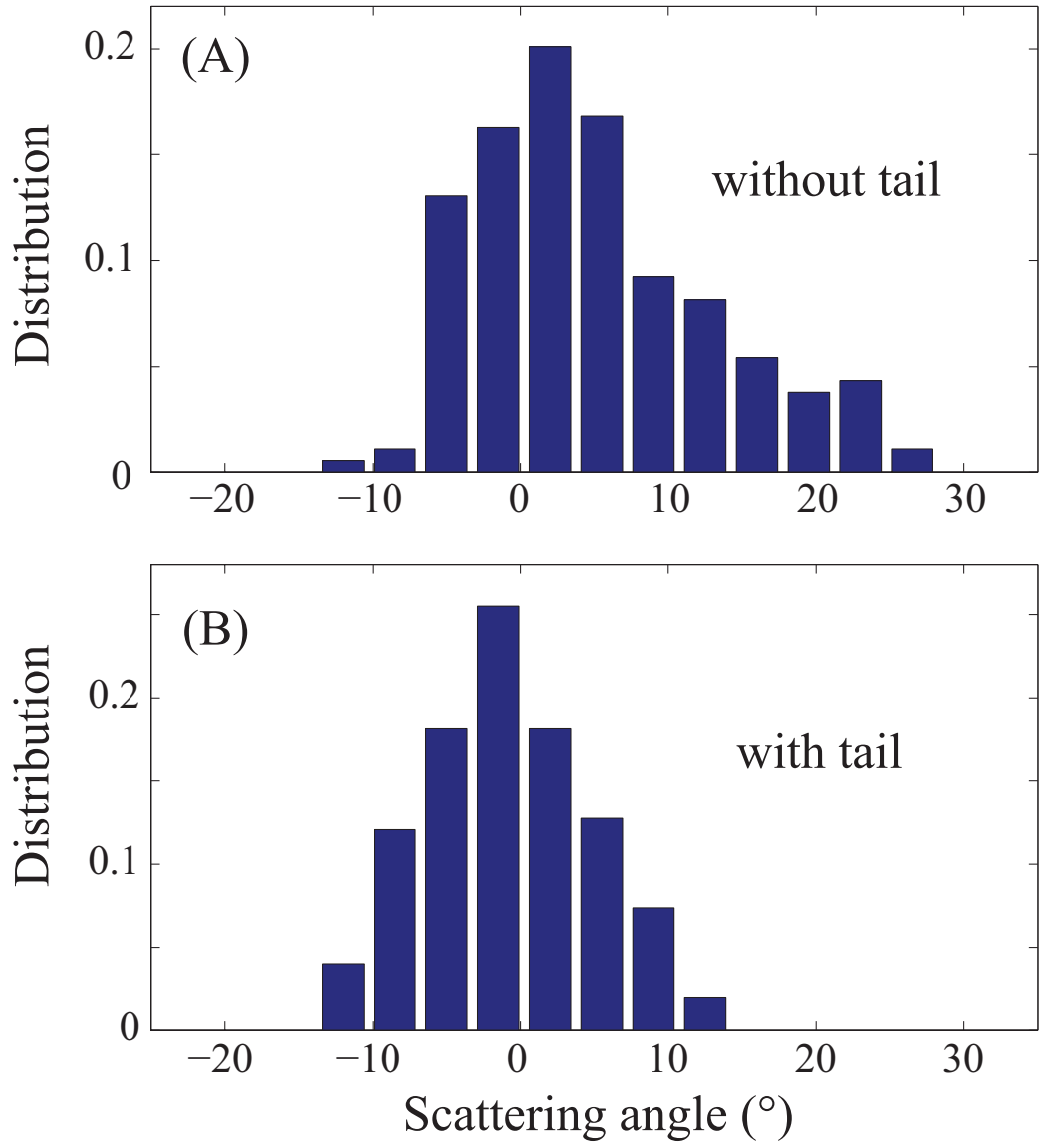

Figure 55: A comparison of scattering angle distribution between with (A) and without (B) tail anticipatory control. The robot trajectory deviation with tail control was reduced from a maximum value of $\approx 28°$ to $\approx 13°$, eliminating large attractive scattering angle components.

leg-boulder interactions during one run, with leg sliding from one contact zone to another, or multiple legs contacting on different boulder zones at the same time. In future work, we will investigate the multi-interactions effect, and model the robot-boulder interaction mode based on the local boulder surface angle, to allow for more accurate and dynamic control of locomotion. Also, we noticed that the scattering correction was relatively less effective for small scattering angles (e.g., $< 5°$). This is largely due to the delayed material response during the tail induced solidification. In future work, we will systematically characterize the tail's morphological and kinematic parameters, to increase the effectiveness in producing GM jamming.

Besides trajectory deviation, the robot also exhibited pitching, rolling, and speed reduction/fluctuations during the boulder interaction. In future work, we will investigate these effects in more detail, and we expect that the development of predictive models can also aid the anticipatory appendage control and further improve robot locomotion performance regarding these issues. Another future direction that we plan to explore is to expand the application of tail assisted GM solidification to achieve different desired trajectories on complex granular terrains. We envision that the development of trajectory control through substrate solidification could significantly reduce the control effort and be useful for exploratory rovers on challenging granular terrains. We will also further investigate the effect of boulder mobility on robot scattering pattern. We posit that these understandings will allow robots to achieve effective locomotion by exploiting and actively manipulating the mobility of the boulder [101] and the property of the sand. We also envision that the development of this "terradynamic" framework for heterogeneous flowable ground will aid in the future design and control of exploratory robots and allow for higher maneuverability on challenging heterogeneous granular terrains.

6.5 Conclusion

We developed an anticipatory control scheme which relied on granular solidification and scattering knowledge. We obtained the scattering information by using a previously developed SCATTER system, which can precisely control and automatically vary properties of the heterogeneous granular substrates. Analysis of robot trajectories in single boulder experiments revealed that the interaction with a single, localized boulder could be modeled as a scattering effect with attractive and repulsive features. The scattering angle depended sensitively on the leg-boulder contact position, but remarkably, this dependence was relatively insensitive to boulder shape, orientation and roughness. We demonstrated that by utilizing this scattering insensitivity, the robot could perform a tail-assisted anticipatory control using a tail induced substrate solidification, and significantly reduce the trajectory deviation caused by boulder interaction. Our scattering study provides a better understanding of the complex interaction between the robot and the heterogeneous ground, and allows robots to evaluate obstacle traversability and predict the probability of outcomes (e.g., possible failure, trajectory deviation, etc.) of different locomotion modes before perturbations. In this manner even simple, low-cost robots can perform successful anticipatory control and manipulate their environments to remain in a favorable locomotor configuration and avoid catastrophic failures.

CHAPTER VII

CONCLUSION AND FUTURE WORK

7.1 Conclusion

In this dissertation, we developed novel ground control techniques to allow systematic creation and variation of granular substrates with arbitrary stiffness and heterogeneity. Using legged robots as physical models, we systematically investigated locomotion on homogeneous and heterogeneous granular ground, and developed interaction models to explain locomotor performance differences among a variety of robotics and biological locomotors with variation in morphology and gait.

We discovered that locomotor performance on homogeneous deformable substrates was determined by the leg penetration ratio. Locomotors with smaller foot pressure were less sensitive to ground stiffness variation, and thus could passively maintain relatively effective performance on low resistance ground. At low gait frequencies, hydrostatic-like forces generated during the yielding of the GM ultimately led to the solidification of the substrate, allowing locomotors to effectively move as if they were walking on a solid surface. At high frequencies, the inertia of the grains being accelerated became important and granular forces became hydrodynamic-like, allowing lightweight locomotors to achieve rapid running by exploiting fluid-like responses of the granular substrate.

Locomotion on heterogeneous granular substrates was more complicated due to force fluctuations introduced by heterogeneities. We developed an automated terrain creation and locomotion testing system, the SCATTER, to precisely control and

automatically vary properties of the heterogeneous granular substrates, facilitating extensive parameter variation and systematic testing for robot locomotion on a wide variety of challenging terrains.

Using the SCATTER system, we systematically analyzed the interaction between a hexapedal robot and the heterogeneous substrates, and found that the interaction of the robot with each heterogeneity (i.e., boulders, rocks, logs, etc.) can be modeled as a scattering potential with attractive and repulsive features. The magnitude of the potential depends sensitively on the leg-heterogeneity contact zone and the heterogeneity mobility within the fine sand, but this dependence was universal and relatively insensitive to heterogeneities' geometry, orientation, or texture. We demonstrated that different interaction modes could be inferred from the fore-aft inclination angles at the initial contact position, which allows estimation of interaction outcomes (e.g., possible failure, trajectory deviation, etc.) before a perturbation occurs. In this manner even simple, low-cost robots can perform successful anticipatory control and manipulate their locomotion environments to remain in a favorable locomotor configuration and avoid catastrophic failures.

7.2 Future work

Below are a few possible directions to be pursued in future study.

7.2.1 Long term dynamics analysis

The single boulder scattering potential analysis provides a way to theoretically model the long term dynamics of robot scattering on large scale boulder field. To systematically test this model, we plan to track and analyze the trajectory of a single-wheel robot on a floating spherical treadmill (a "Kugel",Fig. 56), with different profile of scatterers patterned on the Kugel surface. The trajectory of the robot will reflect in

the rotational displacement of the Kugel, which can be tracked by an optical mouse mounted on the side of the Kugel. We expect that variation in shape, size and spacing of the scatterers will result in different robot diffusion properties. This investigation will provide useful information in diffusion theory as well as robot navigation prediction (e.g., coverage estimation for large scale robot team search and rescue task).

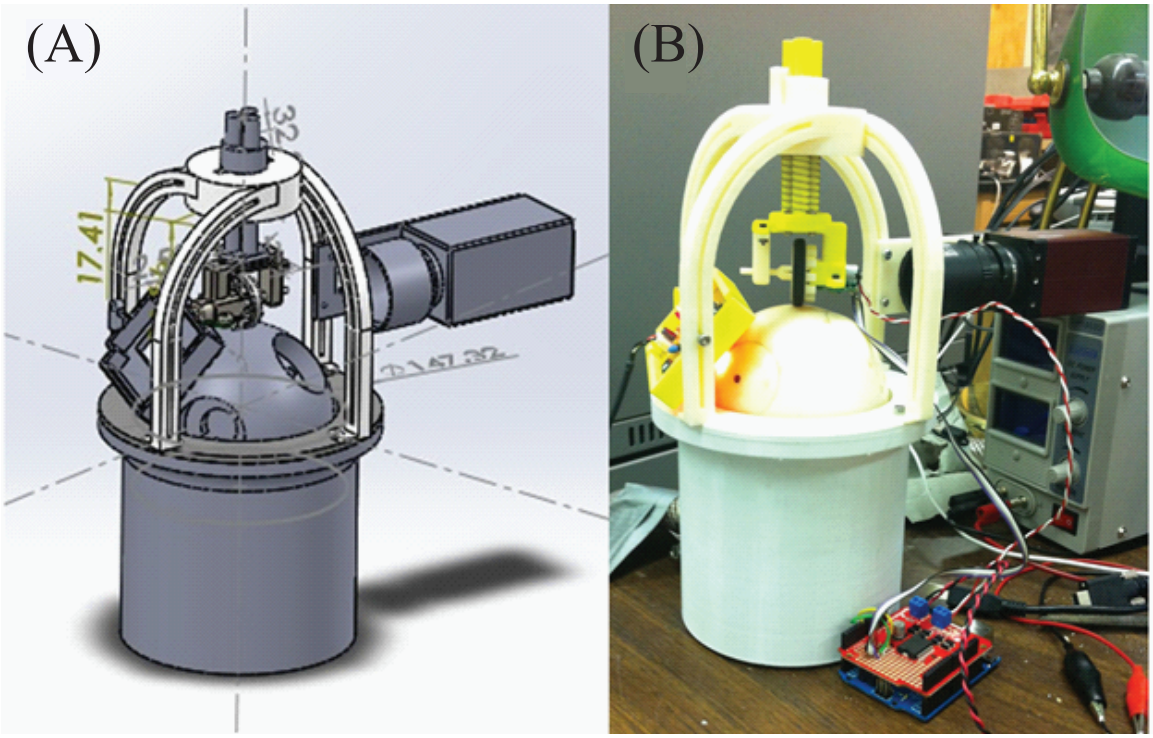

Figure 56: Long term scattering experiment using a Kugel apparatus. (A) The mechanical design of the apparatus. (B) A photo of the apparatus. A motorized wheel is mounted in place on top of an air-fluidized Kugel, whose surface was tiled with a lattice of spring-loaded interchangeable scatterers. Compressed air flows into the Kugel base, evenly fluidizes the Kugel through an air distributer. The scattering trajectory of the robotic wheel was continuously tracked by an optical mouse mounted on the side and recorded by a side-view camera.

7.2.2 Leg shape effect on interaction modes

Our interaction analysis has been largely focused on the positive C shaped legs which was found to produce effective locomotion on hard ground [105] and granular substrates [72]. However, for heterogeneous substrates and sand inclines, other leg shapes

(e.g., flat legs, L shaped legs, and negative C shaped legs, etc.) could potentially produce different leg-boulder interaction modes, leading to higher locomotion performance. In future studies we plan to systematically test different leg shapes and analyze their ground interaction modes and associated robot locomotion performance. These investigations should provide insights into the principles of robot foot design that allows high locomotion performance on more complex terrains.

7.2.3 Gait adaptation to terrain variations

Our terrain interaction analysis studies have revealed that by adjusting locomotor parameters (morphology [80, 69], gait parameters [70], extra appendage actions [98], etc.), robots can passively or actively "manipulate" locomotion environments by triggering different substrate responses [102, 100], to increase the efficiency of locomotion over varying terrain types. However, the missing component has been the ability of the robot autonomously to detect how the terrain has changed and accordingly adapt the properties of its gait. In future work, we plan to integrate terrain sensing and apply our interaction principles to aid in the decision making of robot gait adaptation to terrain variations. By combining our robot-ground interaction results with sensing and planning methods, we expect to allow the robot to make decisions about gait parameter adaptation based on the changes in terrain properties.

7.2.4 "Particle wave" assumption for legged and legless locomotion

In Chapter V, we discovered that when an obstacle (e.g., a cylindrical log) was present in front of the robot, robot trajectories diverged from a straight path and produced a bimodally distributed "position uncertainty"(Fig. 57A) on the other side of the obstacle, similar to the features previously observed in microscopic quantum realm (e.g., diffraction, interference). We suspect that both legged and legless locomotors behave

emergently like "particle wave" that interact with obstacles, where for a legless locomotor (i.e., a snake) its waveform can be described using the undulation amplitude and frequency, and for a legged robot a waveform can be described using the alternating gait frequency and initial leg phase. Preliminary tests of a legged robot (Fig. 57A) and a legless robot (Fig. 57B) traversing through a "single slit" obstacle indicated that the distance between the two distribution peaks depended on both the slit width and the locomotor "wavelength". In future work, we plan to explore in more details to see if a locomotor can effectively interact with an obstacle by actively or passively adjusting its shape/gait wavelength to adapt to the locomotion environments.

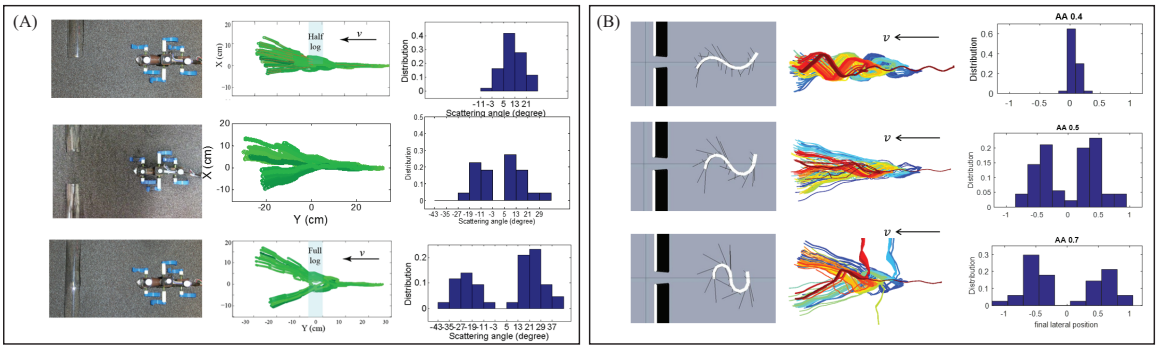

Figure 57: Single slit experiment. (A) A legged robot traversing a log with different opening widths. (B) A legless robot traversing a single slit with different body wavelength. In both (A) and (B), the first column shows the experimental setup, the second column shows the robot trajectories, and the third column shows the distribution histogram of the robot positions captured on the other side of the obstacle.

REFERENCES

[1] "https://www.youtube.com/watch?v=s1WMPLbvGjg."

[2] Aguilar, J. and Goldman, D. I., "Robophysical study of jumping dynamics on granular media." in review.

[3] Aguilar, J., Zhang, T., Qian, F., Kingsbury, M., McInroe, B., Mazouchova, N., Li, C., Maladen, R., Gong, C., Travers, M., Hatton, R. L., Choset, H., Umbanhowar, P. B., and Goldman, D. I., "A review on locomotion robophysics: the study of movement at the intersection of robotics, soft matter and dynamical systems." in review.

[4] Albert, R., Pfeifer, M. A., Barabási, A.-L., and Schiffer, P., "Slow Drag in a Granular Medium," *Phys. Rev. Lett.*, vol. 82, pp. 205–208, Jan. 1999.

[5] Andreotti, B., Forterre, Y., and Pouliquen, O., *Granular media: between fluid and solid*. Cambridge University Press, 2013.

[6] Aoi, S., Egi, Y., and Tsuchiya, K., "Instability-based mechanism for body undulations in centipede locomotion," *Physical Review E*, vol. 87, p. 012717, Jan. 2013.

[7] Bekker, M. G., "Theory of land locomotion," *University of Michigan*, 1956.

[8] Benedict, M., Mattaboni, M., Chopra, I., and Masarati, P., "Aeroelastic Analysis of a Micro-Air-Vehicle-Scale Cycloidal Rotor in Hover," *AIAA Journal*, vol. 49, no. 11, pp. 2430–2443, 2011.

[9] Bhattacharjee, T. and Grice, P., "A Robotic System for Reaching in Dense Clutter that Integrates Model Predictive Control, Learning, Haptic Mapping, and Planning," *Proceedings of the 3rd IEEE/RSJ International Conference on Intelligent Robots and Systems (IROS)*, 2014.

[10] Biewener, A. A. and Full, R. J., "Force platform and kinematic analysis," *Biomechanics: Structures and Systems: A Practical Approach*, pp. 45–73, 1992.

[11] Biewener, A. A. and Daley, M. A., "Unsteady locomotion: integrating muscle function with whole body dynamics and neuromuscular control.," *The Journal of experimental biology*, vol. 210, pp. 2949–2960, Sept. 2007.

[12] Birkmeyer, P., Peterson, K., and Fearing, R. S., "DASH: A dynamic 16g hexapedal robot," in *Intelligent Robots and Systems, 2009. IROS 2009. IEEE/RSJ International Conference on*, pp. 2683–2689, October 2009.

[13] Blickhan, R. and Full, R. J., "Similarity in multilegged locomotion: Bouncing like a monopode," *Journal of Comparative Physiology A*, vol. 173, pp. 509–517, Nov. 1993.

[14] Brown, E., Rodenberg, N., Amend, J., Mozeika, a., Steltz, E., Zakin, M. R., Lipson, H., and Jaeger, H. M., "Universal robotic gripper based on the jamming of granular material," *Proceedings of the National Academy of Sciences*, vol. 107, pp. 18809–18814, Oct. 2010.

[15] Carnot, S., Carnot, H., and Kelvin, W. T. B., *Reflections on the motive power of heat and on machines fitted to develop that power*. J. Wiley, 1890.

[16] Chehata, D., Zenit, R., and Wassgren, C., "Dense granular flow around an immersed cylinder," *Physics of Fluids*, vol. 15, no. 6, pp. 1622–1631, 2003.

[17] Crawford, C. S., *Biology of Desert Invertebrates.* New York: Springer, 1981.

[18] Cruse, H., Bartling, C., Cymbalyuk, G., Dean, J., and Dreifert, M., "A modular artificial neural net for controlling a six-legged walking system," *Biological cybernetics*, vol. 72, no. 5, pp. 421–430, 1995.

[19] Cumberland, D. and Crawford, R. J., "The packing of particles," 1987.

[20] Dickinson, W. W. and Ward, J. D., "Low depositional porosity in eolian sands and sandstones, {N}amib {D}esert," *Journal of Sedimentary Research*, vol. 64, no. 2a, pp. 226–232, 1994.

[21] Ding, L., Gao, H., Deng, Z., Song, J., Liu, Y., Liu, G., and Iagnemma, K., "Foot-terrain interaction mechanics for legged robots: Modeling and experimental validation," *The International Journal of Robotics Research*, vol. 32, pp. 1585–1606, Oct. 2013.

[22] Ding, Y., Gravish, N., and Goldman, D. I., "Drag induced lift in granular media," *Physical Review Letters*, vol. 106, no. 2, p. 028001, 2011.

[23] Esposito, C. J., Tangorra, J. L., Flammang, B. E., and Lauder, G. V., "A robotic fish caudal fin: effects of stiffness and motor program on locomotor performance," *The Journal of Experimental Biology*, vol. 215, no. 1, pp. 56–67, 2012.

[24] Ferris, D. P., Louie, M., and Farley, C. T., "Running in the real world: adjusting leg stiffness for different surfaces.," *Proceedings. Biological sciences / The Royal Society*, vol. 265, pp. 989–994, June 1998.

[25] Fieler, C. and B, "Effects of speed on the hindlimb kinematics of the lizard dipsosaurus dorsalis," *The Journal of experimental biology*, vol. 201, pp. 609–622, Feb. 1998.

[26] Finney, J., "Random packings and the structure of simple liquids. i. the geometry of random close packing," in *Proceedings of the Royal Society of London A: Mathematical, Physical and Engineering Sciences*, vol. 319, pp. 479–493, The Royal Society, 1970.

[27] Geldart, D., "Types of gas fluidization," *Powder technology*, vol. 7, no. 5, pp. 285–292, 1973.

[28] Ghiringhelli, G. L., Masarati, P., Mantegazza, P., and Nixon, M. W., "Multi-Body Analysis of a Tiltrotor Configuration," *Nonlinear Dynamics*, vol. 19, no. 4, pp. 333–357, 1999.

[29] Glasheen, J. W. and McMahon, T. A., "A hydrodhynamic model of locomotion in the Basilisk Lizard," *Nature*, vol. 380, pp. 340–342, Mar. 1996.

[30] Goldman, D. I. and Umbanhowar, P. B., "Scaling and dynamics of sphere and disk impact into granular media," *Physical Review E*, vol. 77, pp. 1–14, Feb. 2008.

[31] Golick, L. A. and Daniels, K. E., "Mixing and segregation rates in sheared granular materials," *Physical Review E*, vol. 80, no. 4, p. 042301, 2009.

[32] Golombek, M., Haldemann, A., Forsberg-Taylor, N., DiMaggio, E., Schroeder, R., Jakosky, B., Mellon, M., and Matijevic, J., "Rock size-frequency distributions on mars and implications for mars exploration rover landing safety and operations," *Journal of Geophysical Research: Planets (1991–2012)*, vol. 108, no. E12, 2003.

[33] Gravish, N. and Goldman, D. I., "Effect of volume fraction on granular avalanche dynamics," *Physical Review E*, vol. 90, no. 3, p. 32202, 2014.

[34] Gravish, N., Umbanhowar, P. B., and Goldman, D. I., "Force and Flow Transition in Plowed Granular Media," *Phys. Rev. Lett.*, vol. 105, p. 128301, Sept. 2010.

[35] Gray, J. and Hancock, G. J., "The propulsion of sea-urchin spermatozoa," *Journal of Experimental Biology*, vol. 32, no. 4, p. 802, 1955.

[36] Haldane, D. W., Peterson, K. C., Garcia Bermudez, F., and Fearing, R. S., "Animal-inspired design and aerodynamic stabilization of a hexapedal millirobot," in *Robotics and Automation (ICRA), 2013 IEEE International Conference on*, pp. 3279–3286, IEEE, 2013.

[37] Heiken, G., Vaniman, D., and French, B. M., *Lunar sourcebook: A user's guide to the Moon*. CUP Archive, 1991.

[38] Hill, G., Yeung, S., and Koehler, S. A., "Scaling vertical drag forces in granular media," *Europhysics Letters (EPL)*, vol. 72, pp. 137–143, Oct. 2005.

[39] Hirose, S., Fukuda, Y., Yoneda, K., Nagakubo, A., Tsukagoshi, H., Arikawa, K., Endo, G., Doi, T., and Hodoshima, R., "Quadruped walking robots at tokyo institute of technology: design, analysis, and gait control methods," *IEEE Robotics and Automation Magazine*, vol. 16, no. 2, pp. 104–114, 2009.

[40] Holmes, P., Full, R. J., Koditschek, D., and Guckenheimer, J., "The dynamics of legged locomotion: Models, analyses, and challenges," *Siam Review*, vol. 48, no. 2, pp. 207–304, 2006.

[41] Hoover, A. M., Burden, S., Shankar Sastry, S., and Fearing, R. S., "Bio-inspired design and dynamic maneuverability of a minimally actuated six-legged robot," *2010 3rd IEEE RAS & EMBS International Conference on Biomedical Robotics and Biomechatronics*, pp. 869–876, Sept. 2010.

[42] III, T. B., Mayor, P., and Durian, D. J., "Depth-dependent resistance of granular media to vertical penetration," *Physical review letters*, vol. 111, pp. 13–16, 2013.

[43] Irschick, D. J. and Jayne, B. C., "Effects of incline on speed, acceleration, body posture and hindlimb kinematics in two species of lizard *Callisaurus draconoides* and *Uma scoparia*.," *The Journal of experimental biology*, vol. 201, no. 2, pp. 273–287, 1998.

[44] Irschick, D. J. and Jayne, B. C., "Comparative three-dimensional kinematics of the hindlimb for high-speed bipedal and quadrupedal locomotion of lizards," *Journal of Experimental Biology*, vol. 202, no. 9, pp. 1047–1065, 1999.

[45] Irschick, D. J. and Jayne, B. C., "Size matters: ontogenetic variation in the three-dimensional kinematics of steady-speed locomotion in the lizard dipsosaurus dorsalis," *Journal of Experimental Biology*, vol. 203, no. 14, pp. 2133–2148, 2000.

[46] J. Shäfer, S. Dippel, and D. E. Wolf, "Force Schemes in Simulations of Granular Materials," *J. Phys. I France*, vol. 6, no. 1, pp. 5–20, 1996.

[47] Jackson, R., *The dynamics of fluidized particles*. Cambridge University Press, 2000.

[48] Jackson, R., *The dynamics of fluidized particles*. Cambridge University Press, 2000.

[49] Jaeger, H. M., Nagel, S. R., and Behringer, R. P., "Granular solids, liquids, and gases," *Reviews of Modern Physics*, vol. 68, no. 4, p. 1259, 1996.

[50] Jayne, B. C. and Irschick, D. J., "Effects of incline and speed on the three-dimensional hindlimb kinematics of a generalized iguanian lizard (Dipsosaurus dorsalis)," *The Journal of experimental biology*, vol. 202, pp. 143–159, Jan. 1999.

[51] Jerkins, M., Schröter, M., Swinney, H. L., Senden, T. J., Saadatfar, M., and Aste, T., "Onset of mechanical stability in random packings of frictional spheres," *Physical review letters*, vol. 101, no. 1, p. 018301, 2008.

[52] Jerkins, M., Schröter, M., Swinney, H. L., Senden, T. J., Saadatfar, M., and Aste, T., "Onset of Mechanical Stability in Random Packings of Frictional Spheres," *Phys. Rev. Lett.*, vol. 101, p. 18301, July 2008.

[53] Johnson, A. M., Libby, T., Chang-Siu, E., Tomizuka, M., Full, R. J., and Koditschek, D. E., "Tail assisted dynamic self righting," in *15th Int. Conf. on Climbing and Walking Robots (CLAWAR)*, 2012.

[54] Kato, N. and Kamimura, S., *Bio-mechanisms of swimming and flying: fluid dynamics, biomimetic robots, and sports science*. Springer Verlag, 2007.

[55] Katsuragi, H. and Durian, D. J., "Unified force law for granular impactcratering," *Nature Physics*, vol. 3, pp. 420–423, Apr. 2007.

[56] Kim, S., Clark, J. E., and Cutkosky, M. R., "isprawl: Design and tuning for high-speed autonomous open-loop running," *The International Journal of Robotics Research*, vol. 25, no. 9, pp. 903–912, 2006.

[57] Kim, S., Spenko, M., and Trujillo, S., "Whole body adhesion: hierarchical, directional and distributed control of adhesive forces for a climbing robot," *Proceedings of IEEE International Conference on Robotics and Automation (ICRA)*, no. April, pp. 10–14, 2007.

[58] Kimura, H., Fukuoka, Y., and Cohen, a. H., "Adaptive Dynamic Walking of a Quadruped Robot on Natural Ground Based on Biological Concepts," *The International Journal of Robotics Research*, vol. 26, pp. 475–490, May 2007.

[59] Kohut, N. J., Pullin, A. O., Haldane, D. W., Zarrouk, D., and Fearing, R. S., "Precise dynamic turning of a 10 cm legged robot on a low friction surface using a tail," in *Robotics and Automation (ICRA), 2013 IEEE International Conference on*, pp. 3299–3306, IEEE, 2013.

[60] Kohut, N. J., Zarrouk, D., Peterson, K. C., and Fearing, R. S., "Aerodynamic steering of a 10 cm high-speed running robot," in *Intelligent Robots and Systems (IROS), 2013 IEEE/RSJ International Conference on*, pp. 5593–5599, IEEE, 2013.

[61] Korff, W. L. and McHenry, M. J., "Environmental differences in substrate mechanics do not affect sprinting performance in sand lizards (*Uma scoparia* and *Callisaurus draconoides*).," *The Journal of experimental biology*, vol. 214, pp. 122–130, Jan. 2011.

[62] Kram, R. and Taylor, R. C., "Energetics of running: a new perspective," pp. 265–267, 1990.

[63] Kuffner, J., Kagami, S., Nishiwaki, K., Inaba, M., and Inoue, H., "Online footstep planning for humanoid robots," *Proceedings of IEEE International Conference on Robotics and Automation (ICRA)*, vol. 1, pp. 932–937, 2003.

[64] Latombe, J.-C., "Robot Motion Planning, Chapter," 1996.

[65] Lee, J. S. and Fearing, R. S., "Anisotropic collapsible leg spines for increased millibot traction," in *International Conference on Robotics and Automation (ICRA)*, IEEE, 2015.

[66] Lejeune, T. M., Willems, P. A., and Heglund, N. C., "Mechanics and energetics of human locomotion on sand.," *The Journal of experimental biology*, vol. 201, pp. 2071–2080, July 1998.

[67] Levihn, M., Nishiwaki, K., Kagami, S., and Stilman, M., "Autonomous environment manipulation to assist humanoid locomotion," in *Robotics and Automation (ICRA), 2014 IEEE International Conference on*, pp. 4633–4638, IEEE, 2014.

[68] Li, C., Hsieh, S. T., and Goldman, D. I., "Multi-functional foot use during running in the zebra-tailed lizard (*Callisaurus draconoides*).," *The Journal of experimental biology*, vol. 215, pp. 3293–3308, Sept. 2012.

[69] Li, C., Pullin, A. O., Haldane, D. W., Lam, H. K., Fearing, R. S., and Full, R. J., "Terradynamically streamlined shapes in animals and robots enhance traversability through densely cluttered terrain," *Bioinspiration & biomimetics*, vol. 10, no. 4, p. 046003, 2015.

[70] Li, C., Umbanhowar, P. B., Komsuoglu, H., and Goldman, D. I., "The Effect of Limb Kinematics on the Speed of a Legged Robot on Granular Media," *Experimental Mechanics*, vol. 50, pp. 1383–1393, Apr. 2010.

[71] Li, C., Umbanhowar, P. B., Komsuoglu, H., Koditschek, D. E., and Goldman, D. I., "Sensitive dependence of the motion of a legged robot on granular media.," *Proceedings of the National Academy of Sciences*, vol. 106, pp. 3029–3034, Mar. 2009.

[72] Li, C., Zhang, T., and Goldman, D. I., "A terradynamics of legged locomotion on granular media.," *Science*, vol. 339, pp. 1408–1412, Mar. 2013.

[73] Libby, T., Moore, T. Y., Chang-Siu, E., Li, D., Cohen, D. J., Jusufi, A., and Full, R. J., "Tail-assisted pitch control in lizards, robots and dinosaurs," *Nature*, vol. 481, no. 7380, pp. 181–184, 2012.

[74] Lipkin, K., Brown, I., Peck, A., Choset, H., Rembisz, J., Gianfortoni, P., and Naaktgeboren, A., "Differentiable and piecewise differentiable gaits for snake robots," in *Intelligent Robots and Systems, 2007. IROS 2007. IEEE/RSJ International Conference on*, pp. 1864–1869, IEEE, 2007.

[75] Lorenz, E. N., *The essence of chaos*. University of Washington Press, 1995.

[76] Majmudar, T. S. and Behringer, R. P., "Contact force measurements and stress-induced anisotropy in granular materials," *Nature*, vol. 435, no. 7045, pp. 1079–1082, 2005.

[77] Maladen, R. D., Ding, Y., Li, C., and Goldman, D. I., "Undulatory swimming in sand: subsurface locomotion of the sandfish lizard," *science*, vol. 325, no. 5938, pp. 314–318, 2009.

[78] Maladen, R. D., Ding, Y., Umbanhowar, P. B., and Goldman, D. I., "Undulatory swimming in sand: experimental and simulation studies of a robotic sandfish," *The International Journal of Robotics Research*, vol. 30, no. 7, pp. 793–805, 2011.

[79] Maladen, R. D., Ding, Y., Umbanhowar, P. B., Kamor, A., and Goldman, D. I., "Mechanical models of sandfish locomotion reveal principles of high performance subsurface sand-swimming.," *Journal of the Royal Society, Interface / the Royal Society*, vol. 8, pp. 1332–45, Sept. 2011.

[80] Maladen, R. D., Umbanhowar, P. B., Ding, Y., Masse, A., and Goldman, D. I., "Granular lift forces predict vertical motion of a sand-swimming robot." 2011.

[81] Marvi, H., Gong, C., Gravish, N., Astley, H., Travers, M., Hatton, R. L., Mendelson, Joseph R. III Choset, H., Hu, D., and Goldman, D. I., "Sidewinding with minimal slip: snake and robot ascent of sandy slopes," *Science*.

[82] Matson, J., "Unfree Spirit: NASA's Mars Rover Appears Stuck for Good," *Scientific American*, vol. 302, no. 4, p. 16, 2010.

[83] May, L. B., Golick, L. A., Phillips, K. C., Shearer, M., and Daniels, K. E., "Shear-driven size segregation of granular materials: Modeling and experiment," *Physical Review E*, vol. 81, no. 5, p. 051301, 2010.

[84] Mazouchova, N., Umbanhowar, P. B., and Goldman, D. I., "Flipper-driven terrestrial locomotion of a sea turtle-inspired robot.," *Bioinspiration & biomimetics*, vol. 8, p. 026007, June 2013.

[85] McCord, M. A. and Rooks, M. J., "SPIE handbook of microlithography, micromachining and microfabrication," in *SPIE, Bellingham*, 2000.

[86] Meirion-Griffith, G. and Spenko, M., "Comprehensive pressure-sinkage model for small-wheeled unmanned ground vehicles on dilative, deformable terrain," *2012 IEEE International Conference on Robotics and Automation*, pp. 4052–4057, May 2012.

[87] Miller, B. D., Rivera, P. R., Dickson, J. D., and Clark, J. E., "Running up a wall: the role and challenges of dynamic climbing in enhancing multimodal legged systems," *Bioinspiration & biomimetics*, vol. 10, no. 2, p. 025005, 2015.

[88] Morrey, J. M., Lambrecht, B., Horchler, A. D., Ritzmann, R. E., and Quinn, R. D., "Highly mobile and robust small quadruped robots," in *Intelligent Robots and Systems, 2003.(IROS 2003). Proceedings. 2003 IEEE/RSJ International Conference on*, vol. 1, pp. 82–87, IEEE, 2003.

[89] Mosauer, W., "Adaptive Convergence in the Sand Reptiles of the {S}ahara and of {C}alifornia: A Study in Structure and Behavior," *Copeia*, vol. 1932, no. 2, pp. 72–78, 1932.

[90] Murphy, M. P., Saunders, A., Moreira, C., Rizzi, A. A., and Raibert, M., "The littledog robot," *The International Journal of Robotics Research*, p. 0278364910387457, 2010.

[91] Nedderman, R., "Statics and kinematics of granular materials," 1992.

[92] Nichol, K., Zanin, A., Bastien, R., Wandersman, E., and van Hecke, M., "Flow-induced agitations create a granular fluid," *Physical review letters*, vol. 104, no. 7, p. 078302, 2010.

[93] Ojha, R., Menon, N., and Durian, D. J., "Hysteresis and packing in gas-fluidized beds," *Physical review. E, Statistical physics, plasmas, fluids, and related interdisciplinary topics*, vol. 62, p. 4442, Sept. 2000.

[94] Pandolf, K. B., Haisman, M. F., and Goldman, R. F., "Metabolic energy expenditure and terrain coefficients for walking on snow," *Ergonomics*, vol. 19, no. 6, pp. 683–690, 1976.

[95] Park, H.-W. and Kim, S., "Quadrupedal galloping control for a wide range of speed via vertical impulse scaling," *Bioinspiration & biomimetics*, vol. 10, no. 2, p. 025003, 2015.

[96] Patla, A. E., Prentice, S. D., Rietdyk, S., Allard, F., and Martin, C., "What guides the selection of alternate foot placement during locomotion in humans," *Experimental Brain Research*, vol. 128, pp. 441–450, Oct. 1999.

[97] Paulson, L. D., "Biomimetic robots," *Computer*, vol. 37, no. 9, pp. 48–53, 2004.

[98] Qian, F., Zhang, T., Korff, W., Umbanhowar, P., Full, R., and Goldman, D., "Principles of appendage design in robots and animals determining terradynamic performance on flowable ground.," *Bioinspiration & biomimetics*, vol. 10, no. 5, p. 056014, 2015.

[99] Qian, F., Daffon, K., Zhang, T., and Goldman, D. I., "An automated system for systematic testing of locomotion on heterogeneous granular media," in *proceedings of the 16th Int. Conf. on Climbing and Walking Robots (CLAWAR)*, pp. 547–554, World Scientific, 2013.

[100] Qian, F. and Goldman, D., "Anticipatory control using substrate manipulation enables trajectory control of legged locomotion on heterogeneous granular media," in *SPIE Defense+ Security*, pp. 94671U–94671U, International Society for Optics and Photonics, 2015.

[101] Qian, F. and Goldman, D. I., "The dynamics of legged locomotion in heterogeneous terrain: universal scattering and sensitivity to initial conditions," *Robotics: Science and Systems (RSS)*, 2015.

[102] Qian, F., Zhang, T., Li, C., Masarati, P., Hoover, A. M., Birkmeyer, P., Pullin, A., Fearing, R. S., Goldman, D. I., and Olin, F. W., "Walking and running on yielding and fluidizing ground," *Robotics: Science and Systems (RSS)*, 2012.

[103] Raibert, M., Blankespoor, K., Nelson, G., Playter, R., and others, "Bigdog, the rough-terrain quadruped robot," in *Proceedings of the 17th World Congress*, vol. 17, pp. 10822–10825, 2008.

[104] Rapaport, D. C., *The art of molecular dynamics simulation*. Cambridge university press, 2004.

[105] Saranli, U., Buehler, M., and Koditschek, D. E., "RHex : A Simple and Highly Mobile Hexapod Robot RHex : A Simple Hexapod Robot," 2001.

[106] Schenker, P. S., Huntsberger, T. L., Pirjanian, P., Baumgartner, E. T., and Tunstel, E., "Planetary rover developments supporting mars exploration, sample return and future human-robotic colonization," *Autonomous Robots*, vol. 14, no. 2-3, pp. 103–126, 2003.

[107] Schneebeli, M., "snow stratigraphy," *Annals of Glaciology*, vol. 26, pp. 1–5, 1998.

[108] Schofield, A. and Wroth, P., "Critical state soil mechanics," 1968.

[109] Schroer, R. T., Boggess, M. J., Bachmann, R. J., Quinn, R. D., and Ritzmann, R. E., "Comparing cockroach and Whegs robot body motions," in *Proceedings of IEEE International Conference on Robotics and Automation (ICRA)*, vol. 4, pp. 3288 —- 3293 Vol.4, 2004.

[110] Schroer, R. T., Boggess, M. J., Bachmann, R. J., Quinn, R. D., and Ritzmann, R. E., "Comparing cockroach and whegs robot body motions," in *Robotics and Automation, 2004. Proceedings. ICRA'04. 2004 IEEE International Conference on*, vol. 4, pp. 3288–3293, IEEE, 2004.

[111] Schröter, M., Nägle, S., Radin, C., and Swinney, H. L., "Phase transition in a static granular system," *Europhysics Letters (EPL)*, vol. 78, p. 44004, May 2007.

[112] Senatore, C. and Wulfmeier, M., "Investigation of Stress and Failure in Granular Soils For Lightweight Robotic Vehicle Applications," *Proceedings of the Ground Vehicle Systems Engineering and Technology Symposium*, pp. 1–12, 2012.

[113] Shibly, H., Iagnemma, K., and Dubowsky, S., "An equivalent soil mechanics formulation for rigid wheels in deformable terrain, with application to planetary exploration rovers," *Journal of Terramechanics*, vol. 42, no. 1, pp. 1–13, 2005.

[114] Spence, A. J., Revzen, S., Seipel, J., Mullens, C., and Full, R. J., "Insects running on elastic surfaces.," *The Journal of experimental biology*, vol. 213, pp. 1907–1920, June 2010.

[115] Sponberg, S. and Full, R. J., "Neuromechanical response of musculoskeletal structures in cockroaches during rapid running on rough terrain," *Journal of Experimental Biology*, vol. 211, no. 3, pp. 433–446, 2008.

[116] Stone, M., Barry, R., Bernstein, D., Pelc, M., Tsui, Y., and Schiffer, P., "Local jamming via penetration of a granular medium," *Physical Review E*, vol. 70, p. 041301, Oct. 2004.

[117] Stone, M. B., Bernstein, D. P., Barry, R., Pelc, M. D., and Tsui, Y.-k., "Getting to the bottom of a granular medium," *Nature*, vol. 427, no. February, pp. 503–505, 2004.

[118] Strogatz, S. H., *Nonlinear dynamics and chaos: with applications to physics, biology and chemistry*. Perseus publishing, 2001.

[119] Takehara, Y., Fujimoto, S., and Okumura, K., "High-velocity drag friction in dense granular media," *EPL (Europhysics Letters)*, vol. 92, no. 4, p. 44003, 2010.

[120] Tryba, A. and Ritzmann, R., "Multi-joint coordination during walking and foothold searching in the Blaberus cockroach. I. Kinematics and electromyograms," *Journal of neurophysiology*, vol. 83, no. 6, pp. 3323–3336, 2000.

[121] Tsinontides, S. C. and Jackson, R., "The mechanics of gas fluidized beds with an interval of stable fluidization," *Journal of Fluid Mechanics*, vol. 255, p. 237, Apr. 1993.

[122] Vásquez, R. A., Ebensperger, L. A., and Bozinovic, F., "The influence of habitat on travel speed, intermittent locomotion, and vigilance in a diurnal rodent," *Behavioral Ecology*, vol. 13, no. 2, pp. 182–187, 2002.

[123] Vernaza, P., Likhachev, M., Bhattacharya, S., Chitta, S., Kushleyev, A., and Lee, D. D., "Search-based planning for a legged robot over rough terrain," in *Robotics and Automation, 2009. ICRA'09. IEEE International Conference on*, pp. 2380–2387, IEEE, 2009.

[124] Vogel, S., *Life in moving fluids: the physical biology of flow*. Princeton Univ Pr, 1996.

[125] Volpe, R., "Rover functional autonomy development for the mars mobile science laboratory," in *Proceedings of the 2003 IEEE Aerospace Conference*, vol. 2, pp. 643–652, 2003.

[126] Waitukaitis, S. R. and Jaeger, H. M., "Impact-activated solidification of dense suspensions via dynamic jamming fronts.," *Nature*, vol. 487, pp. 205–209, July 2012.

[127] Waldron, K. J., Arkin, R. C., Bakkum, D., Merrill, E., and Abdallah, M., "Proprioceptive control for a robotic vehicle over geometric obstacles," tech. rep., DTIC Document, 2005.

[128] Wassgren, C., Cordova, J., Zenit, R., and Karion, A., "Dilute granular flow around an immersed cylinder," *Physics of Fluids*, vol. 15, no. 11, pp. 3318–3330, 2003.

[129] Weyand, P. G., Sternlight, D. B., Bellizzi, M. J., and Wright, S., "Faster top running speeds are achieved with greater ground forces not more rapid leg movements," *Journal of Applied Physiology*, vol. 89, no. 5, pp. 1991–1999, 2000.

[130] Wong, J. Y., *Terramechanics and off-road vehicles*. Elsevier, 1989.

[131] Wong, J.-Y. and Reece, A., "Prediction of rigid wheel performance based on the analysis of soil-wheel stresses part i. performance of driven rigid wheels," *Journal of Terramechanics*, vol. 4, no. 1, pp. 81–98, 1967.

[132] Wood, R. J., Avadhanula, S., Sahai, R., Steltz, E., and Fearing, R. S., "Microrobot design using fiber reinforced composites," *Journal of Mechanical Design*, vol. 130, no. 5, p. 052304, 2008.

[133] Wright, C., Johnson, A., Peck, A., McCord, Z., Naaktgeboren, A., Gianfortoni, P., Gonzalez-Rivero, M., Hatton, R., and Choset, H., "Design of a modular snake robot," *IEEE/RSJ International Conference on Intelligent Robots and Systems (IROS)*, pp. 2609–2614, Nov. 2007.

[134] Zarrouk, D. and Fearing, R. S., "Controlled in-plane locomotion of a hexapod using a single actuator,"

[135] Zug, G. R., "locomotion," *Encyclopaedia Britannica Online*, 2015.